Fall 2014

First-principles investigations of iron-based alloys and their properties

Krista Renee Limmer

Department: Materials Science and Engineering

FIRST-PRINCIPLES INVESTIGATIONS OF IRON-BASED ALLOYS AND THEIR PROPERTIES

by

KRISTA RENEE LIMMER

A DISSERTATION

Presented to the Faculty of the Graduate School of the

MISSOURI UNIVERSITY OF SCIENCE AND TECHNOLOGY

In Partial Fulfillment of the Requirements for the Degree

DOCTOR OF PHILOSOPHY
in
MATERIALS SCIENCE AND ENGINEERING

2014

Approved
Julia Medvedeva, Advisor
David C. Van Aken
Matthew J. O'Keefe
Mohsen Asle Zaeem
Yew San Hor

PUBLICATION DISSERTATION OPTION

The body of this dissertation has been prepared in the style of four manuscripts for publication. Paper I titled "The Role of Ordered Carbon Vacancies in Vanadium Carbide and (V,Nb)C¬x – Energetic, Structural, and Surface Properties" has been prepared for submission to *Acta Materialia*. The second paper "Effect of Nickel, Copper, and Chromium on Stacking Fault Energy of FCC Iron" has been published in the *2014 AISTech Conference Proceedings*. The third paper "Ab-initio simulation of alloying effect on stacking fault energy in fcc Fe" has been prepared for publication in *Computational Materials Science*. The final paper "Carbon interactions with transition metal additions at stacking faults in fcc iron" is prepared for submission to *Acta Materialia*.

The introduction and methodology sections preface the papers to provide pertinent information about the systems studied in this work and the computational methodology applied. Appendices A and B contain supplemental tabulated data from vanadium and niobium carbide and stacking fault energy calculations, respectively.

ABSTRACT

Fundamental understanding of the complex interactions governing structure-property relationships in iron-based alloys is necessary to advance ferrous metallurgy. Two key components of alloy design are carbide formation and stabilization and controlling the active deformation mechanism. Following a first-principles methodology, understanding on the electronic level of these components has been gained for predictive modeling of alloys.

Transition metal carbides have long played an important role in alloy design, though the complexity of their interactions with the ferrous matrix is not well understood. Bulk, surface, and interface properties of vanadium carbide, VC_x, were calculated to provide insight for the carbide formation and stability. Carbon vacancy defects are shown to stabilize the bulk carbide due to increased V-V bonding in addition to localized increased V-C bond strength. The VC_x (100) surface energy is minimized when carbon vacancies are at least two layers from the surface. Further, the Fe/VC interface is stabilized through maintaining stoichiometry at the Fe/VC interface.

Intrinsic and unstable stacking fault energy, γ_{isf} and γ_{usf} respectively, were explicitly calculated in nonmagnetic fcc Fe-X systems for X = Al, Si, P, S, and the 3*d* and 4*d* transition elements. A parabolic relationship is observed in γ_{isf} across the transition metals with minimums observed for Mn and Tc in the 3*d* and 4*d* periods, respectively. Mn is the only alloying addition that was shown to decrease γ_{isf} in fcc Fe at the given concentration. The effect of alloying on γ_{usf} also has a parabolic relationship, with all additions decreasing γ_{isf} yielding maximums for Fe and Rh.

ACKNOWLEDGMENTS

I would like to start by thanking the people who have helped me along in this academic venture. First and foremost, much of what I have learned about density functional theory methodology and application has come from my advisor Julia Medvedeva. In addition to teaching me how to effectively utilize this powerful tool, she has helped me to navigate the numerous opportunities and challenges that accompany such a flexible tool in an interdisciplinary field. Her encouragement for my attending numerous conferences and workshops has tremendously also expanded my understanding. I would be remiss if I did not also thank Nadya Medvedeva for her assistance in learning to use the VASP software, helpful discussion of results, and her advice for avoiding pitfalls. I would also like to thank a number of people in the Materials Science and Engineering Department who have had a positive impact on my life and education. Though I cannot name each person who has significantly affected me, noteworthy individuals include members of my dissertation committee and a number of other faculty who have served as role models in teaching, research, and service. In particular, I would like to thank David Van Aken for his practical guidance and support through my studies, in addition to his modelling of a number of qualities I hope to emulate in and out of the classroom.

I would also like to thank the multiple sources that have funded this work. First, the U.S. Department of Education GAANN Fellowship which allowed me to travel to numerous conferences and pursue fundamental research. Second, the latter part of this research has been supported by the Peaslee Steel Manufacturing Research Center. The relationship with the industrial partners provided direction and allowed me to work on projects with practical applications.

Finally, I would like to express my gratitude to my family, friends, and colleagues who have supported me throughout my studies. Last but not least, my deepest gratitude goes to my husband Matt, who has provided unwavering support, encouragement, and faith that have sustained me through the ups-and-downs.

TABLE OF CONTENTS

LIST OF ILLUSTRATIONS

LIST OF TABLES

1. INTRODUCTION

1.1. STEEL ALLOY DESIGN

The steel industry has long depended on empirical models to improve manufacturing and product performance. The variety of complex competing mechanisms at the atomic and microscopic scale must be understood at a more fundamental level to continue moving the steel industry forward.[1] With increasing performance requirements, steel alloys are becoming increasingly complex. Along with improved performance, increased manufacturability and decreased production energy consumption are also needed to allow the steel industry to remain competitive.

Advanced high strength steels (AHSS) are undergoing industry-driven development to increase the competitiveness of steel against light metals for automotive applications. The US Department of Transportation fuel efficiency regulations have made vehicle light-weighting obligatory, bringing about a need for research to develop the so called, third generation AHSS as indicated in Figure 1.1.[2] First and second generation AHSS depend on key microstructural features for their combined high strength and formability.

In Mn-containing steels, the active deformation mechanism, twin-induced plasticity (TWIP) and transformation-induced plasticity (TRIP), is controlled by stacking fault energy. The effect of alloying elements on stacking fault energies is not currently understood well enough for predictive capabilities. In addition to controlling active deformation mechanisms, carbide and nitride formation and stabilization is of great interest for AHSS and other steel classes. With grain pinning acting as a primary strengthening mechanism, a controlled formation of carbides and nitrides is desired. To gain control, a better fundamental understanding of carbide, nitride, and carbonitride formation and stabilization within complex alloy systems is required.

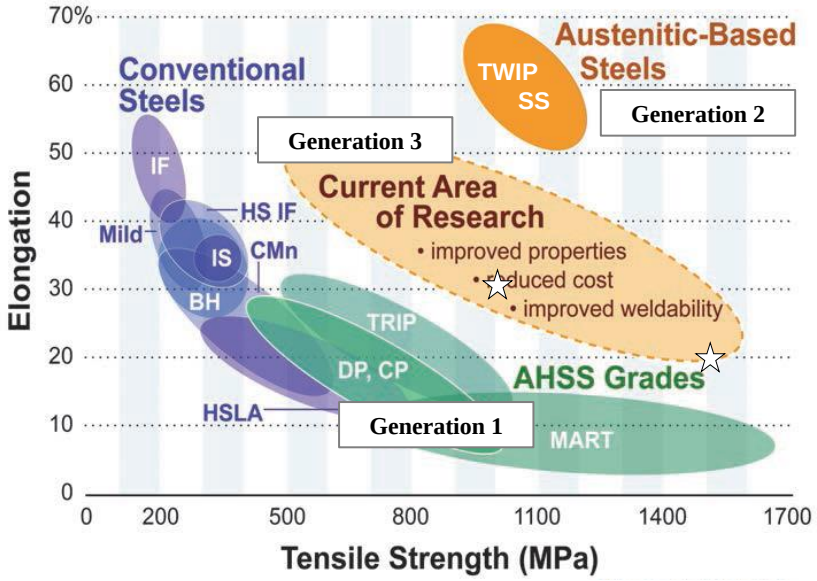

Figure 1.1 Banana plot [2] of tensile strength vs. elongation for steel alloys indicating the primary property targets for third generation AHSS development.

1.2. TRANSITION METAL CARBIDES

High strength steels are strengthened in part by small grain sizes. Nano-sized carbide precipitates act as secondary strengtheners by affecting grain growth through grain pinning.[3]–[5] To achieve these precipitates, many steel alloys contain carbide forming elements such as Cr, W, Mo, V, Ti, Nb, and Zr. Common carbide-forming microalloying additions in high strength low alloy (HSLA) steels are Ti, Nb, and V. In this work vanadium carbide is studied because of its increased solubility in austenite allowing dissolution while heating and fine secondary precipitation. These secondary precipitates serve as nucleation sites for intragranular ferrite during cooling to provide grain refinement.[5]–[8] Many steel classes are designed to contain multiple carbide forming alloying additions. Due to the higher precipitation temperature of NbC and the similar electronic structure of V and Nb, it has been suggested that Nb may compete with

V in carbide formation. The structure and influence of mixed-metal carbides is also not well understood.

1.2.1 Vanadium Carbide Structure & Properties. Vanadium carbide (VC) has the rock salt structure commonly observed in transition metal MC carbides. Like most transition metal carbides, VC has been observed to have carbon vacancies while retaining the MC structure. The carbon range experimentally observed in VC_x is $0.66 < x < 0.88$.[9], [10] While the lower bound is not uncommon, the upper homogeneity boundary of 0.88 is noticeably diminished from the 1.00 generally found in other transition metal carbides.[11]–[13] This decreased boundary gives rise to the ordered cubic structure V_8C_7 [14]–[16] shown in Figure 1.2A corresponding to space group $P4_332$.[17], [18] This ordered structure that has not been observed in other MC carbides[13] was first observed by de Novion[17] and later confirmed by Froidvaux[18]. A second ordered phase, V_6C_5 has been reported with having either a trigonal[19] ($P3_1$) shown in Figure 1.2B or monoclinic[20], [21] (C2 or C2/m) crystal structure. Recent studies have determined that the monoclinic phase is marginally more stable and is stable over a wider temperature range.[22]–[24] The short range-order of the trigonal and monoclinic V_6C_5 phases is identical.[25] The V_8C_7 and V_6C_5 (both trigonal and monoclinic) phases have been observed in steels, and sometimes simultaneously.[3], [13], [26]–[28] The V_4C_3 structure which has been historically reported[19], [21], [22], [29]–[33] is not considered in this study due to recent work which does not support the existence of the phase as a precipitate within Fe-C-V steels.[3], [26]

The VC_x order-disorder transition has been classified as a first-order transition.[11]–[13], [28], [34]–[38] The ordering transition to either V_8C_7 or V_6C_5 occurs between 1100^{o}C and 1300^{o}C and has an enthalpy change of approximately 3.0 kJ/mol.[13], [27], [36] Both ordering transitions result in slight increases of the lattice parameter (0.002-0.005Å).[13] The enthalpy of formation has been determined experimentally for V_8C_7 and V_6C_5 compounds.[39] In addition, thermochemical models have been used to estimate the formation of VC based on experimental data.[32], [38] A first-principles study[40] on ordered VC_x compounds indicated that even without

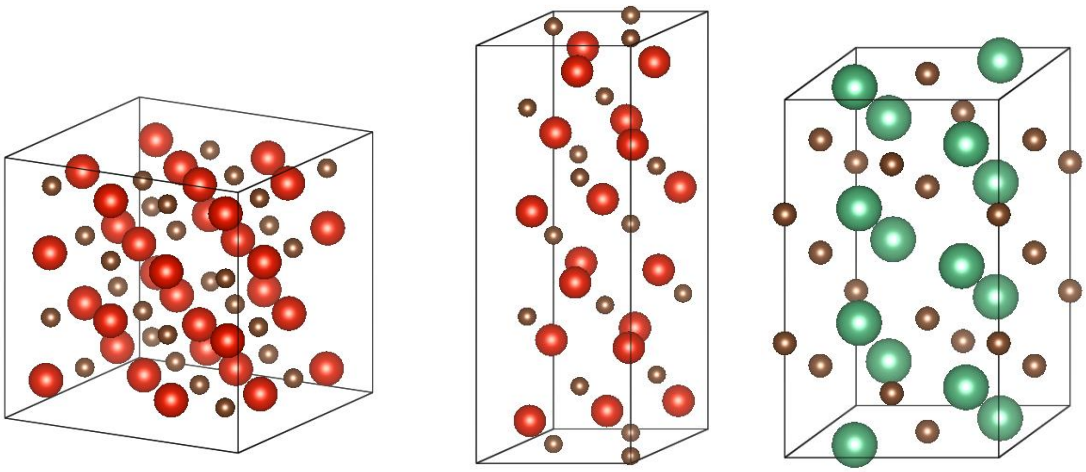

Figure 1.2 a) V_8C_7 cubic carbide corresponding to space group $P4_332$, b) V_6C_5 trigonal carbide corresponding to space group $P3_1$ c) Nb_6C_5 monoclinic carbide corresponding to space group C2/m

relaxation around carbon vacancies, an energy decrease is observed during the ordering transition making the V_8C_7 and V_6C_5 structures more stable than VC.

A recent first-principles study[41] on the mechanical properties of VC compared with cubic V_4C_3 to examine the role of vacancies on elastic properties showed that the introduction of 25% carbon vacancies decreased bulk, shear and elastic moduli by 13.3% 19.2% and 17.7%, respectively. Earlier calculations [42], [43] also indicated decreasing moduli with increasing carbon vacancies although the percentages varied. Calculated mechanical properties of refractory carbides with various first-principles tools[44]–[47] yield comparisons between VC and NbC indicating that NbC has a lower bulk, shear, and elastic moduli than stoichiometric VC. Experimental results [44] also confirm this relationship.

1.2.2 Niobium Carbide: Structure & Properties. Niobium also forms an MC carbide structure while accommodating a wide range of carbon vacancies, similar to vanadium. The homogeneity range for NbC_x is $0.70 < x < 1.00$.[48] NbC_x also has a

stable non-stoichiometric Nb_6C_5 structure which was originally proposed to be a trigonal structure[33] but later determined to be the monoclinic structure also observed in VC_x and is shown in Figure 1.2C.[38] This ordering of the carbon vacancies has only been observed during long anneals at low temperatures (<900^oC) which limit carbon diffusivity and no Nb_8C_7 structure has been observed.[22]

Niobium is another strong carbide former with a similar electronic structure to vanadium, suggesting that Nb may compete with V in carbide formation. Experimental studies have shown mixed metal carbides and carbonitrides when both V and Nb are present in the steel.[26], [49], [50] Experimental results from microalloying with niobium indicate that niobium carbides have a higher precipitation temperature.[5], [51] This higher precipitation temperature allows NbC to be effective in inhibiting static recrystallization of the austenite through grain pinning. [5], [8]

1.2.3 Bonding & Electronic Structure. Transition metal carbides, nitrides, and oxides typically form metal-metal bonds in the presence of carbon vacancies.[12] Zhukov[52] discussed the vacancy formation as a two-part process which undergoes destabilization, breaking M-C bonds, and stabilization through strengthening M-M bonds. In the case of titanium and vanadium however the strengthening from metal-metal bonds may not be sufficient to compensate for the energy required to break the M-C bonds. Rogovoi[53], [54] proposed that both VC_x and NbC_x have increased M-C bond strength in the presence of carbon vacancies. An increased M-C bond strength indicates that the metal atom would shift away from neighboring carbon vacancies towards neighboring carbon atoms. Indeed, experimental static relaxations reveal that the niobium shifts away from the neighboring vacancies in Nb_6C_5.[55], [56] Additionally in V_8C_7 the vanadium octahedra are distorted such that carbon atoms shift towards carbon vacancies.[57] Compton scattering studies showed that in NbC_x Nb-C bonds are strengthened and Nb-Nb bonds are weakened as stoichiometry is approached.[58]

The electronic structure of stoichiometric VC has been examined with first-principles methods and indicates significant charge transfer from V to C in VC.[59], [60] A study on bonding in transition metal MC carbides indicated that the strongest directional bonding involves the C(2p) and TM(3d) orbitals.[61] Further, VC has the

highest percent overlap between the carbon/transition metal spheres indicating strong covalent bonding while ScC has a typical ionic-type rocksalt bonding. The covalent mixing of the valence bonding levels for VC is very high with nearly a 50-50 split in the carbon-metal character.[62]

Bonding studies of M_2C carbides have been completed with first-principles, though not of the ordered substoichiometric transition metal carbides MC_x. M_2C carbides have negative formation energies that decrease with increasing number of valence electrons (for M = V, Nb, Ta, Cr, Mo, and W) which result from highly-directional M-C covalent bonds. M_4C carbides are destabilized with respect to M_2C carbides as a result of directional M-M bonds and simultaneous weakening of M-C bonds.[63] One objective of this work is to elucidate the effect of ordered carbon vacancies on the local electronic structure in VC_x.

1.2.4 Mechanical Properties. NbC_x and TaC_x have been shown to increase hardness and elastic modulus with increasing carbon content at elevated temperatures contrary to what is commonly observed in transition metal nitrides such as TiN_x.[64] In a similar study on yield strength of carbides, VC_x reached a peak strength at x = 0.84 corresponding to the V_6C_5 structure although NbC strengths increased with increasing C content up to x = 0.95, the limit of the experimental study.[65] A recent study[45] on the mechanical properties of VC and NbC yielded bulk modulus results that matched closely with experimental values.

1.2.5 Mixed Metal MC Carbides. Experimental studies have observed mixed metal carbides and carbonitrides when both V and Nb are present in the steel.[26], [49], [50] Experimental results from microalloying with Nb indicate that niobium carbides have a higher precipitation temperature than vanadium carbides.[5], [66] This higher precipitation temperature allows NbC to be effective in inhibiting static recrystallization of the austenite through grain pinning.[5], [8] Precipitated carbides in a Fe-V-Nb-C system have been shown to initiate as Nb-rich carbides that then decompose into NbC and VC_x upon cooling. The VC_x precipitates are suggested to contain Nb-defects because of the observed increased lattice parameter, although minimal V defects were observed within the stable room temperature NbC precipitates.[20], [26] Experimental studies have

shown that partial substitution of vanadium with niobium increases MC carbide volume fraction and improves mechanical properties.[67]–[69] The solubility of Nb in VC_x ordered structures and its impact on the structural properties is unknown.

1.2.6 Surfaces & Interfaces. The structure and properties of carbide surfaces, in particular the interface with an austenitic matrix, is of interest to understand the precipitation and growth of vanadium carbides in steels. Vanadium carbides are of additional interest due to their potential use as a hydrogen trapping agent as indicated by atom-probe studies[70] and numerical analysis[71] that suggests the inherent carbon-vacancy concentration in VC_x promotes hydrogen-trapping.

Surface and interface studies of transition metal carbides have been limited to general surface energy calculations. The surface energy relationship of E[100] < E[110] < E[111] was determined for rocksalt structure transition metal carbides, nitrides, and alkali metal oxides using first principles.[72] Further the (100) surface energy of VC is lower than that of NbC.[73]

Surface chemistry studies have been performed to examine the adhesion of molecules to transition metal carbide surfaces,[74], [75] though interfaces with austenite are little understood. The tungsten carbide - ferrite interface was examined to determine the adhesion properties in a wear and cutting resistance study.[76] The Al/VC interface was studied using first-principles methods and showed that similar to other metal-carbide interface studies, the most favorable interface orientation is for the metalloid site to be positioned directly above the bulk-Al sites.[77] First-principles studies of the ferrite – MC interface for M = (Ti, Mo) have indicated that although the addition of Mo decreases the stability of the carbide, the interfacial energy also decreases, indicating easier carbide formation.[78], [79] It is of interest whether a similar effect may be observed in vanadium carbide as a function of Nb-defects and carbon vacancies with an austenitic interface.

Surface and interface studies may also be used to explain bulk properties of carbides. A Compton scattering study on the electronic properties of NbC_x indicated that as stoichiometry is approached the Nb-C bonds are strengthened while Nb-Nb bonds are

weakened.[58] This observation coupled with a surface vacancy concentration led to the hypothesis that in an attempt to approach stoichiometry non-metal vacancies are created at the crystal surface from non-metal atoms diffusing from the surface to the bulk. The effect of the expected strong V-C bond in vanadium carbide is better elucidated through surface studies in this work.

1.3. STACKING FAULT ENERGY OF MN-STEELS

1.3.1 Manganese Steels. Manganese-containing steels are of renewed interest for meeting the requirements of third generation advanced high strength steels (AHSS) to exceed the strength-ductility combinations of first generation AHSS; such as dual-phase, transformation-induced plasticity (TRIP), complex phase, and martensitic steel; at a cost significantly less than that of second generation AHSS such as twinning-induced plasticity (TWIP) steel.[80] High manganese steels, such as Hadfield steel, containing 15-30 at% Mn are an example of a TWIP steel which gained much attention as a 2nd generation AHSS.[81]–[85] Although the high Mn steel compositions yield favorable results they are expensive and challenging to consistently and safely produce on a large production scale. A middle Mn content of less than 8 wt% is desired.

The active deformation mechanism in austenitic steels is controlled by the stacking fault energy (SFE). The creation of a stacking fault in austenite, or nucleation of a leading partial, may be repeated on every subsequent plane to form a twin, or every other plane to form ε-martensite. It has been suggested that the nucleation of ε-martensite is a critical step in the nucleation process of α-martensite from austenite in the TRIP phenomena, implying a transient metastable state of the ε-martensite.[86], [87] Alternatively, the transformation sequence austenite → ε-martensite → α-martensite has been termed two-stage TRIP, observed in alloys with stable ε-martensite.[88] The possibility to form a twin or to trip to ε-martensite is not well understood. An approximate relationship to SFE has been described such that TRIP steels generally have low SFE, less than 20 mJ/m^2, and TWIP steels have medium SFE or 20-50 mJ/m^2.[89] The stacking fault energy is known to be altered by alloy chemistry, temperature, and strain; this work will address the effects of alloy chemistry. The effect of transition metal elements on the SFE either as alloying additions or residual elements is of concern for

alloy development as these additions may have a significant effect on the SFE and therefore the active deformation mechanism [87], [90], [91].

1.3.2. Stacking Fault Energy Calculations. The SFE values of multicomponent systems are often considered to be proportional to the Gibbs free energies of the fcc to hcp transformation using a regular solution model with estimated parameters from experimental thermodynamic data. These estimations have been made for the Fe-Mn-C and Fe-Mn-Al-Si-C alloys [89], [92]–[94]. Manganese additions have a parabolic influence on stacking fault energy with a minimum between 12-22 at% Mn.[95]–[99] Thermochemical models indicate aluminum and carbon additions increase SFE and first-principles calculations have further established that trend.[94], [98], [100]

Ab-initio methods have been employed to determine the stacking fault energies following both explicit and implicit approaches. The SFE may be explicitly calculated as a total energy difference between the ideal and faulted lattices. This explicit approach has been used to predict the SFE in Fe [98], [101], Fe-N [102], Fe-C [98], [100], Fe-Mn and Fe-Al [98]. An implicit *ab initio* approach to calculate SFE has also been used recently following the axial next-nearest-neighbor Ising (ANNNI) model, where the energies of the fcc, hcp and double hcp phases are calculated to determine the SFE of the fcc phases in the Fe-Mn system [103]–[105]. The implicit approach allows for a more homogeneous description of the bulk environment whereas the explicit calculations provide a more complete understanding of segregation effects as well as the electronic structure changes at the stacking fault [100]. Recent studies have shown that the alloying additions only impact the stacking fault energy with the nearest two-layers of the stacking fault interface.[98], [106]

One of the challenges in first-principle calculations of stacking fault energy in austenite is accurately handling of the magnetic state. The various magnetic states of fcc Fe; nonmagnetic, low-spin ferromagnetic, high-spin ferromagnetic, and collinear and non-collinear antiferromagnetic; have been observed experimentally[107]–[110] and have been calculated using first-principles[111]–[117] to have close lattice parameters and total energies. Figure 1.3 shows the relative phase stability of iron calculated using the FLAPW first-principles code.[118] The paramagnetic state is not readily

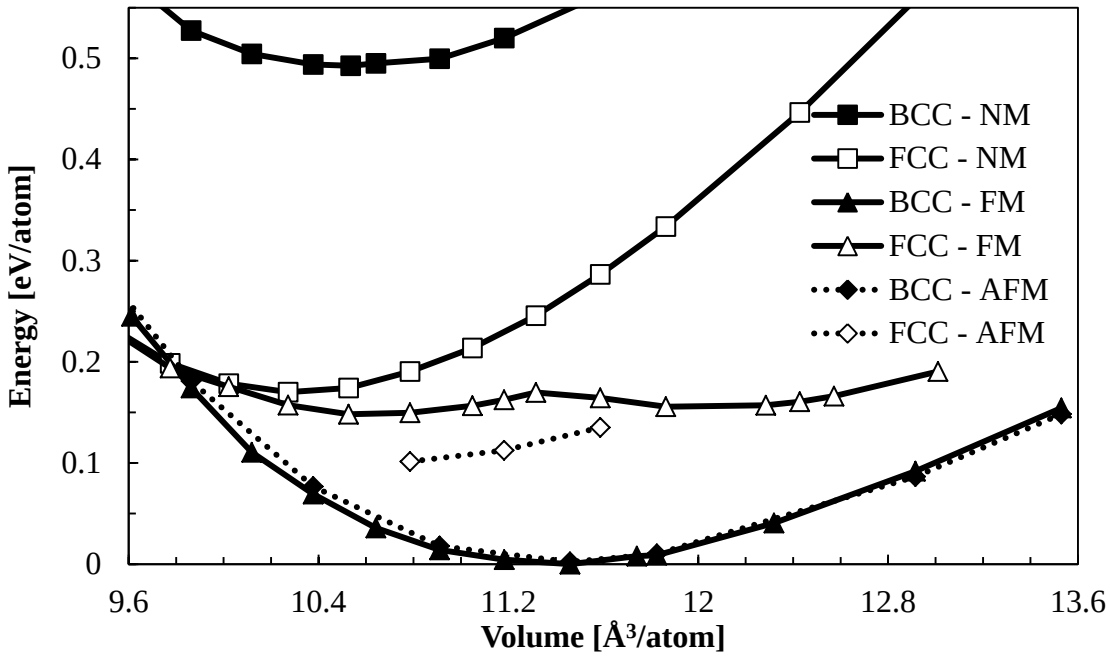

Figure 1.3 Phase Stability of Pure Iron

implemented in current first-principles methods; the increased complexity resulting from the disordered spin-states is impractical at this time.

Previous explicit calculations of stacking fault energy in Fe [98], [101], Fe-N [102], Fe-C [98], [100], Fe-Mn [98] and Fe-Al [98] were non-magnetic. Very close SFE values were obtained for the NM and LS-FM states in Fe and Fe-Mn.[98], [101] The LS-FM state is lower in energy than the HS-FM state and has a lattice parameter closer to those for the AFM states in fcc Fe.[111]–[115] Both NM and LS-FM calculations predict a parabolic dependence of the SFE on Mn concentration in Fe-Mn that is in good agreement with experimental results.[98], [101]

Implicit calculations of stacking fault energy have examined the effect of magnetism and temperature on stacking fault energy.[119], [120] Temperature dependence of stacking fault energy has been studied in the Fe-Mn system as a function

of electronic and magnetic contributions. Magnetic contributions in the paramagnetic Fe-Mn system were shown to shift the relative value of the SFE towards experimental values, although the electronic contribution remained to be the controlling component with regard to changes as a function of temperature.[105] Even so, a recent study has shown that for chemically disordered structures the SFE dependence on composition is strongly changed if paramagnetism is considered instead of a nonmagnetic system.[104]

2. METHODS AND APPROACH

First-principles, or *ab-initio*, methods with no empirical fitting parameters are often used to examine materials at the atomic level. *Ab-initio* quantum mechanical methods such as density functional theory (DFT), Hartree-Fock (HF), Green's Functions (GW), and Quantum Monte Carlo (QMC) are a few of the most common methods. The accessibility of supercomputing resources and parallelization of the first-principles codes have made these calculations more affordable and propelled a growth of atomistic calculations in the materials science community over recent years.[121], [122]

2.1. DENSITY FUNCTIONAL THEORY

Density functional theory (DFT) is one of the most widely used first principles methods for investigating the electronic structure and atomic-level interactions of materials. DFT's popularity is due in part to good scaling of computational expense with the system size as well as the possibility of performing calculations on large complex systems.[123] The fundamental principle of DFT is that any atomistic system can be fully expressed as a functional of its electron density. This electron density can then in principle be used to determine all of the information in the many-body wave-functions; for example the total energy of the system.

The concept of a universal functional, first proposed by Thomas[124] and Fermi[125] in the 1920's, was later proved to exist by Hohenberg and Kohn.[126] The first Hohenberg-Kohn theorem states that there is a one-to-one correspondence between the external potential of an atomisitic system and its ground state electron density. The second Hohenberg-Kohn theorem defines a universal energy functional such that the ground state energy is minimized at the true ground state density. The exact functional for a system of more than one electron is unknown and an approximation is used.

An approximation using exchange-correlation (XC) for the universal ground state functional was made by Kohn and Sham.[127] Their method of mapping the interacting system of electrons onto a non-interacting electron density with the same effective potential is what makes DFT practical and useful. The complicated many-body electron interactions are reduced into an effective potential consisting of the kinetic, Coulombic,

and XC interactions. There is no exact formalism for the XC interactions; therefore approximations are made to make the functional as accurate as possible.

Many approximations to the XC energy exist with the most common being local, gradient dependent, and hybrid functionals. The most widely used approximation is the local-density approximation (LDA) – the first XC functional proposed by Kohn-Sham based on the exact exchange energy for a homogeneous electron gas.[127] LDA has been used for several decades for band-structure and total energy calculations, although it is now known to give less accurate geometries and predicts binding energies too large.[128] The generalized gradient approximation (GGA) has been found to improve the description of total energies, ionization energies, electron affinities of atoms, and atomization energies of molecules and is used in this work.[129], [130] The Vienna Ab-initio Simulation Package[131] (VASP) is used in this work with the generalized gradient approximation (GGA) and PAW-PBE potentials.[129], [132]

In practice, atomistic systems are represented in DFT by positively charged ion cores consisting of the neutrons, protons, and in some cases the non-valence electrons. The Born-Oppenheimer approximation assumes that electrons will instantaneously adjust to changes in the position of the nuclei.[133] The nuclei, considered frozen, are represented by a pseudopotential based on the mass, valence state, and energy of the atomic reference configuration. Full potential calculations make no approximations for the core electrons, resulting in a larger number of electrons considered in the calculation.

2.2. ENERGETICS

Total energy is one of the primary results of DFT calculations. Total energy calculations were shown to be sufficiently accurate and computationally efficient for use in quantum chemical studies of metals and semi-conductors in the mid-1990's after XC functionals and computing algorithms were improved.[123] Energetic values such as total energy, enthalpy of formation, and binding or cohesive energy can be determined from a series of calculations. Enthalpy of formation calculated using the general formula

$$\Delta H^o = \sum nH^o_{f\ products} - \sum mH^o_{f\ reactants} \quad (1)$$

can be computed from the total energy of each bulk component as shown in Equation 2. Similarly the cohesive energy may be calculated using the energy of isolated atoms

instead of the energy of a single atom in a bulk structure as shown in equation 3. There are then two methods, eqn. 2 and eqn. 4, to choose from in calculating the enthalpy of formation depending upon their physical applicability to the problem being modeled.

$$\Delta H^{o}(A_xB_y) = E\left(A_xB_{y_{bulk}}\right) - \left(x \cdot E(A_{bulk}) + y \cdot E(B_{bulk})\right) \quad (2)$$

$$E_{coh}(A_xB_y) = E(A_xB_y) - \left(x \cdot E(A_{iso}) + y \cdot E(B_{iso})\right) \quad (3)$$

$$\Delta H^{o}(A_xB_y) = E_{coh}(A_xB_y) - \left(x \cdot E(A_{coh}) + y \cdot E(B_{coh})\right) \quad (4)$$

In order to reduce error and ensure accuracy when manipulating total energy values, the same pseudopotentials, computational algorithms, and exchange-correlation functional must be used.

First-principles study of point defects in Mg-alloys provided thermodynamic insight concerning metastable phases to aid in alloy development.[134] Defect-formation calculations require the supercells used for the defect-free and defect-containing calculations to be the same size and crystal structure, although the lattice parameter may vary after relaxation of the defect. Defect formation energy is calculable in a similar fashion as shown in Equation 5.

$$\Delta E_f^{defect} = E(A_xB_{y-1}C) - E(A_xB_y) + E(B_{bulk}) - E(C_{bulk}) \quad (5)$$

2.3. STRUCTURAL AND MECHANICAL PROPERTIES

Lattice parameter and ion position optimization is another inherent part of DFT. Crystal structures provided by experimental studies often serve as the initial starting point for first principles calculations. By calculating the directional forces on each ion, ion positions and lattice parameter(s) can be optimized through force relaxation to minimize quantum mechanical strain in the lattice. As the ions shift during the force relaxation, the local bonding arrangement is altered, revealing the optimum – energetically most favorably – ion positioning and bonding at 0K.

Mechanical properties can be calculated using first principles through determining the elastic (stiffness) tensor. Finite distortions of the lattice allow for determination of the

stress-strain relationship and the derivation of the elastic constants through the relationship below.

$$\sigma_i = \sum_{i=1,6} C_{ij}\varepsilon_j \quad (6)$$

A least squares symmetry method[135] can be used to extract the C_{ij} values from ab-initio calculations to reduce the number of simulations required. High symmetry cubic materials require a total of 7 simulations to extract the C_{11}, C_{12}, and C_{44} values, whereas triclinic materials with 21 unique elastic coefficients require a minimum of 13 simulations. The introduction of point defects significantly reduces the symmetry and increases the number of simulations required. Straining the lattice within a simulation can result in extraneous non-physical ionic forces being included in the stress-strain relationship. The ionic Hessian matrix is used to determine and remove the contributions to the elastic constants from the ionic forces. Mechanical properties such as bulk, shear, and elastic moduli are calculated from the elastic tensor. A recent study[45] on the mechanical properties of VC and NbC yielded bulk modulus values that matched closely with experimental ones.

2.4. SURFACES AND INTERFACES

Surface and interface properties, such as chemical adsorption, cleavage energy, surface energy, and interface orientation, are readily calculable within DFT. Chemical adsorption calculations, such as hydrogen adsorption to transition metal surfaces[75], are performed by decreasing the distance of hydrogen ion(s) from the carbide surface and evaluating the resulting energy and electronic structure to indicate the optimum bond structure. To perform cleavage energy calculations, first atoms are arranged in the bulk configuration such that the target cleavage plane is centrally located. Next a separation distance is introduced and gradually increased until there is no interatomic interaction across the separation distance. By examining the stresses as a function of the separation distance, the maximum stress and ideal cleavage energy (γ_s) for fracture can be determined. In addition to calculating bulk cleavage energy, the adhesion of two materials, such as carbide and iron, can be calculated by placing the separation plane at an interface between the two materials.[76] Surface energy may be calculated as shown

in equation 7, where: E_s = surface energy, n = # of layers, E_n = energy per unit cell of the n-layer film, and E_b = bulk energy per unit cell.

$$E_s(n) = \tfrac{1}{2}(E_n - nE_b) \tag{7}$$

Additional surface properties, such as the stacking fault energy and cleavage crack, type can be identified by shearing two parts of a crystal along the desired plane rather than introducing a separation distance. Shearing a close packed plane along a slip direction allows for the calculation of an unstable stacking fault energy (γ_{us}) and the resulting shear stress. The cleavage mode can be distinguished by comparing the energies to cleave through planar separation (γ_s) versus planar slip (γ_{us}) using equation 8.

$$\text{Cleavage-type crack for: } 0.3\,\gamma_s / \gamma_{us} < 1.0 \tag{8}$$

In FCC and HCP materials a generalized stacking fault energy curve can be created. By calculating the change in energy from the undistorted lattice to the sheared lattice the GSFE is generated using equation 9.

$$\text{GSFE}(J/m^2) = 1.6\times10^{-19}(J/eV) \cdot \Delta E(eV) \,/\, S(\text{area}, m^2) \tag{9}$$

The GSFE curve for FCC iron by shearing along the <112> (111) is shown below in Figure 2.1 clearly indicating the unstable and intrinsic stacking fault energies at the 0.5 and 1.0 burgers vector displacement positions respectively.

The explicit calculation of the stacking fault energy described above has been used within this work. Alternatively, implicit methods such as the axial next-nearest neighbor Ising (ANNNI) model may also be used to calculate the stacking fault energy.[103] Following this approach the bulk energy of the fcc, hcp, and dhcp phase at a constant volume are calculated. The SFE is then evaluated as shown in equation 10 below.

$$\text{SFE} = E^{hcp} + 2\,E^{dhcp} - 3\,E^{fcc} \tag{10}$$

The implicit ANNNI approach to calculating stacking fault energy is known to be less accurate as it does not take into account structural relaxations at the stacking fault, but it is computationally more efficient for complex systems.[105]

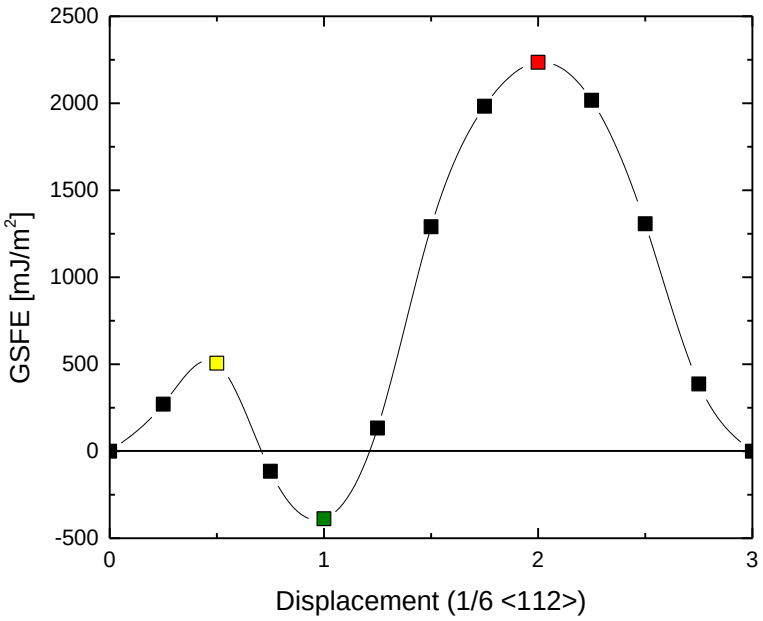

Figure 2.1 Generalized Stacking Fault Energy (GSFE) curve for pure FCC iron where the displacement (burgers vector) is a shift along the <112> direction in the (111) plane. The unstable stacking fault is indicated at 0.5 and the negative intrinsic stacking fault is located at 1.0 displacement.

3. RESEARCH OBJECTIVES AND IMPACT

The objective of this work is to address, at a fundamental level, challenges with innovation in advanced high strength steel alloy design. A first-principles atomistic approach is used to investigate the energetic, structural, and electronic properties of steel alloys for use in the design process. Two of the key components of steel alloy design, carbide formation and stabilization and the ability to control active deformation mechanisms through stacking fault energy, are examined through a series of study objectives outlined below.

- Objective 1: Elucidate the electronic structure level of the stabilizing effect of carbon vacancies on substoichiometric vanadium carbide
    - Hypothesis: Carbon vacancies stabilize vanadium carbide due to a combination of increased local V-C bond strength and increased metallic V-V interaction
- Objective 2: Determine the stability of substoichiometric vanadium carbide with niobium defects
    - Hypothesis: Carbon vacancy ordering in substoichiometic vanadium carbide enables niobium defects to be more easily accommodated than vanadium defects in the near-stoichiometric niobium carbide
- Objective 3: Evaluate the role of carbon vacancies on the surface properties of vanadium carbide and the Fe/VC interface
    - Hypothesis: Carbon vacancies stabilize the Fe/VC interface by relieving interfacial strain due to lattice mismatch
- Objective 4: Identify alloying additions for advanced high strength steel alloy development that may be used to lower the intrinsic and unstable stacking fault energies of fcc Fe
    - Hypothesis: In addition to manganese, other alloying additions may decrease stacking fault energy

- Objective 5: Resolve alloying addition interaction effects on stacking fault energy in FCC iron
    - Hypothesis: Coupling between and local ordering of alloying additions may affect stacking fault energy and the propensity to either form twins or ε-martensite

The results of this work may guide the alloy design decisions made in the steel industry to identify potential alloying alternatives to meet processing and product needs. First-principles methods are utilized in this work to gain fundamental understanding of the processes being studied. First-principles methods, such as density functional theory, allow the changes in alloy chemistry to be systematically examined on the electronic level for impact on material properties.

PAPER

I. THE ROLE OF ORDERED CARBON VACANCIES IN VANADIUM CARBIDE AND (V,NB)C_X – BULK AND SURFACE ENERGETIC AND STRUCTURAL EFFECTS

This paper has been prepared for submission to *Acta Materialia.*

K.R. Limmer[1], N.I. Medvedeva[2], and J.E. Medvedeva[1]

[1]Missouri University of Science and Technology, Rolla, MO 65409, United States

[2]Institute of Solid State Chemistry, Yekaterinburg, Russia

ABSTRACT

The structural and electronic properties of vanadium carbides (VC, V_8C_7, and V_6C_5), niobium carbide, and mixed metal (V, Nb) carbides were examined using ab-initio approach to determine the role of ordered carbon vacancies in phase stability. An increased bond strength observed for both the metal-carbon bonds near carbon vacancy and the metal-metal bonds two coordination spheres away from the vacancy site favors the stability of non-stoichiometric VC_x. Minimal changes in the electronic and structural properties resulted from niobium substitution in vanadium carbide for up to 11 at% Nb. The defect formation energy decreases with increasing Nb concentration and exhibits little dependence on the defect proximity to carbon vacancies. Furthermore, niobium atoms show preference to occupy the topmost positions at the (001) $(V,Nb)C_x$ surface, whereas carbon vacancies reside two or more layers away from the free surface. These distribution trends are expected to affect the nucleation rate and grain size refinement in steels strengthened with VC precipitates.

KEYWORDS

Electronic structure; vanadium carbide; niobium carbide; mixed metal carbide; density functional theory; carbon vacancies

INTRODUCTION

Carbide formation and stabilization in steels is of great interest due to the effect on microstructure and properties of Fe-based alloys. MC carbides are commonly observed in ferrous alloys containing transition metals; notably, in alloys containing strong carbide formers such as Ti, Nb, or V. Nano-sized carbide precipitates may serve as nucleation sites for intragranular ferrite during cooling and govern grain size refinement [1–4].

MC carbides exhibit high flexibility of chemical composition as well as a wide carbon vacancy range denoted by MC_x where x is typically between 0.6 and 1.0 [5–8]. Vanadium carbide, VC_x, has a unique decreased upper homogeneity bound of 0.88 that gives rise to the cubic ordered structure V_8C_7 with space group $P4_332$ which is not observed in other MC carbides [6–16]. A second ordered phase, V_6C_5 has been reported having either a trigonal $P3_1$ [17] or monoclinic C2 or C2/m [18,19] crystal structure. The short-range order of the trigonal and monoclinic V_6C_5 phases is identical; however, the

monoclinic phase has been shown to be marginally more stable and also stable over a wider temperature range [20–24]. The V_8C_7 and V_6C_5 (both trigonal and monoclinic) ordered phases have been observed in V-containing steels [8,19,25–30].

Partial substitution of vanadium with niobium increases the MC carbide volume fraction and improves mechanical properties as shown in experimental studies [31–33]. Having a similar electronic structure, Nb and V are expected to compete in carbide formation. NbC has a higher precipitation temperature than VC allowing NbC to be effective in inhibiting static recrystallization of the austenite through grain pinning [3,4,34]. Precipitated carbides in a Fe-V-Nb-C system initiate as Nb-rich carbides that decompose into NbC and VC_x upon cooling. The VC_x precipitates are thought to contain Nb-defects because of the observed increased lattice parameter, although minimal V-defects were observed within the stable room temperature NbC precipitates [19,26].

An additional insight to the nonmetal/metal stoichiometry and precipitate structure can be gained using carbide surface investigations [35]. The surface energy of transition metal MC carbides was determined to have the relationship E[100] < E[110] < E[111] in a first principles study [36]. Surface calculations of the [100] geometry using FP-LMTO indicated that VC has a lower surface energy than NbC [37]. Vacancy concentration profiles at VC and NbC surfaces have not been studied. In a Compton scattering study Deb [38] hypothesized that NbCx attempts to approach stoichiometry in the bulk by creating carbon vacancies at the crystal surface from carbon atoms diffusing from the surface to the bulk.

In this work, the structural, cohesive, and electronic properties of VC, V_8C_7, V_6C_5 and $(V,Nb)C_x$ are calculated to determine the stabilization mechanisms of the non-stoichiometric carbides. Transition metal carbides, nitrides, and oxides are commonly assumed to form metal-metal bonds in the presence of carbon vacancies [7]. Zhukov discussed the vacancy formation as a two-part process which undergoes destabilization, breaking M-C bonds, and stabilization through strengthening M-M bonds [39]. In the case of titanium and vanadium carbides, however, the strengthening from metal-metal bonds is not sufficient to compensate for the energy required to break the M-C bonds. VC has been shown to have the strongest M-C bonds of the 3d-transition metal carbides [40].

Rogovoi proposed that both VC_x and NbC_x have increased M-C bond strength in the presence of carbon vacancies [41]. Distorted octahedral have been experimentally observed in V_8C_7 and Nb_6C_5 indicating increased M-C bond strength as the metallic atoms shift away from carbon vacancies [42–44]. Another study showed that as stoichiometry is approached in NbC_x, Nb-C bonds are strengthened and Nb-Nb bonds are weakened [45]. One of the objectives of this work is to compare the structural relaxation, charge density redistribution, as well as metal-metal, metal-carbon, and carbon-carbon bonding associated with the presence of ordered carbon vacancies to better understand the role of carbon vacancies in the carbide stability. Furthermore, the effect of the carbon vacancy and niobium defect on the surface energy and cleavage properties of VC is examined to shed light on the structure of carbide precipitates.

CARBIDE STRUCTURE

In the MC rock salt structure, each atom is octahedrally coordinated by the opposite atomic species providing equidistant spacing and 90^o bond angles. Below, we describe the key structural features of the two ordered phases, M_8C_7 and M_6C_5, considered in this study.

First, for the short- and long-range ordering of metallic atoms in the ordered carbide structures, the following notation was introduced: $M^{(6)}$ stands for the atom that is fully coordinated by six C-atoms, and $M^{(5x)}$ is coordinated by five C-atoms and one carbon vacancy, V_C. The letter x designation in the latter is based on the long range ordering associated with the accompanying V_C. Metallic atoms bonded into an alternating sequence of C and V_C in a given direction on the carbon sublattice, are denoted as $M^{(5A)}$. In the orthogonal directions the number of C atoms in between consecutive V_C increases. $M^{(5b)}$ is used to denote a metallic atom bonded into a sequence containing 3 C-atoms in between V_C; and $M^{(5c)}$ is used for 5 or more C-atoms in between V_C. As shown below, the structural and electronic structure properties for $M^{(5b)}$ and $M^{(5c)}$ are not statistically different; therefore, the two are combined in the discussion of the results and are denoted as $M^{(5B)}$.

The cubic M_8C_7 structure, space group $P4_332$, contains ordered carbon vacancies (V_C) such that ¼ of the M-sites retain full six C-coordination, $M^{(6)}$, with the remaining ¾

of the M-sites being coordinated by five C-atoms and one V_C, i.e., $M^{(5A)}$. The vacancy ordering in M_8C_7 results in alternating carbon atoms and vacancies in the carbon-sublattice along each of the main crystallographic directions.

Experimental studies of the M_6C_5 carbides within steels are inconclusive with regard to the long-range order (monoclinic or trigonal) in this phase, as discussed in the introduction. Both the trigonal ($P3_112$) and monoclinic (C2/m) unit cells were examined in this study. The short-range order of the two cells is identical with all of the metal atoms coordinated by five C-atoms and one V_C. Both cells contain metallic atoms of type $M^{(5A)}$ and $M^{(5c)}$; whereas $M^{(5b)}$ appears only in the trigonal cell.

The effect of the point defect placement in the long range linear vacancy-ordering schemes are characterized in the first part of this work and their impact on the formation of mixed vanadium-niobium carbides is subsequently examined.

METHODOLOGY

An ab-initio approach is employed in this study in order to understand the role of the carbon vacancies and niobium defects on the structural and electronic properties of vanadium carbide. The Vienna Ab-initio Simulation Package[46] (VASP) is used with the generalized gradient approximation (GGA).[47] PAW-PBE potentials[48] for vanadium ($3p^6\ 3d^3\ 4s^2$), niobium ($4p^6\ 4d^3\ 5s^2$), carbon ($2s^2\ 2p^2$) are used to give 11- and 4-electron valence states for the metals and carbon respectively. Non-magnetic self-consistent calculations were performed for ideal rock-salt VC and experimentally observed crystal structures V_8C_7 (cubic) and V_6C_5 (trigonal) as reported in the Inorganic Crystal Structure Database [49]. Self-consistent electronic structure calculations were all performed to an energetic convergence criterion of $1x10^{-4}$ eV. All structural calculations utilized a cut-off energy of 342.4 eV. The Γ centered k-point mesh had a minimum of 35 irreducible k-points for all final energy calculations. Structures were optimized using energy-force minimization with the convergence of $1x10^{-3}$ eV/Å. This optimization was used to determine the relaxed lattice constants and atomic positions in vacancy-free VC and in ordered carbon vacancy phases, V_8C_7 and V_6C_5.

To identify phase stability, the enthalpy of formation is calculated according to the following equation:

$$\Delta H_f (M_xC_y) = E (M_xC_y) - x * E (M_{bulk}) - y * E (C_{bulk\ graphite}) \quad (1)$$

Defect formation energy calculations were utilized in the second part of the study to determine niobium solubility in V_xC_y, as shown in equation 2 below. The calculation parameters including the k-point mesh, were kept constant for both the defect-free and the defect-containing structures to ensure accuracy.

$$E_{defect} = E (V_{x-1}NbC_y) - E (V_xC_y) - E (Nb_{bulk}) + E (V_{bulk}) \quad (2)$$

The (001) VC surface was modeled by a slab consisting of nine layers with two V and two C atoms in every layer. Convergence of the surface energy with respect to slab thickness for stoichiometric (001) VC has been previously studied and it was shown that slab with five layers is sufficient to predict the surface energies and relaxations [50]. In order to avoid the interaction between periodically repeating slabs, we used a vacuum of 15 Å thickness and estimated the surface energy as an energy required to cleave the VC bulk along the (001) plane. We used the theoretical lattice constant of bulk VC as the fixed in-plane lattice constant of the VC slab; during the structural relaxation, the atoms were allowed to move only in the out of plane direction. To find the favorable distribution of vacancies and niobium at surface, we performed calculations for carbon vacancy or substitutional Nb atom placed in the topmost, first or second subsurface layers. For all surface calculations, we used a 8x8x2 *k*-point mesh and all atoms were relaxed to a force minimum of 0.05 eV/Å.

RESULTS & DISCUSSION

Carbon Vacancies

Total energy calculations were performed to examine phase stability of ordered vanadium and niobium carbide structures. The enthalpy of formation, ΔH_f, was calculated as described in the methods section above on a per M-atom basis for comparison convenience and are shown in Figure 1. The ΔH_f of VC, -0.86eV, is independent of super cell scaling (2, 18, and 64 atoms) and is less negative than that of both the V_8C_7 and the V_6C_5, -1.02eV and -1.03eV respectively, indicating comparative stability. The results obtained in this study correspond well with the experimental values for V_8C_7 and V_6C_5 [51]. Ozolins' first-principles results [52] are lower for all three compounds, though the energy trend for the ordered vacancy compounds, namely, V_8C_7

being slightly less negative than V_6C_5, is captured. The niobium carbides have a lower ΔH_f than VC_x for each relative structure with NbC being less negative than Nb_6C_5, -0.96eV and -1.04eV respectively. The ΔH_f results confirm that ordered carbon vacancies stabilize both vanadium and niobium MC_x carbides, although the effect is more pronounced in the vanadium system as seen in Figure 1.

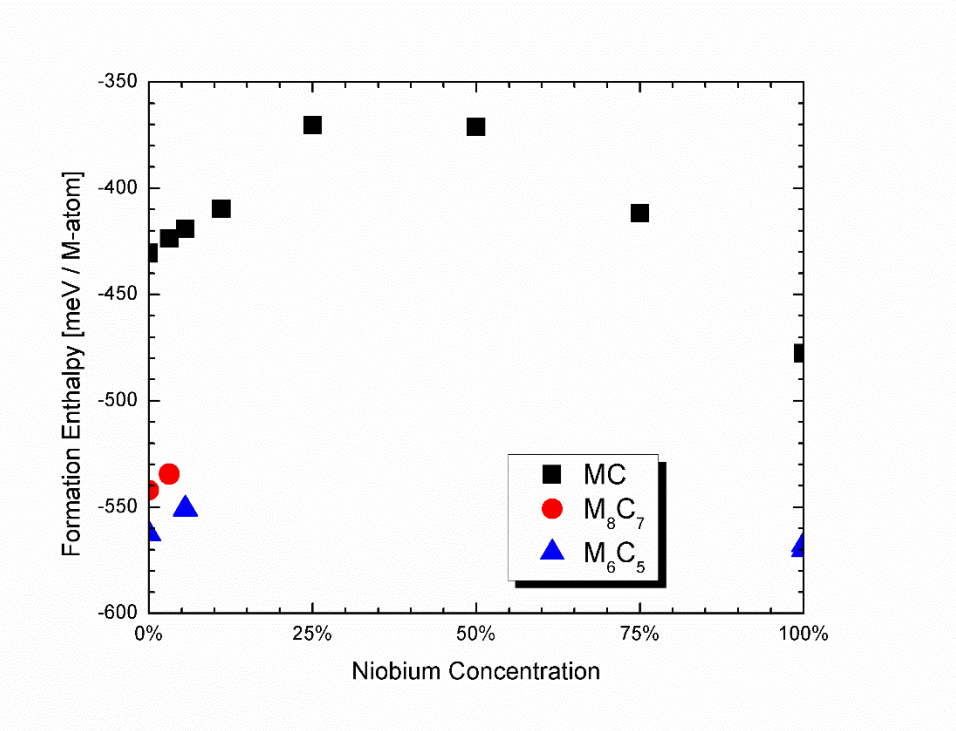

Figure 1. The calculated formation energy of mixed vanadium and niobium carbides.

The role of ordered carbon vacancy in stabilizing the MC_x, M_8C_7, and M_6C_5 structures is examined first through the structural properties. The introduction of V_C significantly reduces the M-C bond length for the $M^{(5x)}$ bond to the carbon atom opposite of the carbon vacancy in both VC_x and NbC_x as shown in Figure 2. M-C bonds associated with $M^{(6)}$ and $M^{(5x)}$ (not opposite to a vacancy) are relatively consistent at 2.08Å and 2.25Å ±0.05Å for VC_x and NbC_x across all unit cells. When the M-C bond is oriented opposite a carbon vacancy the M-C bond length is reduced to 1.92Å and 1.97Å ±0.03Å for $V^{(5A)}$ and $V^{(5B)}$, 2.11Å and 2.15Å ±0.02Å for $Nb^{(5A)}$ and $Nb^{(5B)}$ respectively. Consistent with the shortened M-C bonds, the bond angles are also affected near carbon vacancies. $M^{(5x)}$-C-$M^{(5x)}$ bond angles encircling a carbon vacancy increased from 90° to 99.5°±1.5° and 97.5°±1.0° for VC_x and NbC_x. The bond length and angle changes are more pronounced for the $M^{(5A)}$ sites and in particular in the M_8C_7 structure with all $M^{(5x)}$ sites in the $M^{(5A)}$ class. Following the M-C length trends, M-C/V_C-M distances mirror the

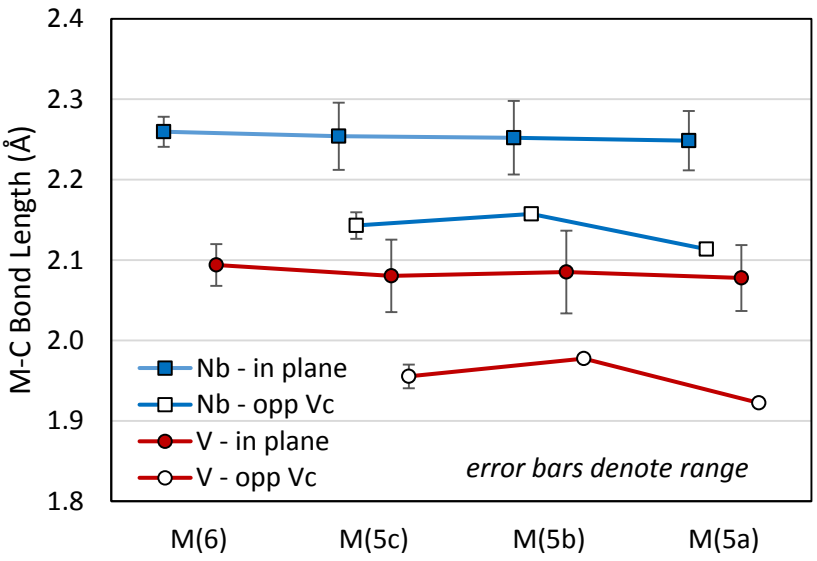

Figure 2. M-C bond length in MC_x, M_8C_7, and M_6C_5 as a function of M-atom site and bond orientation to V_C.

patterns observed in the M-C bonds with M-Vc-M > M-C-M > M-$C_{opposite\ Vc}$-M. Additionally, M-M bonds are lengthened around carbon vacancies from 2.94Å to 3.14Å in VC_x and 3.19Å to 3.36Å in NbC_x. Next nearest M-M bond lengths are unaffected, whereas the second nearest M-M bond lengths are significantly shortened, to 2.85Å and 3.11Å for VC_x and NbC_x, respectively. This decrease in the M-M bond length suggests a strengthened M-M bond two layers from carbon vacancies – in addition to the stronger M-C bonds near the carbon vacancy. Interestingly, nonmetal vacancies in VN have been shown to have the opposite effect; creation of a N vacancy leads to strong V-V bonding and the V-N bonds are weakened near the nonmetal vacancy [53].

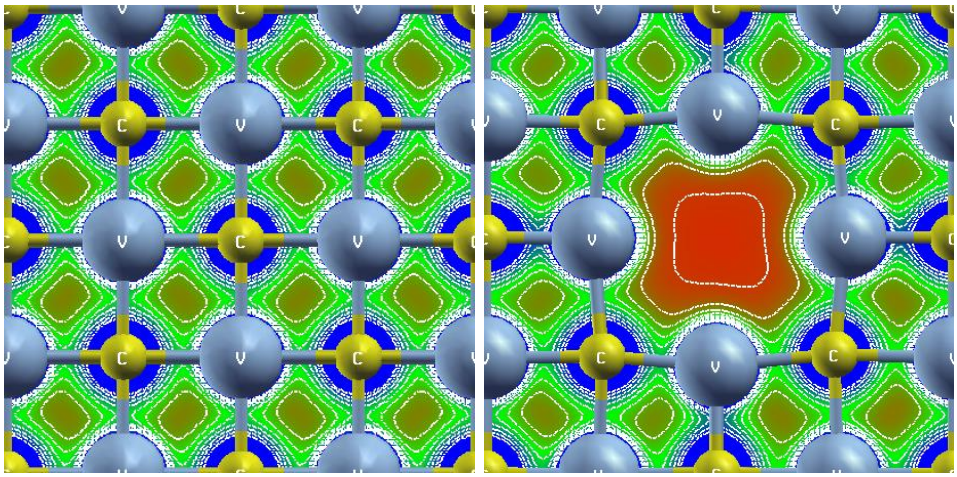

Figure 3. Charge density plot of VC bulk (left) and V8C7 (right) indicate stronger V-C bonding in directions opposite of the carbon vacancy and an electron deficit in the vacancy site. Vanadium atoms near carbon vacancy are visibly shifting away from carbon vacancy.

Next, the local electronic structure was examined to understand the changes in bonding near carbon vacancies. Calculated charge density plots of stoichiometric VC and V_8C_7 are shown in Figure 3. Without carbon vacancies, the electron density is symmetric with V–C bonds having an electron density of 0.57 electrons/$Å^3$. In the V_8C_7 structure, the 6-coordinated vanadium atoms have the same symmetric charge density as in VC, whereas the 5-coordinated vanadium atoms have an increased charge density (0.79 electrons/$Å^3$) in the direction opposite the carbon vacancy with less substantial changes in the V-C bonding perpendicular to the carbon vacancy (0.48-0.61 electrons/$Å^3$).

Since the strong covalent M-C bonding may effectively screen the secondary metallic bonding effects, empty sublattice calculations were performed. Particularly, the strength of the metal-metal bonds in V-only sublattices having VC_x or V8C7 fully-relaxed structure is compared to that in the VC structure. The empty C-sublattice results indicate that V-V bonds have a charge density of 0.20 electrons/ $Å^3$ in a stoichiometric VC structure. The presence of "carbon vacancy" (as in VC_x or V8C7 structure) results in a decrease in the V-V charge density around the vacancy to 0.15 electrons/$Å^3$ as shown in Figure 4. A slight increase, to 0.21 electrons/$Å^3$, in the charge density in the nearest neighbors moving away from the carbon vacancy is indicative of strengthening V-V metallic bonds. The energetic contributions from different bonds were also determined from the empty sublattice calculations and are shown in Table 1. Energetic contributions from same species interactions are given by the total energy of the empty sublattice calculations, and the V-C interactions are obtained by subtracting the energy of the two empty sublattice calculations (i.e, V or C sublattice) from the full system calculation. As the number of "carbon vacancies" in the sublattice increases, the contribution of the V-V interaction also increases. The contribution to the total energy from the V-C bonding remains relatively constant implying an increase in the contribution from each V-C bond.

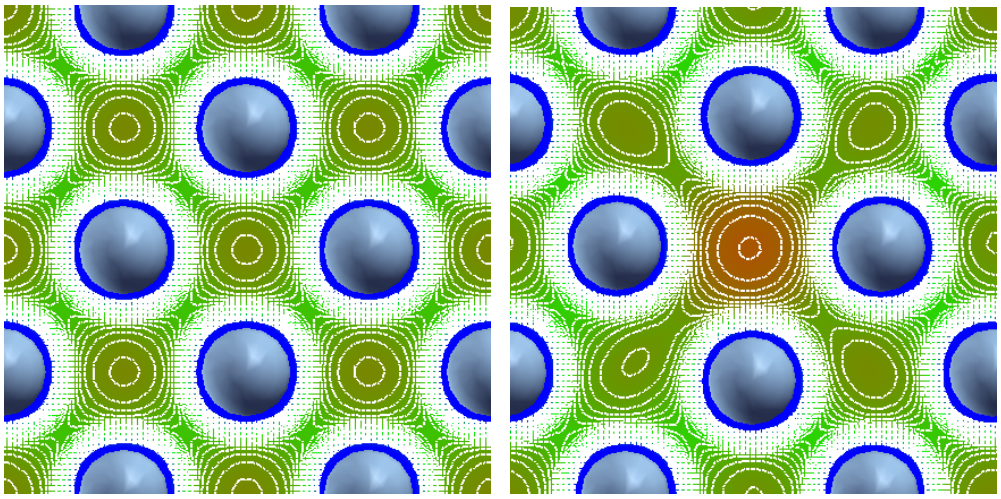

Figure 4. Charge density plot of empty sublattice calculations containing only V atoms for VC (left) and V8C7 (right) indicating a strengthening of V-V bonds two coordination spheres away from carbon vacancies.

Table 1. Energetic contributions from metal-metal, carbon-carbon or metal-carbon interactions towards the total energy as a function of carbon vacancy content. The results are based on empty sublattice calculations.

	M-M interaction	**C-C interaction**	**M-C interaction**
VC	43.6%	15.9%	40.5%
$VC_{0.97}$	44.2%	15.5%	40.3%
V_8C_7	45.9%	13.9%	40.3%
V_6C_5	46.9%	13.3%	39.8%
NbC	46.7%	11.9%	41.3%
$NbC_{0.97}$	47.4%	11.6%	41.0%

The partial density of states for the vanadium atoms, Figure 5, does not reveal any significant differences for vanadium atoms $V^{(6)}$ and $V^{(5a)}$. Evaluating the electronic charge involved in bonding, up to the Fermi level, does show a charge redistribution with more charge for the $V^{(6)}$ sites than $V^{(5)}$ sites, as expected.

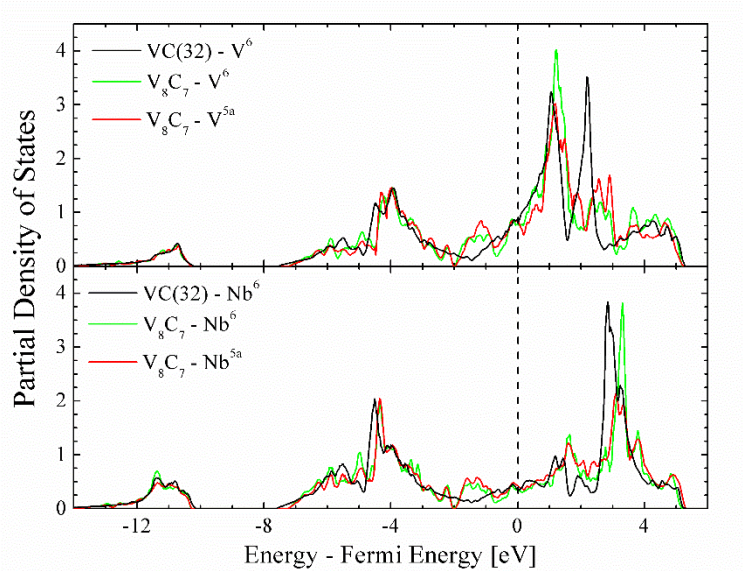

Figure 5. Partial density of states of metal ions in vanadium carbide as a function of coordination.

Mixed Metal Carbide: Nb Substitution

Solubility of substitutional Nb in the metal sublattice was examined in MC_x as well as within the ordered structures M_8C_7 and M_6C_5. Structures were fully optimized to find the equilibrium formation energy, lattice constants, and atomic positions.

The mixed metal carbide formation energy shown in Figure 1 supports phase instability in the VC-NbC system at 0K, in agreement with experimental results of a miscibility gap at low temperatures and a complete solid solution between VC – NbC at high temperatures near the solidus temperatures of the carbides. The formation energy of NbC is determined to be -478 meV/M-atom which is about 48 meV/M-atom lower than the formation energy of VC. Niobium substitution of up to 25% increases the formation energy of VC indicating a miscibility gap that spans the field. The maximum energy, 140 meV between 25-50% Nb, corresponds to a temperature of 1625K. In the mid-1980's a pseudobinary diagram [54] was calculated for the $VC_{0.88}$-NbC system using experimental results [55] showing a miscibility gap spanning the diagram, with a maximum located at 42.1% NbC at 1773K. The expulsion of vanadium from a Nb-rich carbide upon reaching the miscibility gap is indicated in both this study and the CalPhad pseudobinary.

The total energy values before and after the optimization of Nb-substitution in VC_x structures were compared to determine the amount of relaxation that occurs while stabilizing the impurity. Before the structural optimization, the defect formation energy was primarily a function of the site coordination with $M^{(5)}$ sites having a higher energy than $M^{(6)}$ sites, as shown in Table 2. After full lattice and atomic relaxation, the defect formation energy was reduced, and the site coordination no longer has a significant effect, with a defect formation energy difference of ±30meV. The niobium concentration, however, has an effect on the defect formation energy as shown in Table 2, with increased niobium concentration having moderately lower defect formation energy. The inclusion of Nb in V_6C_5 is probable at high temperatures due to the low Nb-defect formation energy within the ordered structure.

The volume increased linearly as a function of niobium content from 18.0 $Å^3$/M-atom for pure VC to 22.9$Å^3$/M-atom in NbC. Carbon vacancies had a negligible effect (less than 1%) on the volume. As may be expected, the Nb-C bond lengths for Nb-defects in the VC system are between those of pure VC and NbC; Nb-C bonds opposite the carbon vacancy are 2.06 ±0.01Å and other Nb-C bonds are 2.16 ±0.02Å. At low Nb-concentrations, the Nb-C-V bond angles around carbon vacancies were found to be 93.5^o $\pm 1.0^o$, significantly closer to the ideal 90^o than those obtained for the V-C-V bond angles

in the pure ordered structures. This shift in bond angles at low Nb-concentrations indicates stronger directional Nb-C bonding.

The metallic substitutions had no substantial impact on the charge density as may be expected due to V and Nb having similar electronic configuration. Niobium additions increased charge density in the M-C bond directions (0.61 vs 0.57 electrons/Å^3). In the 5-coordinated site opposite the carbon vacancy both V-C and Nb-C increase to 0.79 electrons/Å^3. In the planar directions V-C bonds are 0.48-0.61 electrons/Å^3 whereas the Nb defect in the same site results in Nb-C bonds of 0.57-0.66 electrons/Å^3 indicating more symmetric bonding around Nb defects in VC_x.

Table 2. Calculated defect formation energy of niobium impurity in vanadium carbides

Structure	Nb Concentration	Defect Site	Unrelaxed Energy [meV]	Optimized Energy [meV]
VC(32)	3.1%	$V^{(6)}$	902	446
VC(18)	5.6%	$V^{(6)}$	900	405
VC(9)	11.1%	$V^{(6)}$	916	380
V_8C_7	3.1%	$V^{(6)}$	817	442
	3.1%	$V^{(5a)}$	973	469
V_6C_5	5.6%	$V^{(5b)}$	981	382
	5.6%	$V^{(5c)}$	953	375
	5.6%	$V^{(5d)}$	978	392

Carbon Vacancy and Nb Substitution at (001)VC Surface

In this Section we consider how the carbon and niobium atoms are distributed near the (001) VC surface and what is their effect on the surface energy. First, we calculated the surface energy of stoichiometric (001)VC surface to be 1.22 J/m^2, that is in a good agreement with the previous theoretical calculations (1.27 J/m^2) [50]. The relaxation is confined to the two topmost layers and has a rumpling type, where the

surface carbon and vanadium atoms are shifted outwards by 0.07 Å and inwards by 0.11 Å (Figure 6a), respectively. The rippling effect (the axial distance between the vanadium and carbon atoms which belong to the same plane) decreases from 0.18 Å to 0.05 Å going from the surface layer to the first sublayer and it is absent for the second subsurface layer. The distance between the surface vanadium and the nearest carbon in the 1st subsurface layer decreases to 1.93 Å, whereas the distance between the surface carbon and the nearest vanadium in subsurface layer increases to 2.15 Å. As a result, we obtained a 4.8% contraction of the first interplanar spacing of vanadium sublattice, whereas the carbon sublattice slightly expands by about 1% near surface. This relaxed geometry agree with the previously obtained results on the (001)VC surface [50], where the average first interlayer spacing was found to contract by 1.4% and the rippling distance for the V and C atoms which relax inward and outward, respectively, is 0.18 Å.

Next, the distribution of carbon vacancies near the (001) surface is examined. Carbon vacancy in the topmost surface layer enhances the rippling distance between the surface carbon and vanadium atoms by up to 0.32 Å, owing to their increased rumpling with outward and inward shifts of 0.18 Å and 0.14 Å, respectively, Figure 6(b). In the first subsurface layer, all carbon atoms are almost within plane, but a large rippling effect (0.08 Å) exists for vanadium atoms. Due to the vanadium buckling, the average first interplanar V-V spacing decreases by only 2%, whereas the first interplanar C-C distance increases by 7%. Thus, the average first interplanar spacing of the C sublattice should be expanded when carbon vacancies are present at the surface.

For carbon vacancy in the first sublayer, Figure 6(c), there is a rippling relaxation for the vanadium atoms on the surface (0.04 Å) and in the second sublayer (0.12 Å). The topmost C and V atoms move outward and inward by 0.05 Å and 0.15 Å, respectively, (rumpling distance is 0.20 Å). The average first interplanar spacing reduces by 5% for V sublattice and increases by 2% for C sublattice.

When carbon vacancy is in the second subsurface layer (Figure 6d), the surface vanadium atoms shift inward by 0.14 Å, but there is a rippling for vanadium atoms in the first and third layers by about 0.13 Å, as well as for the two surface carbon atoms, which

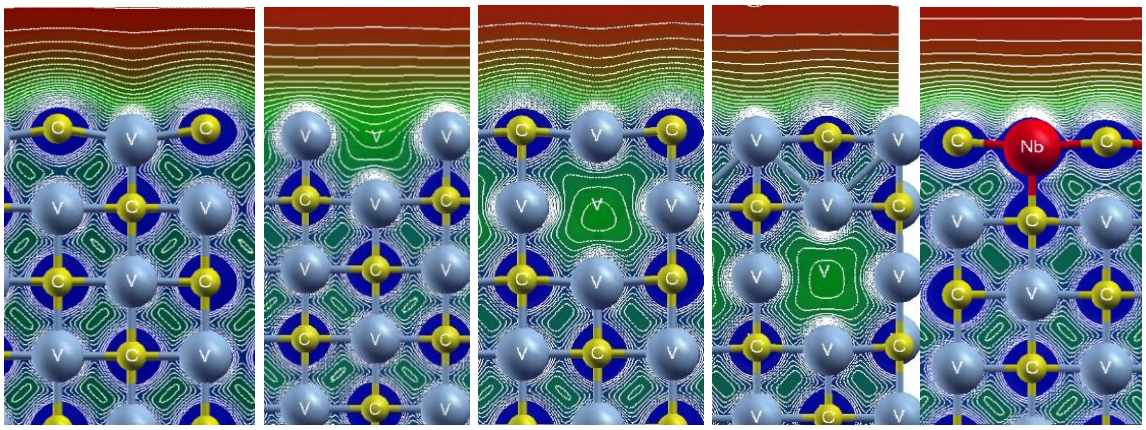

(a) **(b)** **(c)** **(d)** **(e)**

Figure 6. Charge density map for the (001) surface for (a) stoichiometric VC; for the carbon vacancy in the topmost (b), first (c) and second (d) sublayer of VC_x; and (e) for the Nb substitution in the topmost surface layer of (V,Nb)C.

move in plane and in opposite directions by 0.07 Å and 0.04 Å, respectively. As a result, the average first interplanar spacing is contracted by 5% for V sublattice and expanded by 1% for C sublattice, as it was obtained for the stoichiometric surface.

By comparing the total energies of the configurations with carbon vacancy at the surface and in the first and second surface layers, a strong preference of carbon vacancies to be two or more layers away from the surface is found. Once the carbon vacancy reaches the second sublayer, all neighboring vanadium atoms become 5-coordinated with carbon atoms, allowing the vanadium atom above the carbon vacancy to form a bond in the direction opposing the vacancy. Carbon vacancies at the surface and within the first sublayer do not provide this structure (surface vanadium atom has three and four nearest carbon neighbors, respectively). The energy gain for carbon vacancy to be in the first and second subsurface layers in comparison with the surface position are 0.29 and 0.48 eV. The dependence of surface energy on the depth of carbon vacancy (Figure 7) shows that

the surface energy would increase by 0.4 J/m^2 if carbon vacancy were in the topmost layer.

Our theoretical results are in accord with the photo-emission study of (100)$VC_{0.80}$, where a strong 1s core level signal from the surface C atoms was observed. In the experiment on the low-energy electron diffraction on (001)$VC_{0.80}$ [56], the two structural models with the different carbon concentration on surface were considered to explain the results. The authors predict a high carbon concentration on surface (0.4 ± 0.2) and surface rippling with the C subplane being higher than the V subplane.

In marked contrast to carbon vacancy, the niobium substitutional atom prefers to reside at the carbide surface, with an energy gain of 0.26 eV as compared to Nb in the first sublayer. The outward relaxation of niobium is much smaller (<0.02 A) than that of vanadium (0.11 Å), and the average first interplanar spacing demonstrates a contraction

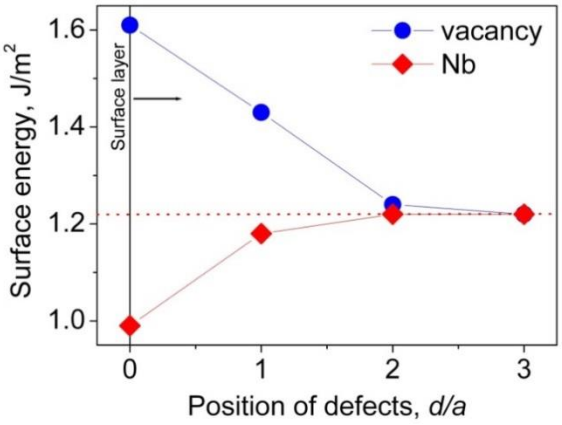

Figure 7. Surface energy as a function of distance to surface in VC indicates a preference for niobium to be at the surface whereas carbon vacancies strongly prefer to be at least 2-layers away from the carbide surface.

by 3.4 % in the metal sublattice and a small expansion (<1%) of the C surface layers. The rippling effect reduces with niobium substituted at the surface (Figure 7e).

CONCLUSIONS

The presence of ordered vacancies was shown to stabilize vanadium carbide. Strengthened metal-carbon covalent bonds were observed near carbon vacancies along with nearest neighbor metal-metal bond strength increasing with moving away from carbon vacancy sites. Carbon vacancies prefer to exist within the bulk of the carbide further stabilizing the non-stoichiometric VC_x. The formation of niobium defects within vanadium carbide was confirmed by examining the defect formation energy. The defect formation in optimized structures is relatively consistent across vanadium carbide structures, with concentration playing a more important role than carbon vacancy existence. Furthermore, the niobium defect is not expected to have significant impact on the structural properties of the vanadium carbide due to its minor structural effects (increased volume and M-C bond lengths) and minimal effect on the electronic structure (charge density and density of states). Niobium defects were shown to prefer substitutional sites at or near carbide surfaces and decrease the cleavage energy when on the cleavage plane.

ACKNOWLEDGEMENTS

This work was funded by a US Department of Education Graduate Assistance in Areas of National Need (GAANN) grant to Krista Limmer through the Department of Materials Science at Missouri University of Science and Technology under contract P200A0900048. The authors gratefully acknowledge David Van Aken for his practical guidance and motivation for this work.

REFERENCES

[1] G. Miyamoto, R. Hori, B. Poorganji, T. Furuhara, ISIJ Int. 51 (2011) 1733.

[2] D.A. Reyes, M. Perez, S. Pecoraro, A. Vincent, T. Epicier, P. Dierickx, 500-501 (2005) 695.

[3] M. Gómez, S.F. Medina, Int. J. Mater. Res. 102 (2011) 1197.

[4] H. Najafi, J. Rassizadehghani, S. Asgari, Mater. Sci. Eng. A 486 (2008) 1.

[5] B. Hutchinson, N. Ridley, Scr. Mater. 55 (2006) 299.

[6] A.I. Gusev, A.A. Rempel, A.J. Magerl, A.A.Rempel, Disorder and Order in Strongly Nonstoichiometric Compounds: Transition Metal Carbides, Nitrides, and Oxides, Springer, New York, 2001.

[7] A.A. Rempel, Physics-Uspekhi 39 (1996) 31.

[8] V.N. Lipatnikov, A.I. Gusev, P. Ettmeier, W. Lengauer, Phys. Solid State 41 (1999) 474.

[9] C.H. De Novion, R. Lorenzelli, P. Costa, Compt. Rend. Acad. Sci. Paris 263 (1966) 775.

[10] C. Froidevaux, D. Rossier, J. Phys. Chem. Solids 28 (1967) 1197.

[11] S.I. Alyamovskii, P. V Gel'd, I.I. Matvcenko, J. Struct. Chem. 2 (1961) 412.

[12] A.W. Henfrey, B.E.F. Fender, Acta Crystallogr. Sect. B 26 (1970) 1882.

[13] M.H. Lewis, J. Billingham, P.S. Bell, Electron Microscopy and Structure of Materials, University of California Press, Berkeley, CA, n.d.

[14] A.I. Gusev, A.A. Rempel, Phys. Status Solidi 93 (1986) 71.

[15] V.N. Lipatnikov, Russ. Chem. Rev. 74 (2005) 697.

[16] R.G. Avatbé, Powder Metall. Met. Ceram. 4 (1965) 122.

[17] J.D. Venables, D. Kahn, R.G. Lye, Philos. Mag. 18 (1968) 177.

[18] J. Billingham, P.S. Bell, M.H. Lewis, Philos. Mag. 25 (1972) 661.

[19] R. Kesri, S. Hamar-Thibault, Acta Metall. 36 (1988) 149.

[20] A.A. Rempel, A.I. Gusev, Phys. Status Solidi 160 (1990) 389.

[21] W.Y. Wang, S.L. Shang, Y. Wang, Z.-G. Mei, K.A. Darling, L.J. Kecskes, S.N. Mathaudhu, X.D. Hui, Z.-K. Liu, Mater. Res. Lett. 2 (2013) 29.

[22] B.-J. Lee, D.N. Lee, L. Byeong-Joo, L. Dong Nyung, Calphad 15 (1991) 283.

[23] T. Epicier, M.G. Blanchin, P. Ferret, G. Fuchs, Philos. Mag. A 59 (1989) 885.

[24] A.I. Gusev, A.A. Rempel, J. Phys. C Solid State Phys. 20 (1987) 5011.

[25] R. Kesri, M. Duran-Charre, Mater. Sci. Technol. 4 (1988) 692.

[26] L. Adnane, R. Kesri, S. Hamar-Thibault, J. Alloys Compd. 178 (1992) 71.

[27] T. Epicier, D. Acevedo, M. Perez, Philos. Mag. 88 (2008) 31.

[28] Y. Oba, S. Koppoju, M. Ohnuma, T. Murakami, H. Hatano, K. Sasakawa, A. Kitahara, J.I. Suzuki, ISIJ Int. 51 (2011) 1852.

[29] G.H. Emmons, W.S. Williams, J. Mater. Sci. 18 (1983) 2589.

[30] G.L. Dunlop, D.A. Porter, Scand. J. Metall. 6 (1977) 19.

[31] H. Chi, D. Ma, J. Liu, Z. Chen, Q. Yong, (2010).

[32] J.-H. Ahn, Y.-J. Kim, S. Lee, H. Chung, Zeitschrift Für Met. 96 (2005) 1426.

[33] S. Kheirandish, ISIJ Int. 41 (2001) 1502.

[34] H. Guanghi, C. Niansun, HSLA Steels: Processing, Properties and Applications, The Minerals, Metals & Materials Society, Warrendale, n.d.

[35] J.G. Chen, B.D. DeVries, B. Fruhberger, C.M. Kim, Z. Liu, x, M, J. Vac. Sci. Technol. A Vacuum, Surfaces, Film. 13 (1995) 1600.

[36] W. Liu, X. Liu, W.T. Zheng, Q. Jiang, Surf. Sci. 600 (2006) 257.

[37] H.W. Hugosson, O. Eriksson, U. Jansson, A. V Ruban, P. Souvatzis, I.A. Abrikosov, Surf. Sci. 557 (2004) 243.

[38] A. Deb, A.K. Chatterjee, Radiat. Phys. Chem. 57 (2000) 135.

[39] V.P. Zhukov, V.A. Gubanov, O. Jepsen, N.E. Christensen, O.K. Andersen, J. Phys. Chem. Solids 49 (1988) 841.

[40] Y. Zhang, J. Li, L. Zhou, S. Xiang, Solid State Commun. 121 (2002) 411.

[41] Y.I. Rogovoi, Powder Metall. Met. Ceram. 38 (1999) 44.

[42] J.P. Landesman, A.N. Christensen, C.H. de Novion, N. Lorenzelli, P. Convert, J. Phys. C Solid State Phys. 18 (1985) 809.

[43] C.H. De Novion, J.P. Landesman, Pure Appl. Chem. 57 (1985) 1391.

[44] D. Rafaja, W. Lengauer, P. Ettmayer, V.. N. Lipatnikov, J. Alloys Compd. 269 (1998) 60.

[45] A. Deb, A.K. Chatterjee, Phys. Rev. B 53 (1996) 13393.

[46] G. Kresse, J. Furthmüller, Phys. Rev. B - Condens. Matter Mater. Phys. 54 (1996) 11169.

[47] J.P. Perdew, J.A. Chevary, S.H. Vosko, K.A. Jackson, M.R. Pederson, D.J. Singh, C. Fiolhais, Phys. Rev. B 46 (1992) 6671.

[48] J.P. Perdew, K. Burke, M. Ernzerhof, Phys. Rev. Lett. 77 (1996) 3865.

[49] F.I.Z. Karlsruhe, (n.d.).

[50] D.J. Siegel, L.G. Hector Jr, J.B. Adams, Acta Mater. 50 (2002) 619.

[51] N.M. Volkova, P. V. Gel'd, Izv. Vyss. Ucheb. Zaved., Tsvet Met. 89 (1963) 23.

[52] V. Ozolins, J. Häglund, Phys. Rev. B 48 (1993) 5069.

[53] Ľ. Benco, J. Solid State Chem. 111 (1994) 440.

[54] A.A. Rempel, A.I. Gusev, G.P. Shveikin, Russ. J. Phys. Chem.(Engl. Transl.) 58 (1984) 1322.

[55] R. Kieffer, H. Nowotny, A. Neckel, P. Ettmayer, L. Usner, Monatshefte Für Chemie 99 (1968) 1020.

[56] J. Rundgren, Y. Gauthier, L.I. Johansson, Surf. Sci. 389 (1997) 251.

[57] O. Kubashevski, A. Evans, C.B. Alcock, Metallurgical Thermochemistry, Pergamon Press, New York, 1958.

II. EFFECT OF NICKEL, COPPER, AND CHROMIUM ON STACKING FAULT ENERGY OF FCC IRON

Published in AISTech 2014 Conference Proceedings, AISTech 2014, Indianapolis, IN, USA

Limmer, K.R., D.C. Van Aken, and J.E. Medvedeva

Missouri University of Science and Technology

205 Straumanis-James Hall

401 West 16th Street

Rolla, MO 65409

Tel: (573) 341-4789

Email: krkt2d@mst.edu

Keywords: stacking fault energy, density functional theory, advanced high strength steel

ABSTRACT

In this study, ab-initio density functional methods are used to examine the effects of nickel, copper, and chromium substitutions on unstable and intrinsic stacking fault energies in FCC iron. The aim of this study was to determine if these alloy additions favor the formation and stability of ε-martensite. Nickel and copper additions are shown to increase intrinsic stacking fault energy whereas chromium is shown to have a parabolic relationship. Effects on the unstable stacking fault energy are also examined indicating chromium decreases the unstable stacking fault energy whereas Ni and Cu have a complex effect and are dependent upon proximity to the stacking fault.

INTRODUCTION

Third generation advanced high strength steels (AHSS) are being designed to exceed the strength-ductility combinations of first generation AHSS; such as dual-phase, transformation induced plasticity (TRIP), complex phase, and martensitic steel; at a cost significantly less than that of second generation AHSS such as twinning induced plasticity (TWIP) steel.[1] High manganese steels, such as Hadfield steel, containing 15-30 at% Mn are one example of a TWIP steel which gained much attention as a 2nd generation AHSS.[2-6] Although the high Mn steel compositions yield favorable results they are expensive and challenging with respect to current steelmaking practices. A middle Mn content of less than 8 wt% is desired. Alternative alloying elements to replace the manganese are being considered in this work to produce ε-martensite and a dual TRIP phenomenon ($\gamma \rightarrow \varepsilon \rightarrow \alpha$) as reported by McGrath et al.[7], but at a lower Mn concentration.

Stacking fault energy plays an important role in two potential deformation mechanisms of austenite: deformation twinning (TWIP) and the transformation to ε-martensite. Stacking faults, generated by a dissociation of dislocations into Schockly partials with a burgers vector of 1/6 <112> on {111} slip planes are used to generate both deformation mechanisms such that the shearing each layer results in a twin and shearing every other layer transforms the region from FCC austenite to HCP ε-martensite. In 3rd generation AHSS a dual-stage TRIP mechanism is targeted in which the austenite transforms to ε-martensite before transforming to α-martensite. Both the unstable stacking fault (USF) and intrinsic stacking fault (ISF) should be considered when examining stacking fault energy due to their role in creating and stabilizing the stacking

fault. A decrease in the unstable stacking fault energy (γ_{us}) reduces the barrier to forming a stacking fault, whereas a reduction in the intrinsic stacking fault energy (γ_{isf}) stabilizes the HCP ε-martensite relative to the FCC austenite.

Alloying additions may strongly affect the SFE and therefore the deformation mechanism in 3rd generation AHSS.[8-11] The primary alloying element, manganese, has a parabolic influence on stacking fault energy with a minimum between 12-22 at% Mn.[12-15] Aluminum and carbon have both been shown to increase γ_{isf}, and Al has been further demonstrated to decrease γ_{us}.[15-18] Silicon additions are expected to decrease γ_{isf} and sustain the $\gamma \rightarrow \varepsilon$ transformation.[18, 19]

Chromium, nickel, and copper are common residual elements found in scrap steel, which may further influence the stacking fault energy and thereby alter the deformation mechanism of 3rd generation AHSS. Experimental and thermochemical modeling studies indicate that copper is expected to increase γisf and chromium is expected to decrease γisf.[18, 20-24] The effect of nickel on stacking fault energy is unclear; studies in high-chrome stainless steel alloys indicate both γus and γisf increase with increasing nickel content whereas a parabolic relationship in the Fe-Ni system with a minimum at 36% Ni was originally thought to exist.[21, 22, 25, 26]

This study employs first-principles density-functional methods to investigate how a single impurity at or near the stacking fault affects the unstable and intrinsic stacking fault energies in FCC Fe. Furthermore, the impurity distribution near the stacking fault and its concentration are taken into account to provide a more accurate description of possible phase transformations facilitated by alloying and to guide future alloy design.

METHOD

Surface and interface properties, such as stacking fault energy, cleavage energy, and interface orientation, are readily calculable with density functional theory (DFT). The Vienna ab initio simulation package (VASP) was employed in this study using projector augmented waves (PAW) for pseudopotentials and the generalized gradient approximation (GGA) for the exchange–correlation functional.[27-29] Calculations were performed on a 24-atom supercell using a 6x6x4 Monkhorst-Pack mesh to generate k-points with convergence in the total energy within 0.02 eV/atom. The 6 layer 24-atom

supercell has been shown sufficiently large to remove interference effects in the periodic structure.[15, 30] A 54-atom supercell based on the 24-atom supercell with a larger stacking fault surface area to accommodate 9-atoms per layer was also used to evaluate decreased impurity concentrations. A 4x4x4 Monkhorst-Pack mesh was used for the 54-atom supercell to generate k-points with energetic convergence within 0.02eV/atom. Atomic positions were not relaxed after creation of the stacking fault to avoid relaxation to the original (ideal) atomic configuration; the resultant forces were examined in the results. The valence electron density for the Fe, Cr, Cu, and Ni atoms were defined by the 4s and 3d electrons.

Generalized stacking fault energies (GSFE) were calculated by a rigid shift along the <112> direction in the (111) slip plane. To achieve this geometry, the 24-atom supercell contained six (111) layers with four atoms per layer, Figure 1.B, with two constant translation vectors $\boldsymbol{a}_1 = a\left(1/2, \sqrt{3}/2, 0\right)$, $\boldsymbol{a}_2 = a\left(-1/2, \sqrt{3}/2, 0\right)$, and a variable vector $\boldsymbol{a}_3 = a\left(0, x, \sqrt{6}\right)$ along the fault displacement where $a = a_{fcc}\sqrt{2}$.[15, 31] Using these vectors the full GSFE curve can be generated using the same Cartesian atomic coordinates within the cell and changing only the x value in $\boldsymbol{a}_3$. The partial burgers vector in FCC materials, $\mathbf{b}_p$, is 1/6 <112> {111}, which corresponds to $x = \sqrt{1/12}$ in the given configuration. The three critical points along the GSFE curve are the unstable stacking fault energy (γ_{us}) at 1/2 $\mathbf{b}_p$, the intrinsic stacking fault energy (γ_{isf}) at 1 $\mathbf{b}_p$, and the maximum value (γ_{max}) at 2 $\mathbf{b}_p$ which corresponds to the identical layers at the stacking fault before returning to the original configuration at 3 $\mathbf{b}_p$. Stacking fault energy was calculated as shown in equation 1, by calculating the energetic change from the undistorted lattice to the sheared lattice.

$$\mathrm{GSFE(J/m^2)} = 1.602\times10^{-19}\mathrm{(J/eV)} \cdot \Delta\mathrm{E(eV)} \,/\, \mathrm{S(area,\ m^2)} \qquad (1)$$

The GSFE curve for FCC-Fe (austenite) is shown below in Figure 1A indicating the unstable and intrinsic stacking fault energies at the 0.5 and 1.0 burgers vector displacement positions respectively. A recent first-principles study confirmed the concept that alloying elements only impact the stacking fault energy at or near the stacking fault interface.[15] Figure 1B shows the stacking sequence for unfaulted FCC. The effect of

distance on the stacking fault energy is examined by considering 25% coverage of impurities in each of the three layers nearest the stacking fault, sites 0-2 in Figure 1C. Concentration effects on stacking fault energy are determined by increasing the impurity concentration along the stacking fault as shown in Figure 1D. Clustering of impurities is investigated using the same 24-atom supercell as a function of total energy differential as the distance between two impurities in bulk FCC iron is increased.

RESULTS

Impurity Proximity to Stacking Fault

In this section the stacking fault energy is calculated as a function of the impurity location with respect to the stacking fault. Impurity concentrations of 25% per layer, corresponding to 4 at% total or 12.5% at the stacking fault, in each of the three layers nearest to the stacking fault were used as illustrated schematically in Figure 1C. To enable either TWIP or the formation of ε-martensite for dual TRIP behavior the intrinsic fault should be further stabilized with respect to austenite through a decrease in γ_{isf}. A decrease of γ_{us} is also desired in order to reduce the barrier to forming a stacking fault that may facilitate the nucleation of dislocations favorable to formation of twins or ε-martensite.

Chromium additions appear to behave similarly to Mn additions, decreasing both γ_{isf} and γ_{us}.values. The magnitude of the decrease of γ_{isf} and γ_{us} for Cr additions of -10 mJ/m^2 and -28 mJ/m^2 respectively, are comparable to the -25 mJ/m^2 and -16 mJ/m^2 decreases observed for Mn additions.[15] As the distance between the chromium impurities is increased, a subsequent increase in the stacking fault energy is observed, approaching the austenite γ_{isf} and γ_{us} values of -359 mJ/m^2 and 490 mJ/m^2, respectively.

The effect of both nickel and copper impurities are similar and are discussed together. Both Ni and Cu significantly increase γ_{isf} , by 124 mJ/m^2 and 126 mJ/m^2, respectively; leading to more than double the effect of Al (increase of 63 mJ/m^2).[15] This significant increase indicates preferential stabilization of the FCC austenite over the HCP ε-martensite, which may be due in part to the FCC structure of bulk Ni and Cu. As the single impurities are moved away from the stacking fault and into the Fe bulk structure, the energy decreases to that of austenite. This was true for the for Cr impurities as well.

The effect of Ni and Cu on the unstable stacking fault energy is more complex. At the stacking fault interface both Ni and Cu decrease γ_{us} by -40 mJ/m^2 and -98 mJ/m^2, respectively. When the impurity concentration is one layer away from the stacking fault, a sharp increase in the γ_{us} is observed, exceeding that of austenite by 34 mJ/m^2 and 47 mJ/m^2 for Ni and Cu impurities, respectively. Further distancing the Ni and Cu (or Cr) impurities from the stacking fault interface again returns γus to the austenitic value as is observed in the intrinsic stacking fault case.

Analysis of the behavior of Cu and Ni impurities near the unstable stacking fault in austenite is continued using the partial density of states. Because the effect was larger for Cu impurities and is easier to discern, Figure 3 compares the partial density of states for copper in austenite. The shape of the curve when the impurity is at the unstable stacking fault (USF) is visually different from the other cases: no fault, 1-layer away and 2-layers away. The area under the partial density of states curve up to the Fermi energy, indicative of the bonding strength, is marginally increased for Cu at the USF at 10.26 states/Cu-atom compared with 10.24 states/Cu-atom in the other three cases. Furthermore, the bonding peak characteristics are different from the other 3 cases. The peak height is decreased from 5.20 ± 0.01 states/eV to 4.83 states/eV and the peak position is shifted from -4.18 eV to -4.14 eV.

Clustering and Concentration at Stacking Fault

In this section both the impurity tendency to cluster in austenite and the effect of the impurity concentration at the stacking fault on γ_{isf} are investigated. Clustering of two impurity atoms in the 24-atom supercell was investigated both within bulk austenite and near the stacking fault. Chromium impurities prefer to segregate within FCC iron with clustering increasing the energy by an average of 148 meV. Nickel impurities have a slight preference for clustering in austenite with clustering decreasing energy by -33 meV. Copper impurities strongly prefer clustering in austenite with an average energy decrease of -248 meV.

Low concentration effects were further examined using the 54-atom supercell. Impurity concentration of of 5.6 at% and 12.5 at% Ni and Cu at the stacking fault are shown in Figure 4 to be nearly linear and were used to approximate the net effect of each

impurity on the stacking fault energy. Ni and Cu impurities increase γ_{isf} by 9.9 mJ/m^2 per at% Ni and 10.0 mJ/m^2 per at% Cu at the stacking fault. Cr exhibits a parabolic behavior with a minimum around 12% Cr at the stacking fault. For Cr concentrations at the stacking fault up to 5.6 at%, γ_{isf} decreases by -1.7 mJ/m^2 per at% Cr and from 25-50% Cr at the stacking fault γ_{isf} increases by 4.8 mJ/m^2 per at% Cr.

Experimental measurements of Ni and Cr concentration effects upon stacking fault energy in austenitic stainless steel alloys indicate Ni decreased γ_{isf} by 2 mJ/m^2 per wt% Ni in the range of 4-20% Ni and chromium increased γ_{isf} by 1 mJ/m^2 per wt% Cr in the range of 10-20% Cr.[24]

In fully examining the effect of Cr concentration on γ_{isf}, calculations were performed for a series of impurity configurations on the (111) planes on both sides of the stacking fault. The 24-atom supercell with 4-atoms per layer gave 8 atomic positions in the two layers nearest the stacking fault. The configurations examined were: (1+1), (2+0), (3+0), (2+1), (4+0), (3+1), and (2+2) such that (i+j) = 2, 3, or 4 denotes the number of Cr atoms near the stacking fault. The results shown in Figure 5 indicate a wide range of stacking fault energies possible at each concentration.

The dominant factor in the stacking fault energy for a given Cr concentration is the exchange of Cr-Cr bonds for Cr-Fe bonds during the formation of the intrinsic stacking fault. Cr was shown to favor segregation compared to clustering, which indicates a preference to form Cr-Fe bonds over Cr-Cr bonds in the FCC iron matrix. Minimum stacking fault energy values occur when the formation of the intrinsic stacking fault breaks Cr-Cr bonds and forms Cr-Fe bonds whereas maximums correspond to the opposite scenario. When the number of Cr-Cr to Cr-Fe bond transitions during stacking fault formation are the same, the stacking fault energy becomes a function of layer coverage, with lowest stacking fault energy corresponding to Cr impurities in the same layer. Such that in the case where (i+j) = 4 has the following relationship: E(4+0) < E(3+1) < E(2+2). As a result, Cr atoms are expected to cluster at the stacking fault. Further work is required to fully understand the role of Cr in stabilization of stacking faults. It is expected that carbon will alter the results as previously shown by Medvedeva et al. for Mn and Al.

CONCLUSIONS

Nickel and copper additions have been shown to increase intrinsic stacking fault energy by 9.9 mJ/m^2 per at% Ni and 10.0 mJ/m^2 per at% Cu at the stacking fault. Chromium concentration has a parabolic behavior with regard to intrinsic stacking fault energy with a minimum around 12 at% Cr at the stacking fault. For Cr concentrations at the stacking fault up to 5.6 at% γisf decreases by -1.7 mJ/m^2 per at% Cr and from 25-50% Cr at the stacking fault γisf increases by 4.8 mJ/m^2 per at% Cr. Chromium also decreases the unstable stacking fault energy whereas Ni and Cu have a complex effect as a function of proximity to the stacking fault.

ACKNOWLEDGEMENTS

This work was supported by the Peaslee Steel Manufacturing Research Center at Missouri University of Science and Technology.

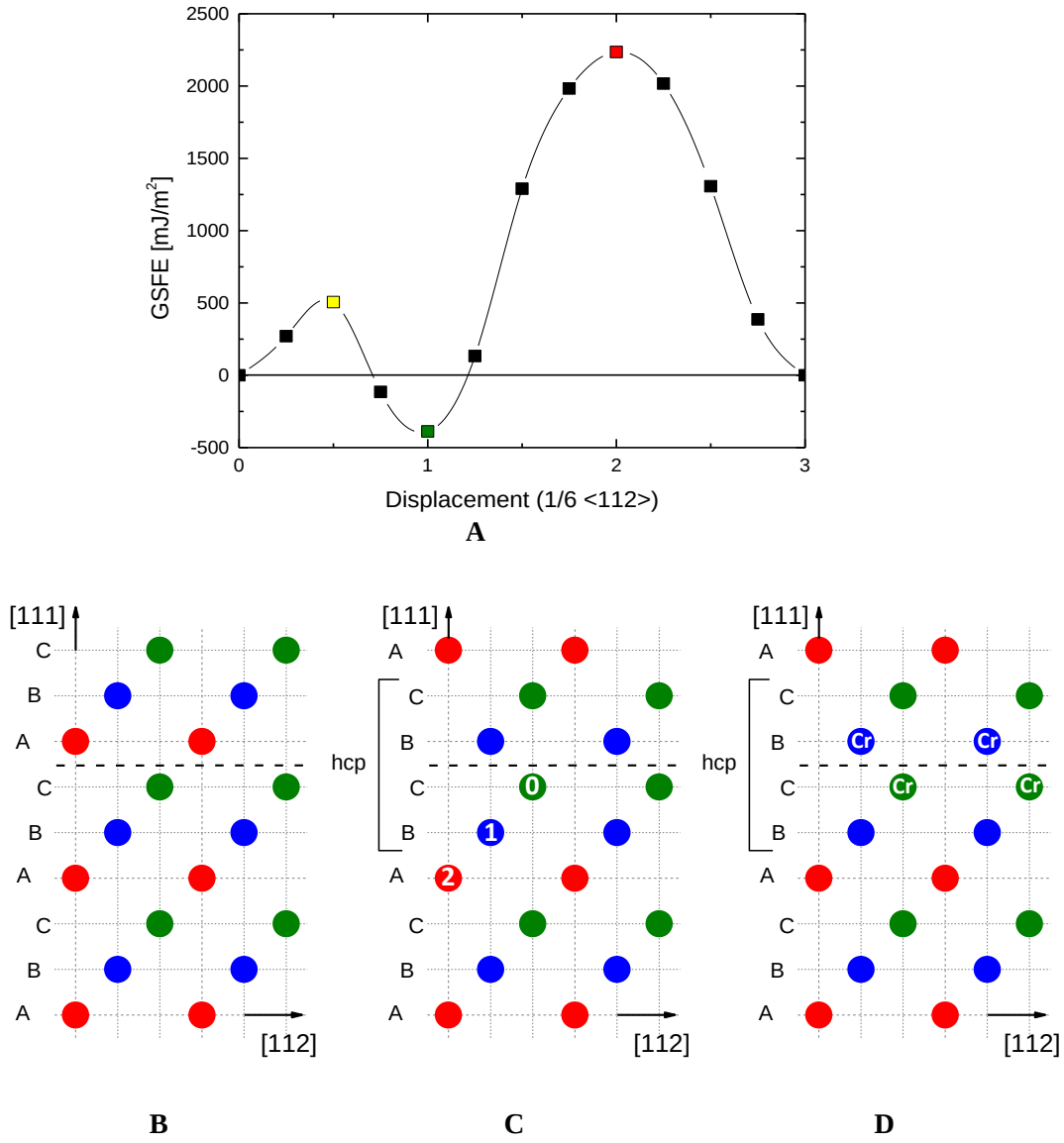

Figure 1. 1.A) generalized stacking fault energy (GSFE) curve for austenite where the displacement is in units of the burgers vector ($\mathbf{b}_p$) a 1/6 shift along the <112> direction in the (111) plane. The unstable stacking fault is indicated at 0.5 and the negative intrinsic stacking fault is located at 1.0 displacement. B) unfaulted austenite. C) intrinsic stacking fault in austenite indicating the three layering positions of single impurities. D) occupation of sites nearest the stacking fault with impurity atoms.

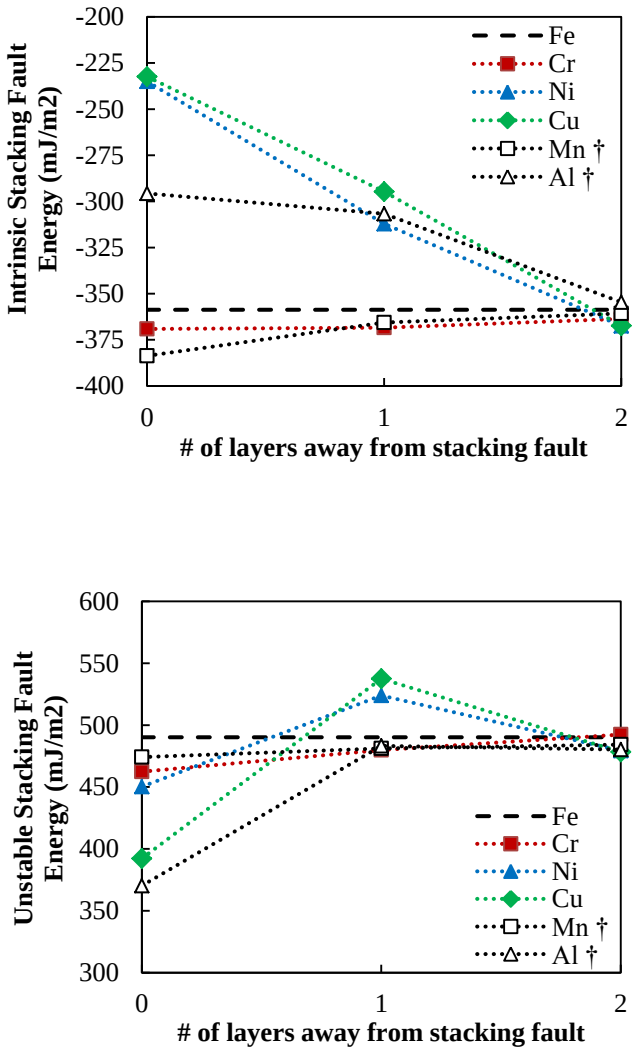

Figure 2. Effect of impurity distance from fault on stacking fault energy for intrinsic and extrinsic stacking faults in austenite; Mn and Al impurity values (†) from Medvedeva et al.[15]

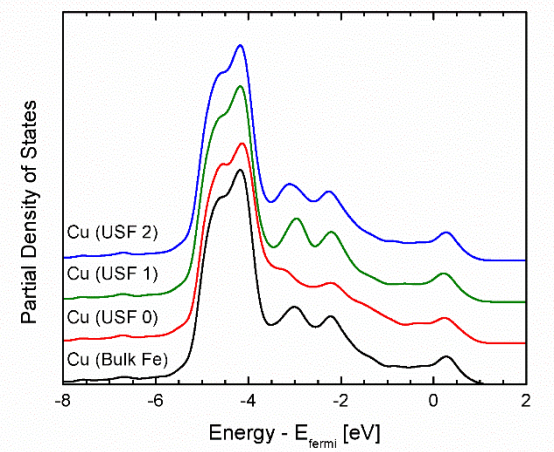

Figure 3. Partial density of states for copper in austenite as a function of distance from unstable stacking fault.

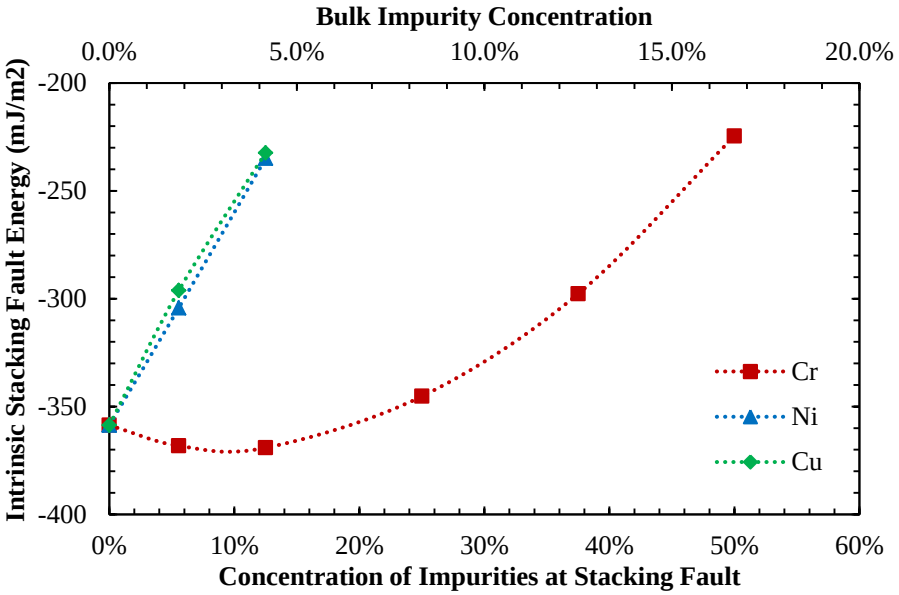

Figure 4. Effect of concentration of impurities at stacking fault on intrinsic stacking fault energy based on average stacking fault energy at each concentration.

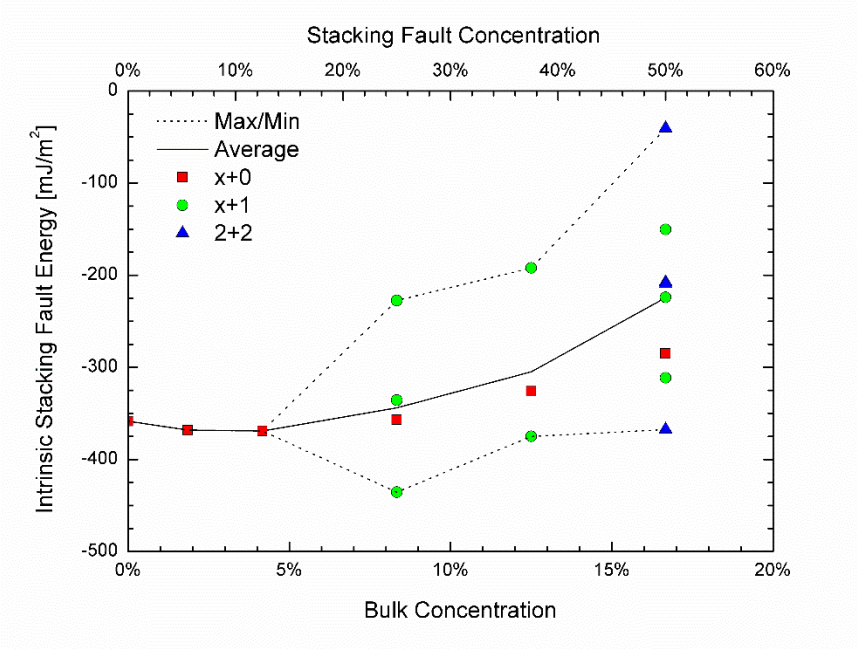

Figure 5. Intrinsic stacking fault energy for varying Cr impurity concentrations and configurations such that (i+j) = 2, 3, or 4 denotes the number of Cr atoms near the stacking fault.

REFERENCES

1. D. K. Matlock and J. G. Speer: 'Third generation of AHSS: microstructure design concepts', in 'Microstructure and Texture in Steels', 185-205; 2009, Springer.

2. Y. N. Dastur and W. C. Leslie: 'Mechanism of Work Hardening in Hadfield Manganese Steel', Metallurgical transactions. A, Physical metallurgy and materials science, 1981, 12 A(5), 749-759.

3. P. H. Adler, G. B. Olson, and W. S. Owen: 'Strain Hardening of Hadfield Manganese Steel', Metallurgical transactions. A, Physical metallurgy and materials science, 1986, 17 A(10), 1725-1737.

4. B. Hutchinson and N. Ridley: 'On dislocation accumulation and work hardening in Hadfield steel', Scripta Materialia, 2006, 55(4), 299-302.

5. D. Canadinc, H. Sehitoglu, H. J. Maier, and Y. I. Chumlyakov: 'Strain hardening behavior of aluminum alloyed Hadfield steel single crystals', Acta Materialia, 2005, 53(6), 1831-1842.

6. E. G. Astafurova, I. V. Kireeva, Y. I. Chumlyakov, H. J. Maier, and H. Sehitoglu: 'The influence of orientation and aluminium content on the deformation mechanisms of Hadfield steel single crystals', International Journal of Materials Research, 2007, 98(2), 144-149.

7. M. C. McGrath, D. C. Van Aken, N. I. Medvedeva, and J. E. Medvedeva: 'Work Hardening Behavior in Steel with Multiple TRIP Mechanisms', Metallurgical and Materials Transactions A: Physical Metallurgy and Materials Science, 2013, 1-10.

8. S. Mahajan and G. Y. Chin: 'Formation of deformation twins in f.c.c. crystals', Acta Metallurgica, 1973, 21(10), 1353-1363.

9. G. B. Olson and M. Cohen: 'A general mechanism of martensitic nucleation: Part I. General concepts and the FCC→HCP transformation', Metallurgical Transactions A, 1976, 7(11), 1897-1904.

10. H. Van Swygenhoven, P. M. Derlet, and A. G. Frøseth: 'Stacking fault energies and slip in nanocrystalline metals', Nature Materials, 2004, 3(6), 399-403.

11. S. Sato, E. P. Kwon, M. Imafuku, K. Wagatsuma, and S. Suzuki: 'Microstructural characterization of high-manganese austenitic steels with different stacking fault energies', Materials Characterization, 2011, 62(8), 781-788.

12. H. Schumann: 'Einfluss der SFE auf den kristallographischen Umgitterungs-mechanismus der γ/α-Umwandlung in hochlegierten Stählen', J. Kristall Technik, 1974, 10(10).

13. P. Y. Volosevich, V. N. Grindnev, and Y. N. Petrov: Phys. Met. Metallogr., 1976, 42(2), 126-130.

14. Y. K. Lee and C. S. Choi: 'Driving force for γ → ε martensitic transformation and stacking fault energy of γ in Fe-Mn binary system', Metallurgical and Materials Transactions A: Physical Metallurgy and Materials Science, 2000, 31(2), 355-360.

15. N. I. Medvedeva, M. S. Park, D. C. Van Aken, and J. E. Medvedeva: 'First-principles study of Mn, Al and C distribution and their effect on stacking fault energies in fcc Fe', Journal of Alloys and Compounds, 2014, 582, 475-482.

16. A. Saeed-Akbari, J. Imlau, U. Prahl, and W. Bleck: 'Derivation and variation in composition-dependent stacking fault energy maps based on subregular solution model in high-manganese steels', Metallurgical and Materials Transactions A: Physical Metallurgy and Materials Science, 2009, 40(13), 3076-3090.

17. A. Abbasi, A. Dick, T. Hickel, and J. Neugebauer: 'First-principles investigation of the effect of carbon on the stacking fault energy of Fe-C alloys', Acta Materialia, 2011, 59(8), 3041-3048.

18. A. Dumay, J. P. Chateau, S. Allain, S. Migot, and O. Bouaziz: 'Influence of addition elements on the stacking-fault energy and mechanical properties of an austenitic Fe–Mn–C steel', Materials Science and Engineering: A, 2008, 483–484(0), 184-187.

19. O. Grässel, L. Krüger, G. Frommeyer, and L. W. Meyer: 'High strength Fe-Mn-(Al, Si) TRIP/TWIP steels development - properties - application', International Journal of Plasticity, 2000, 16(10), 1391-1409.

20. Y. N. Petrov: 'On the electron structure of Mn–, Ni– and Cr–Ni–Mn austenite with different stacking fault energy', Scripta Materialia, 2005, 53(10), 1201-1206.

21. T. Epicier and Y. Kumashiro: 'FIRST HREM OBSERVATION OF THE ORDERED CARBON SUBLATTICE IN A TRANSITION-METAL CARBIDE (VC//1// minus //x)', Philosophical Magazine Letters, 1987, 55(4), 171-179.

22. W. Charnock and J. Nutting: 'The Effect of Carbon and Nickel upon the Stacking-Fault Energy of Iron', Metal science, 1967, 1(1), 123-127.

23. S. Lee, J. Kim, S.-J. Lee, and B. C. De Cooman: 'Effect of Cu addition on the mechanical behavior of austenitic twinning-induced plasticity steel', Scripta Materialia, 2011, 65(12), 1073-1076.

24. R. Schramm and R. Reed: 'Stacking fault energies of seven commercial austenitic stainless steels', Metallurgical Transactions A, 1975, 6(7), 1345-1351.

25. V. Krasnenko and M. G. Brik: 'First-principles calculations of hydrostatic pressure effects on the structural, elastic and thermodynamic properties of cubic monocarbides XC (X = Ti, V, Cr, Nb, Mo, Hf)', Solid State Sciences, 2012, 14(10), 1431-1444.

26. J. Liu, P. Han, M. Dong, G. Fan, G. Qiao, and J. Yang: 'Influence of Ni and N on generalized stacking-fault energies in FeCrNi alloy: A first principle study', Physica B: Condensed Matter, 2012, 407(5), 891-895.

27. G. Kresse and J. Furthmüller: 'Efficient iterative schemes for ab initio total-energy calculations using a plane-wave basis set', Physical Review B - Condensed Matter and Materials Physics, 1996, 54(16), 11169-11186.

28. G. Kresse and D. Joubert: 'From ultrasoft pseudopotentials to the projector augmented-wave method', Physical Review B - Condensed Matter and Materials Physics, 1999, 59(3), 1758-1775.

29. J. P. Perdew, K. Burke, and M. Ernzerhof: 'Generalized gradient approximation made simple', Physical Review Letters, 1996, 77(18), 3865-3868.

30. S. Kibey, J. B. Liu, M. J. Curtis, D. D. Johnson, and H. Sehitoglu: 'Effect of nitrogen on generalized stacking fault energy and stacking fault widths in high nitrogen steels', Acta Materialia, 2006, 54(11), 2991-3001.

31. A. T. Paxton: 'Point, Line and Planar Defects', in 'Electron Theory in Alloy Design', (eds. D. G. Pettifor, et al.), 158-190; 1992, Oxford, The Alden Press Ltd.

III. AB-INITIO SIMULATION OF ALLOYING EFFECT ON STACKING FAULT ENERGY IN FCC FE

Prepared for submission to *Computational Materials Science*

Krista R Limmer[*,1], Julia E Medvedeva[**,1], David C Van Aken[1], and Nadezhda I Medvedeva[2]

[1] Missouri University of Science and Technology, Rolla, MO 65409, United States

[2] Institute of Solid State Chemistry, Yekaterinburg, Russia

[*] Corresponding author: e-mail krkt2d@mst.edu, Phone: +1 330 992 9982

[**] e-mail juliam@mst.edu, Phone: +1 573 341 4789, Fax: +1 573 341 4715

Keywords stacking fault energy, first-principles methods, fcc Fe alloys

ABSTRACT

The effect of 3*d* and 4*d* transition metal (TM) additions on the intrinsic stacking fault energy (SFE) in fcc Fe is studied to elucidate the role of alloying in the deformation mechanisms in austenitic steels. The results of ab-initio calculations reveal that only Mn reduces the SFE, stabilizing the local hcp structure, whereas all other d-additions are expected to decrease the hcp→fcc transformation temperature and restrain the ε-martensite formation. We predict a parabolic dependence of SFE on the atomic number of d-element across the series, with the largest increase in SFE obtained for the early and late elements in the *d*-series that follow (correlate) the difference in the valence electrons between the TM and Fe atoms. To understand the SFE behavior in fcc Fe alloys, the driving forces for the fcc to hcp phase transformations of transition metal X and solid solution Fe-X were considered with an *ab-initio* approach. It is found that the solution model explains the SFE trends for all TM additions except the late TMs with fully occupied d-shells (Cu and Ag).

INTRODUCTION

The active deformation mechanism in austenitic steels is controlled by the stacking fault energy (SFE). The intrinsic stacking fault energy plays an important role in the formation of deformation twins and ε-martensite allowing either twinning induced plasticity (TWIP) or transformation induced plasticity (TRIP) to respectively occur. TRIP was shown to be the dominant mechanism in steels with a low SFE, less than 20 mJ/m^2, whereas TWIP is associated with a medium SFE of about 15-35 mJ/m^2 [1]. To enable the TRIP mechanism, the intrinsic stacking fault should be stabilized with respect to austenite through a decrease in SFE, which may be achieved by altering alloy chemistry, temperature, and strain.

The effect of transition metal elements on SFE – either as alloying additions or residual elements – is of concern for alloy development since these additions may significantly alter SFE and therefore affect the active deformation mechanism [2–4]. The SFE values of multicomponent systems are often considered to be proportional to the Gibbs free energies of the fcc to hcp transformation within a regular solution model with estimated parameters from experimental thermodynamic data. These estimations have been made for the Fe-Mn-C and Fe-Mn-Al-Si-C alloys [1,5–7]. For Mn additions, a

parabolic behavior was calculated with an SFE minimum at 12 at% [8], 15 at% [9], or 22 at% Mn [10].

Ab-initio methods have been employed to determine the stacking fault energies following both explicit and implicit approaches. The SFE may be explicitly calculated as a total energy difference between the ideal and faulted lattices. This explicit approach has been used to predict the SFE in nonmagnetic Fe [11,12], as well as Fe-N [13], Fe-C [12,14], Fe-Mn and Fe-Al [12] alloys. An implicit *ab-initio* approach to calculate SFE has also been used recently following the axial next-nearest-neighbor Ising (ANNNI) model, where the energies of the fcc, hcp and double hcp phases are calculated to determine SFE of the fcc phases in the Fe-Mn system [15–17]. The implicit approach allows for a more homogeneous description of the bulk environment whereas the explicit calculations provide a more complete understanding of segregation effects as well as the electronic structure changes at the stacking fault [14].

In this study, a first-principles approach was employed to describe the effects of 3*d* and 4*d* transition metal alloying additions on the stacking fault energy in fcc Fe. The objective of this work was to contribute towards a systematic understanding of the correlation between composition and stacking fault energy in austenitic steels. Our strategy was to obtain the SFE from the explicit ab-initio simulation of stacking fault defect and to predict how additions can affect stabilization of austenite or ε-martensite. Furthermore, we applied *ab-initio* estimations within a regular solution model in order to find the correlations with the phase transformations. To analyze the calculated trends in SFE, we estimated the driving forces for the fcc to hcp transformations of the 3*d* or 4*d* transition metal X and solid solution Fe-X.

METHOD

The total-energy calculations were performed with the Vienna ab-initio Simulation Package (VASP) [18], using projector augmented waves (PAW) [19,20] and the generalized gradient approximation (GGA) for exchange correlation functional [21]. Calculations were performed on a 24-atom supercell consisting of six (111) layers, where one of four Fe atoms in the stacking fault plane was substituted for alloying addition. This supercell has been shown sufficiently large to remove interference effects across the

layers [12,13]. The supercell configuration corresponds to the impurity concentration of 25% in layer and 4% in bulk. A 6x6x4 Monkhorst-Pack mesh was used for 24-atom supercell to generate k-points with convergence in the total energy within 0.02 eV/atom.

Stacking fault energy was calculated via the total energy difference between undistorted lattice and sheared lattice. The latter was simulated by a rigid shift along the <112> direction in the (111) slip plane that corresponds to the partial Burgers vector in fcc structure, $\mathbf{b}_p$=1/6 <112> {111}. Atomic positions were relaxed in the direction normal to the stacking fault plane until the atomic forces were less than 0.02 eV/Å. In this work, we restricted the explicit calculations of SFE to the nonmagnetic Fe state, following previous investigations [11,12] where similar SFE values were obtained for the ferromagnetic and nonmagnetic states in Fe and Fe-Mn. The stacking fault energy for fcc Fe-X was calculated for the substitutional X addition which was placed at the stacking fault plane. Recent works have shown that SFE decreases linearly as the substitutional point defect is moved from the stacking fault region into the bulk, with the effects absolved upon reaching a depth of two layers from the stacking fault [12,14].

In order to analyze the trends in SFE, a regular solution model was employed, where the driving forces for the fcc to hcp phase transformations of transition metal X and solid solution Fe-X were calculated *ab-initio*.

RESULTS AND DISCUSSION

For pure fcc Fe in non-magnetic state, we predict the SFE value to be -390 mJ/m^2 which is in agreement with the values obtained from previous explicit *ab-initio* calculations [11-14]. For fcc Fe-X, the calculated stacking fault energies demonstrate a parabolic dependence on the atomic number of *d*-impurity across the series (Fig.1a). The calculated SFE values do not follow the atomic size misfit between the impurity and Fe atoms, but rather appear to have an electronic origin correlated with the difference in the number of valence electrons of Fe and the substitutional addition. The 3*d*- and 4*d*-additions which have the same number of valence electrons (e.g., Ru) or 1-2 fewer (e.g., Cr, Mn, or Tc) as compared to that of Fe, slightly affect the SFE, Fig. 1a. In contrast, the additions with a larger or much smaller number of valence electrons than that of Fe increase the SFE strongly. Only Mn addition is found to lower the SFE by ~20 mJ/m^2,

indicating a stabilization of hcp over fcc structure for the considered concentration of 4 at.% Mn in the fcc Fe-Mn alloy.

The crystal structure of alloying elements (hcp for Ti, Zr, Co, Tc, and Ru; bcc for V, Cr, Nb, and Mo; or fcc for Ni, Cu, Pd, and Ag) does not correlate with the obtained SFE trends. Moreover, the calculated energy difference between fcc and hcp structures, $\Delta E^{hcp \rightarrow fcc}$, for the 3*d* and 4*d* transition metals, Fig. 1b, is also a poor predictor of the trends in the SFE obtained in the explicit calculations. Based on the nonmagnetic values of $\Delta E^{hcp \rightarrow fcc}$, which are in agreement with previous nonmagnetic results obtained by the tight-binding method [22], the fcc structure is more stable for the transition metals with a larger number of valence electrons than Fe as well as for V, Cr, Nb, Mo, while the hcp structure is preferred by Ti, Zr, Mn, Fe, Tc, Ru. Thus, the beginning elements in the *d*-series (Ti and Zr) demonstrate a strong preference to have hcp structure, Fig. 1b, however, they provide the largest increase in the SFE (Fig.1a).

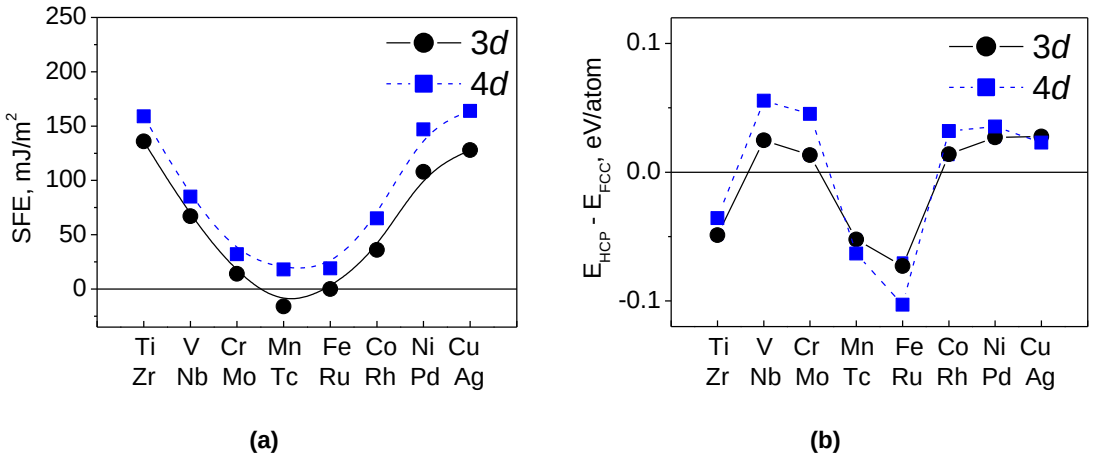

Figure 1. (a) The calculated stacking fault energies for fcc Fe-4 at.%X with respect to fcc Fe and (b) the energy difference between the hcp and fcc structures for transition metals.

The trends obtained within the explicit SFE calculations were further analyzed using the proportionality of the SFE and the Gibbs energy. The Gibbs free energy associated with the phase transformation from fcc to hcp (ΔG) is an indicator of the thermodynamic driving force for stacking fault creation [23]. In this study we estimate the driving force within the framework of a regular solution model as shown in the following equation:

$$\Delta G^{hcp\rightarrow fcc} = c_{Fe}\,\Delta E^{hcp\rightarrow fcc}(Fe) + c_X\,\Delta E^{hcp\rightarrow fcc}(X) + c_{Fe}\cdot c_X\;\Delta E^{hcp\rightarrow fcc}(Fec_{Fe}Xc_X) \qquad (1)$$

where c_{Fe} and c_X are the concentrations of Fe and X in the Fe-X alloy, respectively.

The value of $\Delta E^{hcp\rightarrow fcc}$ for solid solution Fe-X (Fig. 2a) was estimated as a total energy difference between the hcp and fcc structures of $Fe_{0.75}X_{0.25}$ with volumes equal to fcc Fe. The concentration of X in this configuration exactly corresponds to those at the stacking fault plane in our explicit calculations. We find that the $\Delta E^{hcp\rightarrow fcc}$ values are positive and largest for the elements in the beginning of each period with the maximum values corresponding to Ti and Zr that have hcp structure. The elements with the same or greater number of the valence electrons as Fe (Co, Ni in 3*d*-series, and Rh, Pd in 4*d*-series) as well as Mn provide almost equal $\Delta E^{hcp\rightarrow fcc}$. The strongest preference to have hcp structure is obtained for $Fe_{0.75}X_{0.25}$ where X is a TM with filled *d*-states (Cu, Ag), Fig. 2a.

The total $\Delta G^{hcp\rightarrow fcc}$ values calculated according to Eq.1 are shown in Fig. 2b. We find that the $\Delta G^{hcp\rightarrow fcc}$ curves correlate with the parabolic dependences of SFE (Fig.1a) for all additions except for the end elements in the 3*d* and 4*d* series (Ni, Cu, Pd, and Ag). Based on the results of $\Delta E^{hcp\rightarrow fcc}$ for transition metals (Fig. 1b) and solid solutions (Fig. 2a), we conclude that the energy difference between the hcp and fcc structures of solid solution determines the SFE for the early elements (Ti, Zr), whereas the structural stability of the transition metal is important for Fe alloys with late period additions.

Thus, the dependence of stacking fault energy in fcc Fe alloys on the atomic number of *d*-alloying impurity can be explained using simple model calculations. An exception is additions with the filled *d*-states for which the Fe-X alloy demonstrates a strong preference for the hcp structure. Furthermore, the calculations of $\Delta E^{hcp\rightarrow fcc}$ for Fe_{1-}

$_xCu_x$ where x = 0.25, 0.5, 0.75, 1.0 showed that the fcc structure is favorable over hcp only for x = 1.0.

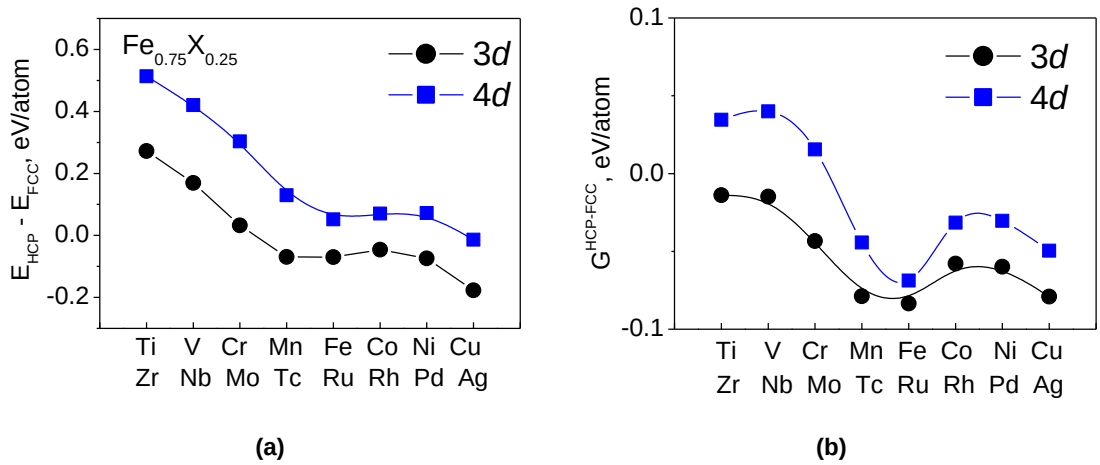

Figure 2. The energy difference between the hcp and fcc structures for (a) solid solution $Fe_{0.75}X_{0.25}$ and (b) total $\Delta G^{hcp\rightarrow fcc}$ (Eq.1).

SUMMARY AND CONCLUSIONS

In summary, a first-principles method was employed to examine the effects of alloying elements on stacking fault energy of fcc iron. A parabolic behavior of the SFE across the periods for 3*d* and 4*d* alloying elements was obtained. We predict that all transition metal additions except manganese increase SFE and the increasing effect correlates with the difference in the number of valence electrons of TM and Fe atoms. Thus, all TM additions except Mn should decrease the hcp→fcc transformation temperature and restrain the ε-martensite formation. The thermodynamic driving forces for the fcc to hcp phase transformations of transition metal X (X=3*d* and 4*d* elements) and solid solution Fe-X were analyzed using a regular solution model. The stacking fault

energies calculated explicitly for fcc Fe-X are in accord with the trends in the solution model, with the exception for the transition metals with the filled *d*-states.

ACKNOWLEDGEMENTS

The authors gratefully recognize the Peaslee Steel Manufacturing Research Center (PSMRC) at Missouri University of Science and Technology for funding this work. This work used the Extreme Science and Engineering Discovery Environment (XSEDE), which is supported by National Science Foundation grant number ACI-1053575. N. Medvedeva acknowledges the support of RBRF, Grant 14-03-00324a.

REFERENCES

[1] S. Allain, J.P. Chateau, O. Bouaziz, S. Migot, and N. Guelton, Mater. Sci. Eng. A 387-389, 158 (2004).

[2] S. Mahajan and G.Y. Chin, Acta Metall. 21, 1353 (1973).

[3] G. Olson and M. Cohen, Metall. Trans. A 7, 1897 (1976).

[4] S. Sato, E.-P. Kwon, M. Imafuku, K. Wagatsuma, and S. Suzuki, Mater. Charact. 62, 781 (2011).

[5] G. Frommeyer, U. Brüx, and P. Neumann, ISIJ Int. 43, 438 (2003).

[6] Y. Petrov, Z. Metallk. 94, 1012 (2003).

[7] A. Saeed-Akbari, J. Imlau, U. Prahl, and W. Bleck, Metall. Mater. Trans. A 40, 3076 (2009).

[8] Y.K. Lee and C.S. Choi, Metall. Mater. Trans. A 31, 355 (2000).

[9] P.U.Y. Volosevich, V.N. Gridnev, Y.U.N. Petrov, and V.N. Grindnev, Phys. Met. Metallography (USSR) 42, 126 (1976).

[10] H. Schumann, Krist. Tech. 9, 1141 (1974).

[11] T. Hickel, A. Dick, B. Grabowski, F. Körmann, and J. Neugebauer, Steel Res. Int. 80, 4 (2009).

[12] N.I. Medvedeva, M.S. Park, D.C. Van Aken, and J.E. Medvedeva, J. Alloy Compd. 582, 475 (2014).

[13] S. Kibey, J.B.J.B. Liu, M.J.J.M. Curtis, D.D.D. Johnson, and H. Sehitoglu, Acta Mater. 54, 2991 (2006).

[14] A. Abbasi, A. Dick, T. Hickel, and J. Neugebauer, Acta Mater. 59, 3041 (2011).

[15] P. Denteneer and W. van Haeringen, J. Phys. C Solid State 20, L883 (1987).

[16] A. Dick, T. Hickel, and J. Neugebauer, Steel Res. Int. 80, 603 (2009).

[17] A. Reyes-Huamantinco, P. Puschnig, C. Ambrosch-Draxl, O.E. Peil, and A.V. Ruban, Phys. Rev. B 86, 060201 (2012).

[18] G. Kresse and J. Furthmüller, Phys. Rev. B 54, 11169 (1996).

[19] P.E. Blöchl, Phys. Rev. B 50, 17953 (1994).

[20] G. Kresse and D. Joubert, Phys. Rev. B 59, 11 (1999).

[21] J.P. Perdew, K. Burke, and M. Ernzerhof, Phys. Rev. Lett. 77, 3865 (1996).

[22] M.J. Mehl and D.A. Papaconstantopoulos, Phys. Rev. B 54, 4519 (1996).

[23] P. Ferreira and P. Müllner, Acta Mater. 46, 4479 (1998).

IV. CARBON INTERACTIONS WITH AUSTENITIC FE-MN-X-C ALLOYS (X= CR AND SI)

In preparation for submission to *Acta Materialia*.

K. R. Limmer and J.E. Medvedeva

INTRODUCTION

Stacking fault energy is a consideration in austenitic high manganese alloy design in order to determine the active deformation mechanism. During deformation of the fcc phase, stacking faults are created in austenite and may be repeated on every subsequent plane to form a twin resulting in twinning-induced plasticity (TWIP) or on every other plane to form ε-martensite followed by α'-martensite via transformation-induced plasticity (TRIP). It has been suggested that the nucleation of ε-martensite is a critical step in the nucleation process of α'-martensite from austenite in the TRIP phenomena, implying a transient metastable state of the ε-martensite.[1,2] Alternatively, the transformation sequence austenite → ε-martensite → α'-martensite has been termed two-stage TRIP, observed in alloys with stable ε-martensite.[3] The probability of forming a twin compared to tripping to ε-martensite is not well understood. An approximate relationship to SFE has been described such that TRIP steels generally have low SFE, less than 20 mJ/m^2, and TWIP steels have medium SFE or 20-50 mJ/m^2.[4] The stacking fault energy is known to be altered by alloy chemistry, temperature, and strain; this work will consider the effects of alloy chemistry.

Recent studies have begun elucidating the effect of alloying additions on the stacking fault energy in Fe-Mn alloys through experimental, thermodynamic modeling, and first-principles calculations. Experimental studies have shown complex results for the effect of Si and Cr with the effect being a function other alloying additions present. Experimentally Si has been shown to decrease SFE in austenitic high Mn and Cr-Ni stainless alloys [5–8] at room temperature, but was also shown to increase SFE at 500K in similar alloys [9]. Thermochemical modelling of a low Mn alloy indicates a complex behavior of Si first increasing SFE before decreasing after 4 mass % [10]. Recent *ab-initio* results suggest that Si decreases the Néel temperature as well as strongly affects local magnetic ordering below the Néel temperature resulting in conflicting hcp/fcc phase stability results [11]. Additionally, the nonmagnetic contribution to the stacking fault energy was shown to increase as a function of increasing Si content, and above the Néel temperature be the significant component of the stacking fault energy [12]. Similarly, the effect of Cr on the stacking fault energy has been shown experimentally increase SFE [9,13,14] and also decrease SFE in similar alloys [6,15]. Thermochemical modeling

suggests that Cr decreases SFE [10] Previous *ab-inito* work [16] has indicated that as a sole alloying addition in fcc Fe, Cr increases stacking fault energy at a concentration of 4 at% when it is located at the stacking fault. This first-principles work examines the interaction between Cr and Si in a Fe-Mn-Al-C alloy on electronic level to enable predictions of stacking fault energy in this alloy class.

METHODOLOGY

The first-principles calculations were performed with the Vienna *ab-initio* Simulation Package (VASP) [17], using projector augmented waves (PAW) [18,19] and the generalized gradient approximation (GGA) for exchange correlation functional [20]. The valence electron density was defined as the 4s and 3d electrons of Fe, Mn and Cr, 3s and 3p electrons of Si, and 2s and 2p electrons of C using the PAW Perdew-Burke-Ernzerhof (PBE) pseudopotentials. A kinetic energy cut-off of 350 eV was used in all calculations. The 32-atom cubic fcc supercell, depicted in Figure 1, used to determine alloying element interactions was sampled with a 4x4x4 Monkhurst-Pack grid giving accuracy within 0.5 meV/atom, which is sufficient for determining site preferences. Full relaxation of the ion positions and lattice parameter were conducted to resolve forces on each atom to less than 0.01 eV/Å. Binding energies, E_b, were calculated as shown below in equation 1.

$$E_b\,(\text{Fe-X-Z}) = [E(\text{Fe-X}) + E(\text{Fe-Z})] - [E(\text{Fe-X-Z}) + E(\text{Fe})] \quad (1)$$

Following this notation, positive and negative binding energies correspond to attractive and repulsive interactions between alloying additions X and Z respectively.

Stacking fault energy calculations were performed on a 36-atom supercell consisting of nine (111) layers. The stacking fault energies were calculated by a rigid shift along the <112> direction in the (111) slip plane corresponding to the partial Burgers vector in fcc materials, $\mathbf{b}_p$=1/6 <112> {111}. Stacking fault energy was calculated as the energy change from between the sheared lattice and the undistorted lattice. Atomic positions were relaxed in the direction normal to the stacking fault until forces on each atom were less than 0.02 eV/Å.

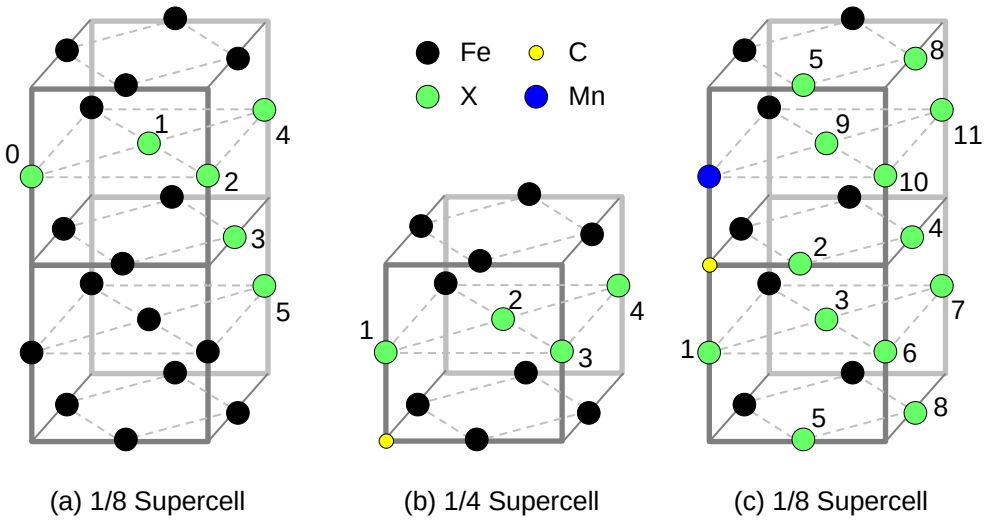

Figure 1. Schematic of atomic placements in 32-atom cubic supercell for alloying interaction calculations of composition (a) $Fe_{30}X_2$ (b) $Fe_{31}XC$ and (c) $Fe_{30}MnXC$.

RESULTS AND DISCUSSION

Alloying interactions and distribution in nonmagnetic fcc Fe

An optimized lattice parameer of 3.446 Å was utilized for nonmagnetic fcc Fe which is in good agreement with previous *ab-inito* results [21–23]. Interstitial carbon was introduced in in an octaheral site giving rise to a lattice parameter increase to 3.470 Å and local distortion of Fe-Fe bonds around the occupied octahedral site in agreement with past *ab-initio* calculations and experimental results [23,24]. Upon relaxation the Fe-C distance increased from 1.72 to 1.87 Å.

Chromium substitution at 3 at.% in nonmagnetic fcc Fe ($Fe_{31}Cr$) resulted in a lattice parameter increase from 3.446 to 3.454 Å and an outward shift of Fe atoms around the Cr impurity from 2.44 to 2.46 Å. Calculations for two Cr substitutional atoms ($Fe_{30}Cr_2$) showed a repulsive interaction for Cr atoms in nearest neighbor sites (E_b equal to -0.07 eV). Weak attractive interactions were predicted for sites 2 and 4 (E_b equal to +0.05 and +0.04 eV respectively). Negative binding energies of -0.01 and -0.03 eV were

calculated for sites 3 and 5 indicating again a repulsive ineraction. This energy profile indicates a segregation preference to increase the planar concentration of Cr in fcc Fe without introducing nearest neighbor interactions.

Silicon substitutions at 3 at.% ($Fe_{31}Si$) also increased atomic spacing around the Si impurity from 2.44 to 2.46 Å and marginally increased the nonmagnetic fcc Fe lattice parameter to 3.450 Å. Calculations of 6 at.% Si substitution ($Fe_{30}Si_2$) resulted in repulsive interactions between Si atoms for all sites with the most repulsive sites being 1 and 4, with E_b equal to -0.24 and -0.23 eV, respectively. The sites with the least repulsive interactions, 3 and 5, correspond to the third coordination sphere and the most remote site possible within the 32-atom cell (E_b equal to -0.03 and -0.06 eV, respectively). Silicon ordering in fcc Fe has not been studied experimentally to the extent of Si in bcc Fe, in which Fe_3Si ($D0_3$ structure) is well documented. Si ordering in Fe_3Si is such that the Si atoms occupy third coordination sphere sites similar to the prediction of site 3 having the lowest site preference energy (Table 1).

Table 1. Site preference energies (meV) for impurities in fcc Fe corresponding to site positions in Figure 1. Zero energy corresponds to the lowest site energy.

Site	$Fe_{30}Cr_2$	$Fe_{30}Si_2$	$Fe_{31}CrC$	$Fe_{31}SiC$	$Fe_{30}MnCrC$	$Fe_{30}MnSiC$
1	123	208	0	686	0	686
2	0	71	21	0	35	705
3	61	0	69	125	64	0
4	11	199	38	108	106	132
5	84	27			155	186
6-11					53-86	48-125

Carbon interactions with alloying additions of Si and Cr were also examined in $Fe_{31}XC$ alloys. Substitution around the carbon site results in distortion of the octahedra with lengthening of the X-C distance to 1.96 and 2.01Å for Cr and Si respectively, and shortening of the Fe-C distance in the 180^o X-C-Fe pair to 1.84 and 1.83Å respectively; remaing Fe-C distances remain unchanged. The binding energy between Cr and C is attractive for each site considered, with the highest binding energy calculated for the nearest neighbor site (E_b = +0.09). Interactions between Si and C are strongly repulsive in the nearest neighbor site (E_b = -0.62) and attractive in the second coordination sphere (E_b = +0.06). The site preferences and binding energies exhibited by Cr and Si with respect to C are similar to those of Mn and Al, respectively, although the repulsive interaction between Si and C in nearest neighbor positions is calculated to be more than twice that of the Al and C interaction in the same configuration of -0.28eV [25].

Interactions of Si and Cr with C and Mn ($Fe_{30}MnXC$) are examined assuming Mn and C are situated in nearest neighbor sites, following previous experimental and *ab-initio* calculation results indicating an attractive binding energy [25,26]. The Cr addition prefers to occupy site 1 to form a 180^o Cr–C–Mn pair with a binding energy of 0.13 eV. The next most preferred site is position 2, introducing weakly repulsive Cr – Mn neighbor interactions while maintaining the strong attractive Cr – C interaction. Alternatively the most preferable position for Si is site 3, in the second coordination sphere of the C. Site 9, also within the second coordination sphere of the C atom and also a nearest neighbor of the Mn has increase in site energy by 49 meV indicating Si prefers to avoid Mn. Aluminum was shown to have a similar site preference in relation to a Mn–C pair, although the energy increase as a function of neighboring a Mn is more pronounced for Al than Si.

These calculations show energetically preferred ordering of Si and Cr in relation to Mn and C within a nonmagnetic fcc Fe alloy. The diffusion of C towards Cr atoms is likely due to the attractive interactions, and in alloys containing Mn, a Mn – C – Cr pair is also energetically favored. Previous work has demonstrated C diffuses away from stacking faults enabling a decrease of the stacking fault energy and growth of the fault [27].

REFERENCES

[1] H. Aydin, E. Essadiqi, I.-H.H. Jung, S. Yue, Mat. Sci. Eng. A-Struct. 564 (2013) 501.

[2] G.B. Olson, M. Cohen, Metall. Trans. A 7 (1976) 1897.

[3] M.C. McGrath, D.C. Van Aken, N.I. Medvedeva, J.E. Medvedeva, Metall. Mater. Trans. A (2013) 1.

[4] S. Allain, J.P. Chateau, O. Bouaziz, S. Migot, N. Guelton, Mater. Sci. … 387-389 (2004) 158.

[5] G. Frommeyer, U. Brüx, P. Neumann, ISIJ Int. 43 (2003) 438.

[6] R.E. Schramm, R.P. Reed, Metall. Trans. A 6 (1975) 1345.

[7] P. Gallagher, Metall. Trans. 1 (1970) 2429.

[8] X. Tian, Y. Zhang, Mat. Sci. Eng. A-Struct. 516 (2009) 73.

[9] K. Ishida, T. Nishizawa, Trans Jap Inst Met 15 (1974) 225.

[10] A. Dumay, J.-P.P. Chateau, S. Allain, S. Migot, O. Bouaziz, Mat. Sci. Eng. A-Struct. 483-484 (2008) 184.

[11] T. Gebhardt, D. Music, M. Ekholm, I.A. Abrikosov, J. Von Appen, R. Dronskowski, D. Wagner, J. Mayer, J.M. Schneider, Acta Mater. 59 (2011) 1493.

[12] X. Tian, Y. Zhang, Mat. Sci. Eng. A-Struct. 516 (2009) 78.

[13] X. Tian, H. Li, Y.S.S. Zhang, Acta Metall. Sin. (English Lett. 16 (2003) 211.

[14] C.G. Rhodes, A.W. Thompson, Metall. Trans. A 8 (1977) 1901.

[15] Y. Petrov, Zeitschrift Für Met. 94 (2003) 1012.

[16] K.R. Limmer, J.E. Medvedeva, D.C. Van Aken, N.I. Medvedeva, Ab-Initio Simulation of Alloying Effect on Stacking Fault Energy in Fcc Fe, n.d.

[17] G. Kresse, J. Furthmüller, Phys. Rev. B - Condens. Matter Mater. Phys. 54 (1996) 11169.

[18] P.E. Blöchl, Phys. Rev. B 50 (1994) 17953.

[19] G. Kresse, D. Joubert, Phys. Rev. B 59 (1999) 11.

[20] J.P. Perdew, K. Burke, M. Ernzerhof, Phys. Rev. Lett. 77 (1996) 3865.

[21] H.C. Herper, E. Hoffmann, P. Entel, Phys. Rev. B 60 (1999) 3839.

[22] D.E. Jiang, E.A.E. Carter, Phys. Rev. B 71 (2005) 045402.

[23] N.I. Medvedeva, D.C. Van Aken, J.E. Medvedeva, J. Phys. Condens. Matter 22 (2010) 316002.

[24] R.C. Ruhl, M. Cohen, Trans. AIME 245 (1969).

[25] N.I. Medvedeva, M.S. Park, D.C. Van Aken, J.E. Medvedeva, J. Alloys Compd. 582 (2014) 475.

[26] V. Massardier, E. Le Patezour, M. Soler, J. Merlin, Metall. Mater. Trans. A 36 (2005) 1745.

[27] T. Hickel, S. Sandlöbes, R.K.W. Marceau, A. Dick, I. Bleskov, J. Neugebauer, D. Raabe, Acta Mater. 75 (2014) 147.

[28] A. Dick, T. Hickel, J. Neugebauer, Steel Res. Int. 80 (2009) 603.

[29] S. Kibey, J.B.J.B. Liu, M.J.J.M. Curtis, D.D.D. Johnson, H. Sehitoglu, Acta Mater. 54 (2006) 2991.

[30] T. Hickel, A. Dick, B. Grabowski, F. Körmann, J. Neugebauer, Steel Res. Int. 80 (2009) 4.

SECTION

4. SUMMARY AND CONCLUSIONS

First-principles methods were used to investigate interactions at the electronic level for two key components of advanced high strength steel alloy design: carbide formation and stacking fault energy. Bulk, surface, and interface properties of vanadium carbide as a function of substoichiometry and niobium defects were investigated as well as the effect of alloying additions on the stacking fault energy of fcc iron.

Carbon vacancies were shown to stabilize substoichiometric vanadium carbide VCx through a combination of increased local V-C bond strength and an increased metallic V-V interactions. The ordered structures V_8C_7 and V_6C_5 resulted in localized Vc – V – C – V – Vc ordering giving rise to a pair of strong V-C bonds. Metallic V-V interactions were increased in the second coordination sphere of a carbon vacancy. Examination of the VC_x free surface showed that the surface energy is minimized when there are no carbon vacancies in the outer two layers, enabling the (surface/Vc) – V – C – V – Vc ordering. In the case of the Fe/VCx interface however, carbon vacancies act to stabilize the interface.

Niobium defects in substoichiometric VC_x were shown have no substitutional site preference to be near a carbon vacancy. Additionally, carbon vacancies were shown to be more effective at stabilizing VC than NbC, resulting in more significant local structure relaxations around carbon vacancies in VC_x than NbC_x indicating a stronger directional bonding interaction for Nb than V. VC and NbC were shown to be completely immiscibile at 0K although at elevated temperatures a solid solution would likely exist enabling mixed-metal (V,Nb)C precipitation in steel, as indeed observed experimentally. Furthermore, niobium-defects in VC were shown to minimize surface energy when located at the carbide surface.

Explicit calculations of stacking fault energy indicate that only Mn additions decrease the intrinsic stacking fault energy of FCC iron. The effect of Cr was shown to be negligible at low concentrations whereas the effect of Si may be complex and reduce the

stacking fault energy at high concentrations. Intrinsic stacking fault energy was shown to follow a parabolic trend across the 3d and 4d elements with minimums for Mn and Tc, both having one fewer valence electron than Fe. All 4d elements increased stacking fault energy as a result of additional strain due to misfit. The unstable stacking fault energy was shown to decrease for all alloying additions considered and again followed a parabolic trend, with maximums at Fe and Rh in the 3*d* and 4*d* elements respectively. Thermodynamic modeling of SFE using an implicit approach indicated that inclusion of magnetic effects has a significant effect on implicit calculations of SFE as compared with the energetic shifting effect in the explicit calculations.

5. RECOMMENDATIONS FOR FUTURE WORK

5.1. IRON / VANADIUM CARBIDE INTERFACE

Transition metal carbides TiC and VC have recently been experimentally observed to act as hydrogen traps in high strength steels.[70], [136] Alloying with carbide formers for the purpose of trapping hydrogen and thereby reducing or eliminating hydrogen embrittlement would be beneficial for the high-Mn and third generation AHSS steel systems. Following the results of the first paper, indicating the surface energy of vanadium carbide is stabilized when carbon stoichiometry is maintained in the outer two atomic layers and that niobium defects further stabilize the surface, the role of carbon vacancies and niobium defects on the Fe/VC_x interface behavior should be examined.

Preliminary calculations have been performed for the nonmagnetic ferrite/VCx interface. The Kurdjumov-Sachs orientation relationship was assumed, yielding an interface orientation of $(001)_{VC}$ // $(001)_{\alpha}$ and $[110]_{VC}$ // $[100]_{\alpha}$. The layer alignment was such that the surface Fe-atoms are aligned vertically with the C-atoms in the surface layer of the carbide as this configuration has been shown to be preferred in similar metal – metal carbide/nitride systems. The slab thickness of 5-layers and 9-layers for the Fe and VC_x respectively were determined to be sufficiently thick to converge the surface energy. The interface simulation cell consisted of an Fe-slab, followed by a VC-slab and again a repetition of the Fe-slab to create two identical Fe/VC interfaces. The Fe-slabs were separated by a minimum vacuum of 10Å to prevent interaction. Each slab was fully relaxed to within 0.05eV/Å force acting on each ion. In these preliminary results, the interface was not relaxed, however due to the observed surface rippling, the interface should be relaxed to ensure the relative interface stability does not change.

Calculations were performed for four VC-slab configurations: stoichiometric VC, VCx with 50% carbon vacancies in the outer, first sublayer, and second sublayer. For symmetry, the carbon vacancies were introduced from both free surfaces. As carbon vacancies move into the bulk of the vanadium carbide, the interface is stabilized as shown in Figure 5.1. Further the separation distance is decreased by 1% as the carbon vacancies are moved into the bulk of the vanadium carbide.

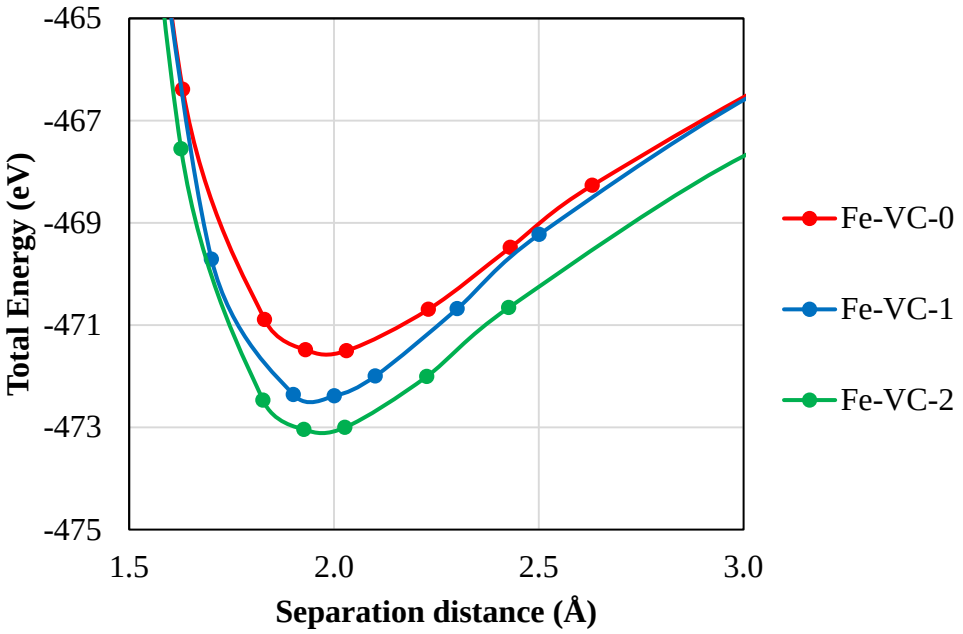

Figure 5.1 Total energy as a function of slab separation distance for Fe/VCx

Estimates of the work of adhesion were calculated based on the universal binding energy relation (UBER) and are shown in Figure 5.2.[137] Equation 11 represents the UBER for the given geometry where W_{ad} is the work of adhesion, E_i are the total energies of the *i* components, and SA is the surface area one interface.

$$W_{ad} = (2 * E_{Fe\text{-}slab} + E_{VC\text{-}slab} - E_{Fe/VC/Fe}) / (2 * SA_{Fe/VC}) \quad (11)$$

W_{ad} is minimized when the carbon vacancies are two sublayers removed from the interface corresponding to the lowest energy state, corresponding to the same W_{ad} as the stoichiometric VC. Similar calculations were performed for Fe-slabs containing carbon in octahedral interstitial sites with the most stable configuration corresponding to carbon

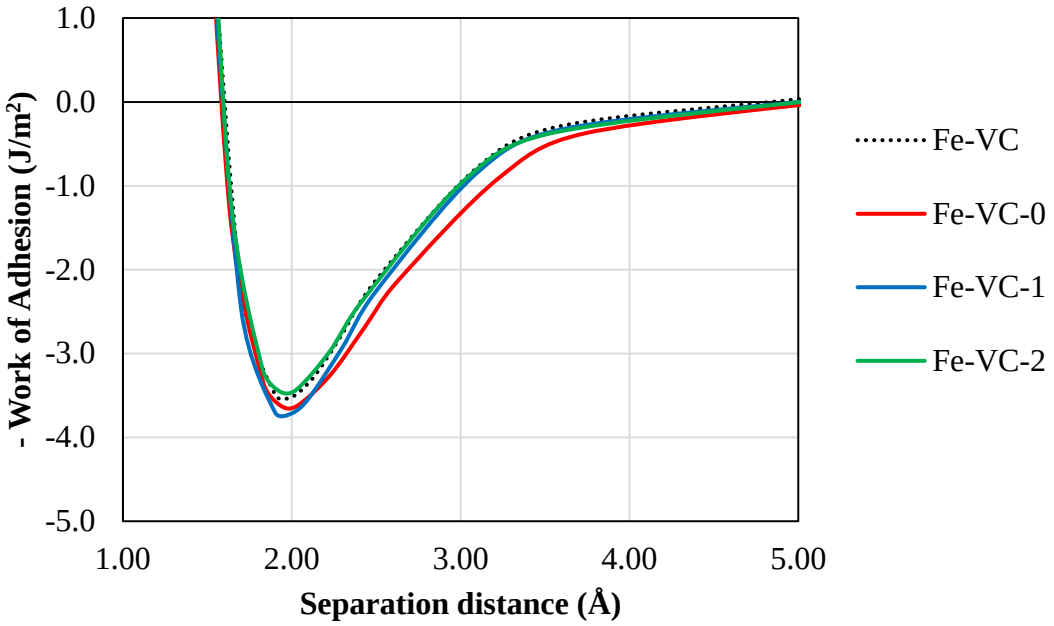

Figure 5.2 Work of adhesion as a function of separation distance for Fe/VCx derived using the Universal Binding Energy Relation

atoms removed from the two layers nearest the interface and removed into the Fe-bulk. These results suggest a positive driving force for carbon diffusion out of a stoichiometric carbide into the surrounding ferritic matrix.

Additional calculations should be performed to confirm these preliminary results allowing for relaxation of the Fe/VC interface as the surface rippling observed in the VC-slab may be altered when in proximity to the Fe-slab. Further the hydrogen trapping potential of the fcc Fe / VC interface as a function of carbon vacancies and niobium concentration should be assessed. Additionally, effects of magnetism should also be taken into account.

5.2. MAGNETO-VOLUME INSTABILITY EFFECT ON STACKING FAULT ENERGY IN FCC IRON

The formation of a stacking fault results in localized volumetric changes. In the fcc structure, iron has both a low-spin and high-spin ferromagnetic state corresponding to local minima in the volume – free energy curve shown in Figure 1.3. The formation of a stacking fault may alter the local magnetic state in a ferromagnetic iron system and thereby significantly affect the resulting stacking fault energy. Therefore, magnetic calcualtions of the low-spin and high-spin ferromagnetic states as well as antiferromagnetic states on Fe are expected to shed light on the role of magneto-volume effects in the deformation mechanisms.

5.3. TWIP- AND TRIP-ABILITY OF FCC IRON FROM FIRST-PRINCIPLES

The intrinsic stacking fault energy (SFE) of fcc iron is commonly used to characterize the dominant deformation mechanism in austenitic alloys as it may be determined experimentally. The influence of the unstable stacking fault energy, which may be described as the barrier to forming a stacking fault, is not well understood. In the development of third generation advanced high strength steels the question whether a stacking fault proceeds to nucleate a twin or a ε-martensite plate remains unsolved. The progression from an unfaulted lattice, to a stacking fault, to a twin or ε-martensite plate is schematically represented in Figure 5.3.

The twinnability, or probability of forming a twin, of an fcc material has been described mathematically using the stacking fault energy, unstable stacking fault energy, and unstable twinning energy and has been calculated for fcc metals, excluding austenite.[138]–[140] A fundamental examination of the effects of alloying additions on the propensity to form a twin or an ε-martensite plate following an initial stacking fault, a second probability termed tripability must also be calculated. Initial unrelaxed results for pure Fe are presented in Figure 5.4.

The energy barrier to form either a twin or an ε-martensite plate is significantly higher than that of forming an unstable stacking fault, although the formation of an epsilon plate has a slightly lower energy barrier of 2953 mJ/m^2 compared to 3191 mJ/m^2.

The result of force relaxation may alter the results and should be considered in future work.

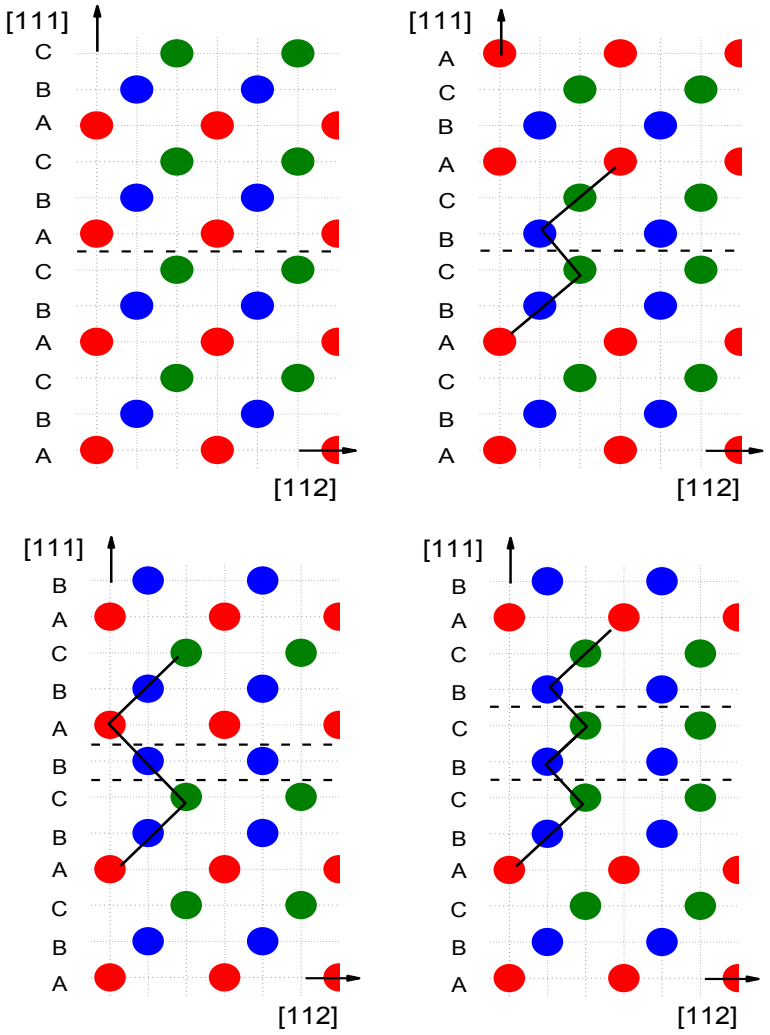

Figure 5.3 Schematic representation of the formation of a twin or ε-martensite plate in fcc iron. A) unfaulted fcc Fe lattice B) nucleation of leading partial dislocation or stacking fault C_1) nucleation of twinning partial C_2) nucleation of ε-martensite plate

Alloying effects may also significantly affect the twinnability and tripability of fcc iron. Alloying additions of Mn, Cr, Al, and Si are the most prominent in current alloy design and should be considered. Additionally, the location of alloying elements with respect to the original stacking fault and twining- or tripping-plane may significantly affect the results.

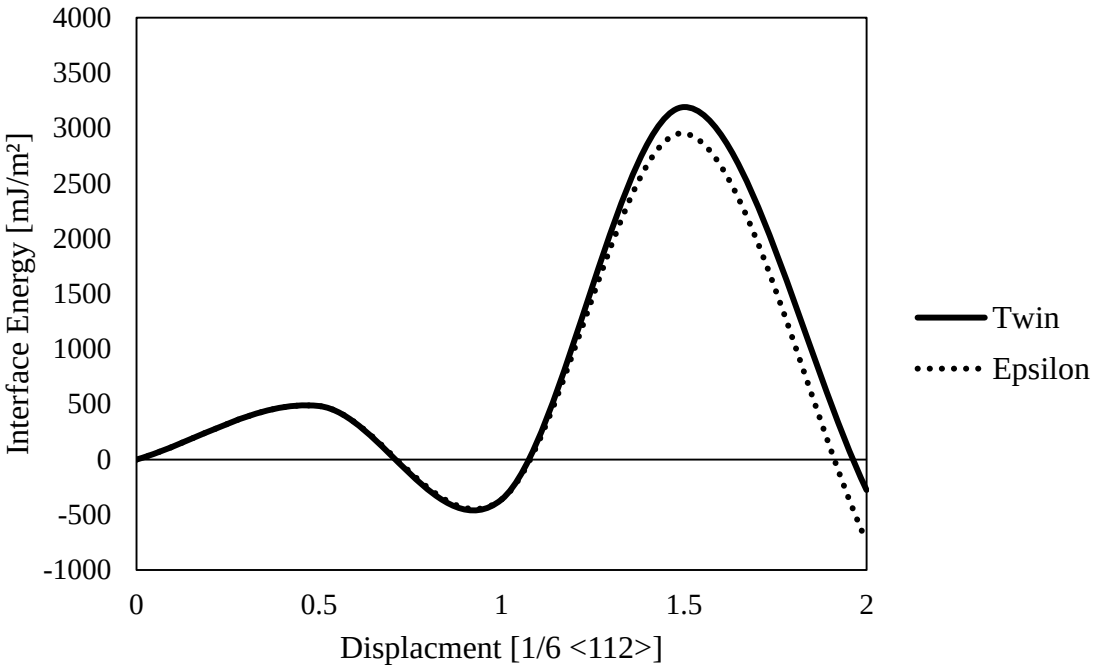

Figure 5.4 Interface energy of fcc iron after the creation of an unstable sacking fault (x = 0.5), an intrinsic stacking fault (x = 1.0), and the unstable energy to create a twin or ε-martensite plate (x = 1.5)

APPENDIX A

SUPPLEMENTAL DATA: VANADIUM AND NIOBIUM CARBIDE ENERGY AND STRUCTURE

Table B.1. Raw data from VASP carbide stability calculations. Optimized energy is after full relaxation of lattice parameter and ion positions to forces less than 0.02 eV/Å.

		# of atoms			Total Energy (eV)			Enthalpy of Formation (eV)				Defect F. Energy (eV)	
Structure	Description	V	C	Nb	initial	optimized	ΔE	initial	per M-atom	optimized	per atom	per M-atom	initial	optimized
C (graphite)	element	0	4	0		-36.803								
V	element	1	0	0		-8.950								
Nb	element	0	0	1		-10.087								
VC	bulk	1	1	0		-19.012				-0.861	-0.431	-0.861		
VC(4)	bulk	4	4	0		-76.047				-3.444	-0.430	-0.861		
VC(4)	25%Nb	3	4	1		-76.703				-2.963	-0.370	-0.741		0.481
VC(4)	50%Nb	2	4	2		-77.848				-2.970	-0.371	-0.743		0.473
VC(4)	75%Nb	1	4	3		-79.310				-3.295	-0.412	-0.824		0.149
NbC(4)	bulk	0	4	4		-80.974				-3.821	-0.478	-0.955		
NbC(4)	25%V	1	4	3		-79.310				-3.295	-0.412	-0.824		0.526
NbC(4)	50%V	2	4	2		-77.848				-2.970	-0.371	-0.743		0.851
NbC	bulk	0	1	1		-20.243				-0.955	-0.478	-0.955		
VC(32)	bulk	32	32	0		-608.387				-27.565	-0.431	-0.861		
	Nb-V1	31	32	1	-608.622	-609.078	-0.456	-26.662	-0.833	-27.118	-0.424	-0.847	0.902	0.446
V8C7	bulk	32	28	0		-576.545				-32.525	-0.542	-1.016		
	Nb-V1	31	28	1	-576.865	-577.240	-0.375	-31.708	-0.991	-32.083	-0.535	-1.003	0.817	0.442
	Nb-V2	31	28	1	-576.709	-577.214	-0.504	-31.552	-0.986	-32.057	-0.534	-1.002	0.973	0.469
VC(18)	bulk	18	18	0		-342.210				-15.497	-0.430	-0.861		
	Nb-V1	17	18	1	-342.448	-342.942	-0.494	-14.598	-0.811	-15.092	-0.419	-0.838	0.900	0.405
V6C5	bulk	18	15	0		-317.675				-18.565	-0.563	-1.031		
	Nb-V1	17	15	1	-317.832	-318.431	-0.599	-17.584	-0.977	-18.183	-0.551	-1.010	0.981	0.382
	Nb-V2	17	15	1	-317.859	-318.438	-0.578	-17.611	-0.978	-18.190	-0.551	-1.011	0.953	0.375
	Nb-V3	17	15	1	-317.835	-318.421	-0.586	-17.587	-0.977	-18.173	-0.551	-1.010	0.978	0.392
VC(9)	bulk	9	9	0		-171.110				-7.754	-0.431	-0.862		
	Nb-V1	8	9	1	-171.331	-171.868	-0.536	-6.838	-0.760	-7.374	-0.410	-0.819	0.916	0.380

Table B.2. Calculation Parameters

Structure	Description	k-points			NKPTS (irr kpts)	ENCUT (eV)	NBANDS
C	element	13	13	11	126	342.4	12
V	element	15	15	15	120	342.4	12
Nb	element	15	15	15	120	342.4	12
VC	bulk	17	17	17	165	342.4	12
VC(4)	bulk	15	15	15	120	342.4	48
	25%Nb	15	15	15	120	342.4	48
	50%Nb	15	15	15	288	342.4	48
NbC(4)	bulk	15	15	15	120	342.4	48
	25%V	15	15	15	120	342.4	48
NbC	bulk	17	17	17	165	342.4	12
VC(32)	bulk	11	11	11	56	342.4	360
	Nb-V1	11	11	11	56	342.4	360
V8C7	bulk	9	9	9	35	342.4	348
	Nb-V1	9	9	9	125	342.4	348
	Nb-V2	9	9	9	365	342.4	350
VC(18)	bulk	11	11	9	120	342.4	212
	Nb-V1	11	11	9	120	342.4	212
V6C5	bulk	11	11	9	120	342.4	194
	Nb-V1	11	11	9	545	342.4	194
	Nb-V2	11	11	9	545	342.4	194
	Nb-V3	11	11	9	545	342.4	194
VC(9)	bulk	11	11	11	146	342.4	106
	Nb-V1	11	11	11	666	342.4	106

Table B.3. Empty Sublattice Calculation Raw Data

	Energy (eV)			Interaction (%)			M-C bonds		M-M bonds	
	Total	M only	C only	M - C	Total	M only	C only	M - C	# bonds	% / bond	# bonds	% / bond
$(VC)_{32}$	-608.4	-265.2	-97.0	-246.2	100%	43.6%	15.9%	40.5%	192	0.211%	192	0.227%
$V_{32}C_{31}$	-600.0	-265.1	-92.9	-242.0	100%	44.2%	15.5%	40.3%	186	0.217%	192	0.230%
V_8C_7	-576.5	-264.4	-80.0	-232.1	100%	45.9%	13.9%	40.3%	168	0.240%	192	0.239%
V_6C_5	-317.7	-148.8	-42.3	-126.5	100%	46.9%	13.3%	39.8%	90	0.442%	108	0.434%
$(NbC)_{32}$	-647.8	-302.8	-77.4	-267.7	100%	46.7%	11.9%	41.3%	192	0.215%	192	0.243%
$Nb_{32}C_{31}$	-638.9	-302.7	-74.0	-262.3	100%	47.4%	11.6%	41.0%	186	0.221%	192	0.247%
Nb_6C_5	-225.6	-113.7	-22.5	-89.5	100%	50.4%	10.0%	39.7%	60	0.661%	72	0.700%

APPENDIX B

SUPPLEMENTAL DATA: TABULATED STACKING FAULT ENERGY DATA

Table C.1. Raw data for stacking fault energy calculations of 6-layer nonmagnetic fcc Fe supercells with 1 of 4 atoms in a layer adjacent to the stacking fault substituted by X.

Alloying Addition	Energy (eV)					SFE [mJ/m²]			
	unfaulted	ISF	ISF (relaxed)	USF	USF (relaxed)	ISF	ISF (relaxed)	USF	USF (relaxed)
Al	-190.340	-190.514	-190.670	-189.883	-189.965	-134	-255	353	289
Si	-192.724	-193.005	-193.079	-192.260	-192.345	-218	-276	360	294
P	-192.527	-192.818	-192.873	-192.069	-192.211	-227	-270	357	246
S	-189.604	-189.838	-189.904	-189.189	-189.363	-182	-233	323	188
Ti	-194.421	-194.472	-194.690	-193.873	-193.998	-39	-207	421	325
V	-195.563	-195.852	-195.957	-194.992	-195.087	-224	-305	442	368
Cr	-195.717	-196.171	-196.241	-195.122	-195.205	-353	-407	462	398
Mn	-195.195	-195.706	-195.776	-194.573	-194.656	-398	-452	484	420
Fe	-194.308	-194.779	-194.847	-193.666	-193.747	-367	-420	501	437
Co	-193.104	-193.483	-193.540	-192.474	-192.549	-295	-340	491	432
Ni	-191.454	-191.720	-191.779	-190.880	-190.946	-207	-253	447	396
Cu	-188.958	-189.150	-189.245	-188.460	-188.526	-148	-222	386	335
Zn	-186.474	-186.638	-186.784	-186.031	-186.106	-127	-239	342	284
Zr	-193.809	-193.524	-193.949	-193.236	-193.434	216	-106	434	284
Nb	-195.816	-195.781	-196.033	-195.227	-195.382	27	-165	449	331
Mo	-196.733	-196.985	-197.106	-196.136	-196.265	-193	-286	458	359
Tc	-196.368	-196.785	-196.863	-195.751	-195.874	-321	-382	475	380
Ru	-195.105	-195.525	-195.600	-194.446	-194.571	-324	-381	507	411
Rh	-193.185	-193.485	-193.557	-192.513	-192.625	-231	-286	517	430
Pd	-190.450	-190.566	-190.660	-189.827	-189.931	-89	-160	478	398
Ag	-186.301	-186.265	-186.433	-185.749	-185.858	28	-101	422	338
Cd	-183.995	-183.871	-184.143	-183.488	-183.616	94	-112	385	287

BIBLIOGRAPHY

[1] T. Hickel, B. Grabowski, F. Körmann, and J. Neugebauer, "Advancing density functional theory to finite temperatures: Methods and applications in steel design," *J. Phys. Condens. Matter*, vol. 24, no. 5, p. 053202, Feb. 2012.

[2] World Steel Association, "World Auto Steel." [Online]. Accessed August 2014, Available: http://www.worldautosteel.org/.

[3] T. Epicier, D. Acevedo, and M. Perez, "Crystallographic structure of vanadium carbide precipitates in a model Fe-C-V steel," *Philos. Mag.*, vol. 88, no. 1, pp. 31–45, Jan. 2008.

[4] M. Sawada, K. Adachi, and T. Maeda, "Effect of V, Nb and Ti addition and annealing temperature on microstructure and tensile properties of AISI 301L stainless steel," *ISIJ Int.*, vol. 51, pp. 991–998, 2011.

[5] M. Gómez and S. F. Medina, "Role of microalloying elements in the microstructure of hot rolled steels," *Int. J. Mater. Res.*, vol. 102, pp. 1197–1207, 2011.

[6] G. Miyamoto, R. Hori, B. Poorganji, and T. Furuhara, "Interphase precipitation of VC and resultant hardening in V-added medium carbon steels," *ISIJ Int.*, vol. 51, pp. 1733–1739, 2011.

[7] D. A. Reyes, M. Perez, S. Pecoraro, A. Vincent, T. Epicier, and P. Dierickx, "Vanadium carbide dissolution during austenitisation of a model microalloyed FeCV steel," vol. 500–501, pp. 695–702, 2005.

[8] H. Najafi, J. Rassizadehghani, and S. Asgari, "As-cast mechanical properties of vanadium/niobium microalloyed steels," *Mater. Sci. Eng. A*, vol. 486, pp. 1–7, 2008.

[9] V. N. Lipatnikov, "Phase equilibria, phases and compounds in the V–C system," *Russ. Chem. Rev.*, vol. 74, no. 8, pp. 697–723, Aug. 2005.

[10] R. G. Avatbé, "The thermodynamic stability of monocarbides of transition metals from sub groups IV – VI," *Powder Metall. Met. Ceram.*, vol. 4, pp. 122–128, 1965.

[11] A. I. Gusev, A. A. Rempel, A. J. Magerl, and A.A.Rempel, *Disorder and Order in Strongly Nonstoichiometric Compounds: Transition Metal Carbides, Nitrides, and Oxides*. New York: Springer, 2001.

[12] A. A. Rempel, "Atomic and vacancy ordering in nonstoichiometric carbides," *Physics-Uspekhi*, vol. 39, pp. 31–56, 1996.

[13] V. N. Lipatnikov, A. I. Gusev, P. Ettmayer, and W. Lengauer, “Phase transformations in non-stoichiometric vanadium carbide,” *J. Phys. Condens. Matter*, vol. 11, pp. 163–184, 1999.

[14] S. I. Alyamovskii, P. V Gel’d, and I. I. Matvcenko, “Cusic phases of vanadium carbides,” *J. Struct. Chem.*, vol. 2, pp. 412–415, 1961.

[15] M. H. Lewis, J. Billingham, and P. S. Bell, *Electron Microscopy and Structure of Materials*. Berkeley, CA: University of California Press.

[16] A. W. Henfrey and B. E. F. Fender, “A neutron diffraction investigation of V8C7,” *Acta Crystallogr. Sect. B*, vol. 26, pp. 1882–1883, 1970.

[17] C. H. De Novion, R. Lorenzelli, and P. Costa, “Superlattice structure in vanadium carbide VC 1-x,” *Compt. Rend. Acad. Sci. Paris*, vol. 263, pp. 775–778, 1966.

[18] C. Froidevaux and D. Rossier, “NMR investigation of the atomic and electronic structure of vanadium and niobium carbides,” *J. Phys. Chem. Solids*, vol. 28, pp. 1197–1209, 1967.

[19] J. D. Venables, D. Kahn, and R. G. Lye, “Structure of the ordered compound V6C5,” *Philos. Mag.*, vol. 18, no. 151, pp. 177–192, 1968.

[20] R. Kesri and S. Hamar-Thibault, “Structures ordonnees a longue distance dans les carbures mc dans les fontes,” *Acta Metall.*, vol. 36, pp. 149–166, 1988.

[21] J. Billingham, P. S. Bell, and M. H. Lewis, “A superlattice with monoclinic symmetry based on the compound V6C5,” *Philos. Mag.*, vol. 25, no. 3, pp. 661–671, Nov. 1972.

[22] B.-J. Lee, D. N. Lee, L. Byeong-Joo, and L. Dong Nyung, “A thermodynamic study on the V-C and FE-V systems,” *Calphad*, vol. 15, pp. 283–291, Sep. 1991.

[23] T. Epicier, M. G. Blanchin, P. Ferret, and G. Fuchs, “High-resolution electron microscopy imaging of the carbon vacancy superlattice in the ordered carbide VC1−x,” *Philos. Mag. A*, vol. 59, pp. 885–906, Nov. 1989.

[24] A. I. Gusev and A. A. Rempel, “Vacancy distribution in ordered Me6C5-type carbides,” *J. Phys. C Solid State Phys.*, vol. 20, pp. 5011–5025, 1987.

[25] A. A. Rempel and A. I. Gusev, “Short-Range Order in Superstructures,” *Phys. Status Solidi*, vol. 160, pp. 389–402, 1990.

[26] L. Adnane, R. Kesri, and S. Hamar-Thibault, “Vanadium carbides formed from the melt by solidification in Fe-V-X-C alloys (X = Cr, Mo, Nb),” *J. Alloys Compd.*, vol. 178, pp. 71–84, 1992.

[27] R. Kesri and M. Duran-Charre, “Metallurgical structure and phase diagram of Fe-C-V system: comparison with other systems forming MC carbides,” *Mater. Sci. Technol.*, vol. 4, pp. 692–699, 1988.

[28] G. H. Emmons and W. S. Williams, “Thermodynamics of order-disorder transformations in vanadium carbide,” *J. Mater. Sci.*, vol. 18, pp. 2589–2602, 1983.

[29] G. L. Dunlop and D. A. Porter, “SECONDARY PRECIPITATION OF ORDERED V6C5 AND (V, Ti)6C5 PARTICLES IN FERRITE,” *Scand. J. Metall.*, vol. 6, pp. 19–20, 1977.

[30] M. Nöhrer, S. Zamberger, and H. Leitner, “Strain-Induced Precipitation Behavior of a Nb-Ti-V Steel in the Austenite Phase Field,” *Steel Res. Int.*, vol. 84, pp. 827–836, 2013.

[31] A. Osawa and M. Oya, “No Title,” *Sci. Rep. Tohoku Univ. First Ser.*, vol. 19, 1930.

[32] Y. Herrera, I. C. Grigorescu, J. Ramirez, C. Di Rauso, and M. H. Staia, “Microstructural characterization of vanadium carbide laser clad coatings,” *Surf. Coatings Technol.*, vol. 108, pp. 308–311, 1998.

[33] R. G. Baker and J. Nutting, “Precipitation Processes in Steels,” *Iron Steel Inst.*, vol. ISI Specia, pp. 1–22, 1959.

[34] V. N. Lipatnikov, A. I. Gusev, P. Ettmeier, and W. Lengauer, “Order-disorder phase transformations and specific heat of nonstoichiometric vanadium carbide,” *Phys. Solid State*, vol. 41, pp. 474–480, 1999.

[35] L. W. Shacklette and W. S. Williams, “Scattering of electrons by vacancies through an order-disorder transition in vanadium carbide,” *J. Appl. Phys.*, vol. 42, pp. 4698–4703, 1971.

[36] W. S. Williams, “Influence of Vacancy Ordering on Thermophysical Properties of Vanadium Carbide,” *High Temp. - High Press.*, vol. 4, pp. 627–638, 1972.

[37] A. I. Gusev, “Sequence of phase transformations in the formation of superstructures of the M6C5 type in nonstoichiometric carbides,” *J. Exp. Theor. Phys.*, vol. 109, pp. 417–433, 2009.

[38] A. A. Rempel, A. I. Gusev, and G. P. Shveikin, “Thermodynamic Calculation of the Phase Diagrams of the VC 0.88-NbC, VC 0.88-TaC, VC 0.88-HfC, NbC-TaC, and NbC-HfC Systems,” *Russ. J. Phys. Chem.(Engl. Transl.)*, vol. 58, no. 9, pp. 1322–1325, 1984.

[39] N. M. Volkova and P. V. Gel'd, "Heats of formation of cubic vanadium carbides," *Izv. Vyss. Ucheb. Zaved., Tsvet Met.*, vol. 89, p. 23, 1963.

[40] V. Ozolins and J. Häglund, "First-principles study of effective cluster interactions and enthalpies of formation of substoichiometric VC1-x," *Phys. Rev. B*, vol. 48, no. 8, pp. 5069–5076, 1993.

[41] H. Liu, J. Zhu, Y. Liu, and Z. Lai, "First-principles study on the mechanical properties of vanadium carbides VC and V4C3," *Mater. Lett.*, vol. 62, pp. 3084–3086, 2008.

[42] V. P. Zhukov and V. A. Gubanov, "The study of the energy band structures of TiC, VC, Ti4C3 and V4C3 by the LMTO-ASA method," *J. Phys. Chem. Solids*, vol. 48, pp. 187–195, 1987.

[43] W. Wolf, R. Podloucky, T. Antretter, and F. D. Fischer, "First-principles study of elastic and thermal properties of refractory carbides and nitrides," *Philos. Mag. B*, vol. 79, pp. 839–858, 1999.

[44] F. Vines, C. Sousa, P. Liu, J. A. Rodriguez, and F. Illas, "A systematic density functional theory study of the electronic structure of bulk and (001) surface of transition-metals carbides," *J. Chem. Phys.*, vol. 122, 2005.

[45] K. B. Joshi and U. Paliwal, "First-principles study of structural and bonding properties of vanadium carbide and niobium carbide," *Phys. Scr.*, vol. 80, 2009.

[46] Y. Liu, Y. Jiang, R. Zhou, and J. Feng, "First principles study the stability and mechanical properties of MC (M = Ti, V, Zr, Nb, Hf and Ta) compounds," *J. Alloys Compd.*, vol. 582, pp. 500–504, Jan. 2014.

[47] P. Soni, G. Pagare, and S. P. Sanyal, "Structural, high pressure and elastic properties of transition metal monocarbides: A FP-LAPW study," *J. Phys. Chem. Solids*, vol. 72, pp. 810–816, 2011.

[48] E. K. Storms and N. H. Krikorian, "THE NIOBIUM—NIOBIUM CARBIDE SYSTEM," *J. Phys. Chem.*, 1960.

[49] T. N. Baker, "Processes, microstructure and properties of vanadium microalloyed steels," *Mater. Sci. Technol.*, vol. 25, pp. 1083–1107, 2009.

[50] M. J. Crooks, A. J. Garratt-Reed, J. B. V Sande, and W. S. Owen, "Precipitation and Recrystallization in Some Vanadium and Vanadium-Niobium Microalloyed Steels," *Metall. Trans. A*, vol. 12, pp. 1999–2013, 1981.

[51] S. Shanmugam, M. Tanniru, R. D. K. Misra, D. Panda, and S. Jansto, "Precipitation in v bearing microalloyed steel containing low concentrations of Ti and Nb," *Mat. Sc. Tech.*, vol. 21, pp. 883–892, 2005.

[52] V. P. Zhukov, V. A. Gubanov, O. Jepsen, N. E. Christensen, and O. K. Andersen, "Calculated energy-band structures and chemical bonding in titanium and vanadium carbides, nitrides and oxides," *J. Phys. Chem. Solids*, vol. 49, pp. 841–849, 1988.

[53] Y. I. Rogovoi, "Effect of structural vacancies on the nature of metal - Metal and metal - Carbon bonds in cubic monocarbides," *Powder Metall. Met. Ceram.*, vol. 38, no. 405, pp. 44–50, 1999.

[54] Y. I. Rogovoi, "Potentials of metal-metal and metal-carbon bonds in cubic monocarbides," *Powder Metall. Met. Ceram.*, vol. 36, pp. 84–92, 1997.

[55] J. P. Landesman, A. N. Christensen, C. H. de Novion, N. Lorenzelli, and P. Convert, "Order-disorder transition and structure of the ordered vacancy compound Nb 6 C 5 : powder neutron diffraction studies," *J. Phys. C Solid State Phys.*, vol. 18, p. 809, 1985.

[56] C. H. De Novion and J. P. Landesman, "Order and Disorder in Transition Metal Carbides and Nitrides: Experimental and Theoretical Aspects," *Pure Appl. Chem.*, vol. 57, pp. 1391–1402, 1985.

[57] D. Rafaja, W. Lengauer, P. Ettmayer, and V. . N. Lipatnikov, "Rietveld analysis of the ordering in V8C7," *J. Alloys Compd.*, vol. 269, no. 1–2, pp. 60–62, May 1998.

[58] A. Deb and A. K. Chatterjee, "Compton scattering study on the electronic properties of niobium carbide and niobium nitride," *Radiat. Phys. Chem.*, vol. 57, pp. 135–144, 2000.

[59] A. Kalemos, T. H. Dunning Jr, and A. Mavridis, "The electronic structure of vanadium carbide, VC," *J. Chem. Phys.*, vol. 123, pp. 1–8, 2005.

[60] G. L. Gutsev, L. Andrews, and C. W. Bauschlicher Jr, "Similarities and differences in the structure of 3d-metal monocarbides and monoxides," *Theor. Chem. Acc.*, vol. 109, pp. 298–308, 2003.

[61] T. Das, S. Deb, and A. Mookerjee, "Study of electronic structure and elastic properties of transition metal and actinide carbides," *Phys. B Condens. Matter*, vol. 367, pp. 6–18, 2005.

[62] S. V Didziulis, K. D. Butcher, and S. S. Perry, “Small Cluster Models of the Surface Electronic Structure and Bonding Properties of Titanium Carbide, Vanadium Carbide, and Titanium Nitride,” *Inorg. Chem.*, vol. 42, pp. 7766–7781, Jan. 2003.

[63] F. Z. Abderrahim, H. I. Faraoun, and T. Ouahrani, “Structure, bonding and stability of semi-carbides M 2C and sub-carbides M 4C (M=V, Cr, Nb, Mo, Ta, W): A first principles investigation,” *Phys. B Condens. Matter*, vol. 407, pp. 3833–3838, 2012.

[64] S. H. Jhi, S. G. Louie, M. L. Cohen, and J. Ihm, “Vacancy hardening and softening in transition metal carbides and nitrides,” *Phys. Rev. Lett.*, vol. 86, pp. 3348–3351, 2001.

[65] G. E. Hollox, “Microstructure and mechanical behavior of carbides,” *Mater. Sci. Eng.*, vol. 3, pp. 121–137, 1968.

[66] H. Guanghi and C. Niansun, *HSLA Steels: Processing, Properties and Applications*. Warrendale: The Minerals, Metals & Materials Society.

[67] H. Chi, D. Ma, J. Liu, Z. Chen, and Q. Yong, “Effect of Different Nb-V Contents on Microstructure and Mechanical Properties of CR8-type Work Die Steel,” 2010.

[68] J.-H. Ahn, Y.-J. Kim, S. Lee, and H. Chung, “Effect of niobium on the mechanical properties of powder-metallurgy processed high-speed steels,” *Zeitschrift für Met.*, vol. 96, pp. 1426–1430, 2005.

[69] S. Kheirandish, “Effect of Ti and Nb on the formation of carbides and the mechanical properties in as-cast AISI-M7 high-speed steel,” *ISIJ Int.*, vol. 41, pp. 1502–1509, 2001.

[70] J. Takahashi, K. Kawakami, and T. Tarui, “Direct observation of hydrogen-trapping sites in vanadium carbide precipitation steel by atom probe tomography,” *Scr. Mater.*, vol. 67, no. 2, pp. 213–216, Jul. 2012.

[71] K. Kawakami and T. Matsumiya, “Numerical analysis of hydrogen trap state by TiC and V 4C 3 in bcc-Fe,” *ISIJ Int.*, vol. 52, pp. 1693–1697, 2012.

[72] W. Liu, X. Liu, W. T. Zheng, and Q. Jiang, “Surface energies of several ceramics with NaCl structure,” *Surf. Sci.*, vol. 600, pp. 257–264, 2006.

[73] H. W. Hugosson, O. Eriksson, U. Jansson, A. V Ruban, P. Souvatzis, and I. A. Abrikosov, “Surface energies and work functions of the transition metal carbides,” *Surf. Sci.*, vol. 557, pp. 243–254, 2004.

[74] H. H. Hwu and J. G. Chen, “Surface chemistry of transition metal carbides,” *Chem. Rev.*, vol. 105, pp. 185–212, 2005.

[75] J. R. Kitchin, J. K. Nørskov, M. A. Barteau, and J. G. Chen, “Trends in the chemical properties of early transition metal carbide surfaces: A density functional study,” *Catal. Today*, vol. 105, pp. 66–73, 2005.

[76] N. C. Chen, P. He, and D. C. Li, “First principles calculation of adhesion at Fe/WC interface,” *Adv. Mater. Res.*, vol. 129–131, pp. 808–813, Aug. 2010.

[77] D. J. Siegel, L. G. Hector Jr, and J. B. Adams, “First-principles study of metal–carbide/nitride adhesion: Al/VC vs. Al/VN,” *Acta Mater.*, vol. 50, pp. 619–631, 2002.

[78] N. Y. Park, J. H. Choi, P. R. Cha, W. S. Jung, S. H. Chung, and S. C. Lee, “First-principles study of the interfaces between fe and transition metal carbides,” *J. Phys. Chem. C*, vol. 117, pp. 187–193, 2013.

[79] J. H. Jang, C.-H. Lee, Y.-U. Heo, and D.-W. Suh, “Stability of (Ti, M)C (M = Nb, V, Mo and W) carbide in steels using first-principles calculations,” *Acta Mater.*, vol. 60, pp. 208–217, 2012.

[80] D. K. Matlock and J. G. Speer, “Third generation of AHSS: microstructure design concepts,” in *Microstructure and Texture in Steels*, Springer, 2009, pp. 185–205.

[81] Y. N. Dastur and W. C. Leslie, “Mechanism of Work Hardening in Hadfield Manganese Steel,” *Metall. Trans. A*, vol. 12 A, pp. 749–759, 1981.

[82] B. Hutchinson and N. Ridley, “On dislocation accumulation and work hardening in Hadfield steel,” *Scr. Mater.*, vol. 55, pp. 299–302, 2006.

[83] P. H. Adler, G. B. Olson, and W. S. Owen, “Strain Hardening of Hadfield Manganese Steel,” *Metall. Trans. A*, vol. 17 A, pp. 1725–1737, 1986.

[84] E. G. Astafurova, I. V Kireeva, Y. I. Chumlyakov, H. J. Maier, and H. Sehitoglu, “The influence of orientation and aluminium content on the deformation mechanisms of Hadfield steel single crystals,” *Int. J. Mater. Res.*, vol. 98, pp. 144–149, 2007.

[85] D. Canadinc, H. Sehitoglu, H. J. Maier, and Y. I. Chumlyakov, “Strain hardening behavior of aluminum alloyed Hadfield steel single crystals,” *Acta Mater.*, vol. 53, pp. 1831–1842, 2005.

[86] H. Aydin, E. Essadiqi, I.-H. H. Jung, and S. Yue, “Development of 3rd generation AHSS with medium Mn content alloying compositions,” *Mater. Sci. Eng. A*, vol. 564, pp. 501–508, Mar. 2013.

[87] G. B. Olson and M. Cohen, “A general mechanism of martensitic nucleation: Part I. General concepts and the FCC→ HCP transformation,” *Metall. Trans. A*, vol. 7, no. December, pp. 1897–1904, 1976.

[88] M. C. McGrath, D. C. Van Aken, N. I. Medvedeva, and J. E. Medvedeva, “Work Hardening Behavior in Steel with Multiple TRIP Mechanisms,” *Metall. Mater. Trans. A*, pp. 1–10, 2013.

[89] S. Allain, J. P. Chateau, O. Bouaziz, S. Migot, and N. Guelton, “Correlations between the calculated stacking fault energy and the plasticity mechanisms in Fe–Mn–C alloys,” *Mater. Sci. Eng. A*, vol. 387–389, no. 1–2 SPEC. ISS., pp. 158–162, Dec. 2004.

[90] S. Mahajan and G. Y. Chin, “Formation of deformation twins in f.c.c. crystals,” *Acta Metall.*, vol. 21, no. 10, pp. 1353–1363, Oct. 1973.

[91] S. Sato, E.-P. Kwon, M. Imafuku, K. Wagatsuma, and S. Suzuki, “Microstructural characterization of high-manganese austenitic steels with different stacking fault energies,” *Mater. Charact.*, vol. 62, no. 8, pp. 781–788, Aug. 2011.

[92] G. Frommeyer, U. Brüx, and P. Neumann, “Supra-Ductile and High-Strength Manganese-TRIP/TWIP Steels for High Energy Absorption Purposes.,” *ISIJ Int.*, vol. 43, no. 3, pp. 438–446, 2003.

[93] Y. Petrov, “Effect of carbon and nitrogen on the stacking fault energy of high-alloyed iron-based austenite,” *Zeitschrift für Met.*, vol. 94, no. 9, pp. 1012–1016, 2003.

[94] A. Saeed-Akbari, J. Imlau, U. Prahl, and W. Bleck, “Derivation and Variation in Composition-Dependent Stacking Fault Energy Maps Based on Subregular Solution Model in High-Manganese Steels,” *Metall. Mater. Trans. A*, vol. 40, no. 13, pp. 3076–3090, Oct. 2009.

[95] Y. K. Lee and C. S. Choi, “Driving force for γ→ ε martensitic transformation and stacking fault energy of γ in Fe-Mn binary system,” *Metall. Mater. Trans. A*, vol. 31, no. February, pp. 355–360, 2000.

[96] P. U. Y. Volosevich, V. N. Gridnev, Y. U. N. Petrov, and V. N. Grindnev, “Influence of Mn and the Stacking Fault Energy of Fe-Mn Alloys,” *Phys. Met. Met.*, vol. 42, no. 2, pp. 126–130, Jan. 1976.

[97] H. Schumann, “Einfluss der SFE auf den kristallographischen Umgitterungs-mechanismus der γ/α-Umwandlung in hochlegierten Stählen,” *J. Krist. Tech.*, vol. 10, 1974.

[98] N. I. Medvedeva, M. S. Park, D. C. Van Aken, and J. E. Medvedeva, “First-principles study of Mn, Al and C distribution and their effect on stacking fault energies in fcc Fe,” *J. Alloys Compd.*, vol. 582, pp. 475–482, Jan. 2014.

[99] H. Schumann, “Influence of the Stacking Fault Energy on the Crystallographic Mechnisms of γ/α-transformation in high-alloy steel,” *J. Krist. Tech.*, vol. 9, no. 10, pp. 1141–1152, 1974.

[100] A. Abbasi, A. Dick, T. Hickel, and J. Neugebauer, “First-principles investigation of the effect of carbon on the stacking fault energy of Fe–C alloys,” *Acta Mater.*, vol. 59, no. 8, pp. 3041–3048, May 2011.

[101] T. Hickel, A. Dick, B. Grabowski, F. Körmann, and J. Neugebauer, “Steel Design from Fully Parameter-Free Ab Initio Computer Simulations,” *Steel Res. Int.*, vol. 80, no. 1, pp. 4–8, 2009.

[102] S. Kibey, J. B. J. B. Liu, M. J. J. M. Curtis, D. D. D. Johnson, and H. Sehitoglu, “Effect of nitrogen on generalized stacking fault energy and stacking fault widths in high nitrogen steels,” *Acta Mater.*, vol. 54, no. 11, pp. 2991–3001, Jun. 2006.

[103] P. Denteneer and W. van Haeringen, “Stacking-fault energies in semiconductors from first-principles calculations,” *J. Phys. C Solid …*, vol. 20, pp. L883–L887, 1987.

[104] A. Dick, T. Hickel, and J. Neugebauer, “The Effect of Disorder on the Concentration-Dependence of Stacking Fault Energies in Fe 1-x Mn x – a First Principles Study,” *Steel Res. Int.*, vol. 80, pp. 603–608, 2009.

[105] A. Reyes-Huamantinco, P. Puschnig, C. Ambrosch-Draxl, O. E. Peil, and A. V. Ruban, “Stacking-fault energy and anti-Invar effect in Fe-Mn alloy from first principles,” *Phys. Rev. B*, vol. 86, no. 6, p. 060201, Aug. 2012.

[106] T. Hickel, S. Sandlöbes, R. K. W. Marceau, A. Dick, I. Bleskov, J. Neugebauer, and D. Raabe, “Impact of nanodiffusion on the stacking fault energy in high-strength steels,” *Acta Mater.*, vol. 75, pp. 147–155, Aug. 2014.

[107] K. Haneda, Z. X. Zhou, A. H. Morrish, T. Majima, and T. Miyahara, “Low-temperature stable nonometer-size fee-Fe particles with no magnetic ordering,” *Phys. Rev. B*, vol. 46, no. 21, pp. 832–838, 1992.

[108] L. Del Bianco, C. Ballesteros, J. Rojo, and A. Hernando, “Magnetically ordered fcc structure at the relaxed grain boundaries of pure nanocrystalline Fe,” *Phys. Rev. Lett.*, vol. 81, no. 20, pp. 4500–4503, 1998.

[109] W. A. A. Macedo, F. Sirotti, G. Panaccione, A. Schatz, W. Keune, W. N. Rodrigues, and G. Rossi, "Magnetism of atomically thin fcc Fe overlayers on an expanded fcc lattice: Cu 84 Al 16 (100)," *Phys. Rev. B*, vol. 58, no. 17, pp. 534–538, 1998.

[110] Y. Tsunoda, Y. Nishioka, and R. M. Nicklow, "Spin fluctuations in small γ-Fe precipitates," *J. Magn. Magn. Mater.*, vol. 128, no. 1–2, pp. 133–137, Nov. 1993.

[111] H. C. Herper, E. Hoffmann, and P. Entel, "Ab initio full-potential study of the structural and magnetic phase stability of iron," *Phys. Rev. B*, vol. 60, no. 6, pp. 3839–3848, 1999.

[112] D. Jiang and E. Carter, "Carbon dissolution and diffusion in ferrite and austenite from first principles," *Phys. Rev. B*, vol. 67, no. 21, p. 214103, Jun. 2003.

[113] M. Acet, E. F. Wassermann, and W. Pepperhoff, "Relevance of magnetic instabilities to the phase stabilities of Fe alloys," *Philos. Mag. B*, vol. 80, no. 2, pp. 127–139, Feb. 2000.

[114] L. T. Kong and B. X. Liu, "Distinct magnetic states of metastable fcc structured Fe and Fe–Cu alloys studied by ab initio calculations," *J. Alloys Compd.*, vol. 414, no. 1–2, pp. 36–41, Apr. 2006.

[115] N. I. Medvedeva, D. C. Van Aken, and J. E. Medvedeva, "Magnetism in bcc and fcc Fe with carbon and manganese," *J. Phys. Condens. Matter*, vol. 22, no. 31, p. 316002, Aug. 2010.

[116] M. Uhl, L. M. Sandratskii, and J. Kübler, "Spin fluctuations in γ-Fe and in Fe3Pt Invar from local-density-functional calculations," *Phys. Rev. B*, vol. 50, pp. 291–301, 1994.

[117] K. Knöpfle, L. Sandratskii, and J. Kübler, "Spin spiral ground state of γ-iron," *Phys. Rev. B*, vol. 62, no. 9, pp. 5564–5569, 2000.

[118] M. Weinert, E. Wimmer, and A. J. Freeman, "Total-energy all-electron density functional method for bulk solids and surfaces," *Phys. Rev. B*, vol. 26, pp. 4571–4578, 1982.

[119] L. Vitos, J.-O. O. Nilsson, and B. Johansson, "Alloying effects on the stacking fault energy in austenitic stainless steels from first-principles theory," *Acta Mater.*, vol. 54, no. 14, pp. 3821–3826, Aug. 2006.

[120] L. Vitos, P. a Korzhavyi, J.-O. O. Nilsson, and B. Johansson, "Stacking fault energy and magnetism in austenitic stainless steels," *Phys. Scr.*, vol. 77, no. 6, p. 065703, Jun. 2008.

[121] K. Burke, “Perspective on density functional theory,” *J. Chem. Phys.*, vol. 136, no. 15, pp. 150901–150901–9, 2012.

[122] J. Hafner, C. Wolverton, and G. Ceder, “Toward computational materials design: The impact of density functional theory on materials research,” *MRS Bull.*, vol. 31, pp. 659–665, 2006.

[123] G. Kresse and J. Furthmüller, “Efficiency of ab-initio total energy calculations for metals and semiconductors using a plane-wave basis set,” *Comput. Mater. Sci.*, vol. 6, pp. 15–50, 1996.

[124] L. H. Thomas, “The calculation of atomic fields,” in *Mathematical Proceedings of the Cambridge Philosophical Society*, 1927, vol. 23, pp. 542–548.

[125] E. Fermi, “A statistical method for the determination of some atomic properties and the application of this method to the theory of the periodic system of elements,” *Z. Phys*, vol. 48, p. 29, 1928.

[126] P. Hohenberg and W. Kohn, “Inhomogeneous electron gas,” *Phys. Rev.*, vol. 136, pp. B864–B871, 1964.

[127] W. Kohn and L. J. Sham, “Self-consistent equations including exchange and correlation effects,” *Phys. Rev.*, vol. 140, pp. A1133–A1138, 1965.

[128] K. Capelle, “A bird’s-eye view of density-functional theory,” *Brazilian J. Phys.*, vol. 36, pp. 1318–1341, 2006.

[129] J. P. Perdew, J. A. Chevary, S. H. Vosko, K. A. Jackson, M. R. Pederson, D. J. Singh, and C. Fiolhais, “Atoms, molecules, solids, and surfaces: Applications of the generalized gradient approximation for exchange and correlation,” *Phys. Rev. B*, vol. 46, no. 11, pp. 6671–6687, 1992.

[130] A. García, C. Elsässer, Z. Jing, S. G. Louie, and M. L. Cohen, “Use of gradient-corrected functionals in total-energy calculations for solids,” *Phys. Rev. B*, vol. 46, pp. 9829–9832, 1992.

[131] G. Kresse and J. Furthmüller, “Efficient iterative schemes for ab initio total-energy calculations using a plane-wave basis set,” *Phys. Rev. B - Condens. Matter Mater. Phys.*, vol. 54, no. 16, pp. 11169–11186, Oct. 1996.

[132] J. P. Perdew, K. Burke, and M. Ernzerhof, “Generalized gradient approximation made simple,” *Phys. Rev. Lett.*, vol. 77, no. 18, pp. 3865–3868, Oct. 1996.

[133] M. Born and R. Oppenheimer, “Zur quantentheorie der molekeln,” *Ann. Phys.*, vol. 389, pp. 457–484, 1927.

[134] D. Shin and C. Wolverton, “First-principles density functional calculations for Mg alloys: A tool to aid in alloy development,” *Scr. Mater.*, vol. 63, pp. 680–685, 2010.

[135] Y. Le Page and P. Saxe, “Symmetry-general least-squares extraction of elastic data for strained materials from ab initio calculations of stress,” *Phys. Rev. B*, vol. 65, p. 104104, 2002.

[136] J. Takahashi, K. Kawakami, Y. Kobayashi, and T. Tarui, “The first direct observation of hydrogen trapping sites in TiC precipitation-hardening steel through atom probe tomography,” *Scr. Mater.*, vol. 63, no. 3, pp. 261–264, Aug. 2010.

[137] J. R. Smith, T. Hong, and D. J. Srolovitz, “Metal-ceramic adhesion and the Harris functional,” *Phys. Rev. Lett.*, vol. 72, no. 25, pp. 4021–4024, 1994.

[138] E. B. Tadmor and N. Bernstein, “The Twinnability of FCC Metals : A Detailed Analysis by The Twinnability of FCC Metals : A Detailed Analysis,” Haifa, Israel, 2004.

[139] E. B. Tadmor and N. Bernstein, “A first-principles measure for the twinnability of FCC metals,” *J. Mech. Phys. Solids*, vol. 52, no. 11, pp. 2507–2519, Nov. 2004.

[140] B. Q. Li, M. L. Sui, and S. X. Mao, “Twinnability Predication for fcc Metals,” *J. Mater. Sci. Technol.*, vol. 27, no. 2, pp. 97–100, Feb. 2011.

VITA

Krista Renee Limmer, née Kalac, was born and raised in Chatham, Ohio. She graduated from Cloverleaf Local High School in 2006 after completing her junior and senior years of high school on the main campus of the University of Akron. Krista graduated *magna cum laude* with Engineering Honors from Alfred University in 2010 with a Bachelor of Science in Materials Science and Engineering and a Bachelor of Arts in Mathematics. During her undergraduate studies, Krista worked as a calculus tutor, resident assistant, and campus tour guide. She also worked for two summers as an intern at Owens Corning, as well as one summer on an undergraduate research project with the Center for Advanced Ceramic Technologies at Alfred University. After meeting her husband Matt during the first of the Owens Corning summer internships, Krista and Matt decided to both attend Missouri S&T for graduate school. In 2010 Krista applied for and received a GAANN fellowship at Missouri S&T. After a year of working with Dr. Rajiv Mishra on friction stir processing of high-strength magnesium alloys, his departure from the university presented Krista with an opportunity to redefine her doctoral research and begin working with Dr. Julia Medvedeva. At the end of her doctoral studies, Krista worked for six months in the Department of Ferrous Metallurgy at RWTH Aachen University in Germany. Krista received her Ph.D. in Materials Science and Engineering from Missouri University of Science and Technology in December 2014.